

ON-LINE OIL CONDITION MONITORING FOR MARINE GEARBOXES

This thesis addresses the importance of oil condition monitoring in marine reduction gearboxes and compares the sensitivity and usage of three different sensors, each with its own working principle.

Johannes Kalaoja

Supervisors

Surya T. Kandukuri
Andreas Klausen
Kjell G. Robbersmyr

This Master's Thesis is carried out as a part of the education at the University of Agder and is therefore approved as a part of this education. However, this does not imply that the University answers for the methods that are used or the conclusions that are drawn.

University of Agder, 2020
Faculty of Engineering and Science
Department of Engineering Sciences

Acknowledgements

This thesis is a part of the Master's program in Mechatronics, at the Department of Engineering Sciences, at the University of Agder. The task in hand proved to be educational, containing key aspects in the field of mechatronics and condition monitoring. I am pleased with the final results, after a semester of dedicated work.

I would like to thank my supervisors, Surya T. Kandukuri, Andreas Klausen, and Kjell G. Robbersmyr, for their much appreciated support and inputs. I would also like to thank the laboratory personnel for providing help related to this thesis.

Johannes Kalaoja

Signature:

Date:

Abstract

Failures in marine reduction gearboxes lead to substantial costs. With the use of oil condition monitoring, these failures can be foreseen so that preemptive measures can be taken. The development of oil condition monitoring equipment has come a long way, and it is time to start using this technology.

There are various reasons why a gearbox failure, and as most of them are a result of inadequate lubrication, several things can be done to reduce these failures. By testing 3 different sensors in a gearbox lubrication system, this study goes through each sensor technology and aims to figure out what is important to consider when selecting a sensor for oil condition monitoring.

The sensors discussed and tested are Gill 4212 Oil Condition Monitoring Sensor, Poseidon Trident QW3100, and Parker Kittiwake Metal Wear Debris Sensor. To test these sensors, several experiments, with a variety of added contaminants, are designed to find the strengths and weaknesses of each sensor. In the end, a conclusion is made on how the tested sensors meet those requirements and what can be done in the future to find an even better sensor configuration to prevent gearbox failures.

Contents

Acknowledgements	i
Abstract	iii
List of Tables	viii
List of Figures	viii
Nomenclature	xi
1 Introduction	1
1.1 Background	1
1.2 History of Oil Condition Monitoring	1
1.3 State-of-the-Art	1
1.4 Problem	3
1.5 Objective	4
1.6 Thesis Structure	4
2 Theory	5
2.1 Gear Materials	5
2.2 Oil Debris Prediction	6
2.3 Gearbox Failure Modes	7
2.4 Surface Stress Estimation	10
2.5 Lubricant Contamination	11
2.5.1 Metallic Debris	12
2.5.2 Non-metallic Debris	14
2.5.3 Water	15
2.6 Sensors	17
2.6.1 Gill 4212	17
2.6.2 Poseidon Trident QW3100	19
2.6.3 Parker Kittiwake MWDS	20
2.7 Hypothesis	21
3 Methods	23
3.1 Setup	23
3.1.1 Test Rig	24
3.1.2 Gearbox	25
3.1.3 Lubrication System	26
3.1.4 Sensor Location	27
3.1.5 Design of Sensor Block	27
3.2 Sensor Wiring and Setting up the Software	29
3.2.1 Gill 4212	30
3.2.2 Poseidon Trident QW3100	32
3.2.3 Parker Kittiwake MWDS	33

3.3	Design of Experiments	34
3.3.1	Adding Water	36
3.3.2	Adding AISI 316L	37
3.3.3	Adding AISI M2	38
3.3.4	Adding Iron Silicate	39
3.4	Sensor Calibration	40
4	Analysis	41
4.1	Temperature	41
4.2	Calibration	41
4.2.1	Gill 4212	41
4.3	Initial Testing	43
4.3.1	Gill 4212	43
4.3.2	Poseidon Trident QW3100	43
4.3.3	Parker Kittiwake MWDS	44
4.4	Experiment no. 1	46
4.4.1	Run no. 1	46
4.4.2	Run no.2	47
4.4.3	Run no. 3	47
4.4.4	Summary	48
4.5	Experiment no. 2	50
4.5.1	Run no. 1	50
4.5.2	Run no. 2	50
4.5.3	Run no. 3	50
4.5.4	Summary	51
4.6	Experiment no. 3	51
4.6.1	Run no. 1	51
4.6.2	Run no. 2	52
4.6.3	Run no. 3	52
4.6.4	Summary	52
4.7	Experiment no. 4	54
4.7.1	Run no. 1	54
4.7.2	Run no. 2	54
4.7.3	Run no. 3	55
4.7.4	Run no. 4	55
4.7.5	Summary	55
4.8	Experiment no. 5	56
4.8.1	Run no. 1	56
4.8.2	Run no. 2	56
4.8.3	Run no. 3	57
4.8.4	Summary	57
5	Discussions	59
5.1	Results of Experiments	59
5.1.1	Water	59
5.1.2	AISI 316L	59
5.1.3	AISI M2	59
5.1.4	Iron Silicate	60
5.1.5	Contamination for Future Experiments	60
5.2	Ease of Installation	61
5.3	Ease of Use	61
5.4	Marine Reduction Gearboxes	62

5.5	Costs	63
6	Conclusion	64
6.1	Limitations	65
6.2	Future Work	65
	Bibliography	65
	Appendices	A1
A	Wiring Diagram	A1
B	Plumbing diagram	B1
C	Sensor Block Drawing	C1
D	M22x1.5 Plug	D1
E	MATLAB scripts	E1
E.1	Script for plotting Gill 4212 sensor data	E1
E.2	Script for plotting Poseidon Trident QW3100 sensor data	E4
E.3	Script for plotting Parker Kittiwake MWDS sensor data	E8
E.4	Script for logging Poseidon Trident QW3100 sensor data	E12
F	Results	F1
F.1	Experiment no. 1	F1
	F.1.1 Run no. 1	F1
	F.1.2 Run no. 2	F4
	F.1.3 Run no. 3	F7
F.2	Experiment no. 2	F10
	F.2.1 Run no. 1	F10
	F.2.2 Run no. 2	F13
	F.2.3 Run no. 3	F16
F.3	Experiment no. 3	F19
	F.3.1 Run no. 1	F19
	F.3.2 Run no. 2	F22
	F.3.3 Run no. 3	F25
F.4	Experiment no. 4	F28
	F.4.1 Run no. 1	F28
	F.4.2 Run no. 2	F30
	F.4.3 Run no. 3	F32
	F.4.4 Run no. 4	F34
F.5	Experiment no. 5	F36
	F.5.1 Run no. 1	F36
	F.5.2 Run no. 2	F39
	F.5.3 Run no. 3	F42

List of Tables

2.1	Debris size from the different kinds of failure modes	10
2.2	Oil debris contamination limit for an industrial gearbox	11
2.3	Oil conductivity for common types of gear oil	12
2.4	Chrome- and nickel-equivalents for AISI 316L and AISI M2	13
2.5	Chemical composition of AISI 316L stainless steel	14
2.6	Properties of AISI 316L stainless steel	14
2.7	Chemical composition of AISI M2 high-speed steel	14
2.8	Properties of AISI M2 high-speed steel	14
2.9	Chemical composition of iron silicate blasting powder	15
2.10	Properties of iron silicate	15
2.11	Water saturation limits for the different types of oil	15
2.12	Life extension factor of a lubricant when reducing moisture	16
2.13	Properties of Water	16
2.14	Electromagnetic properties for the different substances	17
2.15	Maximum range fine debris	18
2.16	Maximum range coarse debris	18
2.17	Guideline oil reference number	19
2.18	Poseidon Trident QW3100 holding registers	20
2.19	Parker MWDS classification bins	21
2.20	Substance detectability prediction for the different sensors	22
3.1	Bill of materials	24
3.2	Wire color codes for the Gill 4212	30
3.3	The RS-485 configurations for the Poseidon Trident QW3100	32
3.4	Wire color codes for the Poseidon Trident QW3100	32
3.5	Wire color codes for the Parker MWDS	33
3.6	The different experiments being conducted	34
3.7	Steps for adding water	36
3.8	Steps for adding AISI 316L stainless steel	37
3.9	Steps for adding AISI M2 high-speed steel	38
3.10	Steps for adding iron silicate	39
6.1	Specifications for the tested sensors	65

List of Figures

1.1	Kytola OILAN A4	2
1.2	Parker MWDS	2

1.3	Eaton CCT 01 transmitter and PFS 01 laser sensor	2
1.4	Stauff offers a lot of sensors to measure lubricant contamination	3
1.5	Parker XRF Analyser	3
2.1	Hardness profile of a case-hardened AISI 4140 specimen	5
2.2	Bathtub curve indicating the stages of wear rates	6
2.3	Debris generation and wear process in a gearbox	7
2.4	Examples of how the different failure modes can look like	7
2.5	Typical shapes for bending and Hertzian fatigue endurance limits for steels plotted in an S-N curve	8
2.6	4 common types of wear in a tribological system	9
2.7	Effect of the ratio between the abraded and abrasive hardness	9
2.8	Schaeffler diagram of AISI 316L and AISI M2	13
2.9	Water dissolution limit in a common gear oil as a function of temperature	16
2.10	The different options for sensor location	17
2.11	Gill 4212 Oil Condition Monitoring Sensor	18
2.12	Poseidon Trident QW3100 Oil Condition and Water Contamination Monitor	19
2.13	Parker Kittiwake Metal Wear Debris Sensor	21
3.1	Overview of the setup	23
3.2	Gearbox test rig setup	24
3.3	Magnetic and non-magnetic drain plug	25
3.4	Brevini PD2010	25
3.5	Bosch Rexroth oil filter	25
3.6	Hose nipple for plumbing	26
3.7	Marco UP3/OIL-R gear pump	26
3.8	Section view of the assembled sensor block	28
3.9	Sensor block	29
3.10	M22x1.5 plug to replace the Gill 4212	29
3.11	National Instruments USB-6008 DAQ	30
3.12	Overview of the Data Acquisition Tool	31
3.13	Gill Sensor Configuration Tool	31
3.14	Advantech B+B SmartWorx Isolated USB to RS-422/485 Converter	32
3.15	Screenshot of the Parker DebrisSCAN sensor connecting tab	33
3.16	Screenshot of the Parker DebrisSCAN sensor graphical interface tab	34
3.17	Sample glass and syringe used for adding the contamination	35
4.1	Steady state temperature of the gearbox	41
4.2	Fine debris calibration with the Gill 4212	41
4.3	Fine debris calibration testing with the Gill 4212	42
4.4	Gill 4212 oil condition calibration process	42
4.5	Initial data acquisition with the Gill 4212	43
4.6	Initial data acquisition with the Poseidon Trident QW3100	44
4.7	Initial data acquisition with the Parker Kittiwake MWDS	45
4.8	Parker MWDS results on particle filtering	46
4.9	Gill sensor data after experiment no. 1-3	48
4.10	Poseidon water-in-oil sensor data for experiment no. 1	49
4.11	Poseidon temperature sensor data for experiment no. 1	49
4.12	Poseidon interfacial impedance data for experiment no. 2	51
4.13	Particle debris on Gill 4212 probe after experiment no. 3	53
4.14	Gill fine particles data for experiment no. 3	53
4.15	Parker ferrous particle per minute data for experiment no. 3	54
4.16	Poseidon interfacial impedance data for experiment no. 4	55

4.17	Parker ferrous particle per minute data for experiment no. 4	56
4.18	Parker ferrous particle per minute data for experiment no. 5	57
4.19	Poseidon interfacial impedance data for experiment no. 5	58
5.1	Alternate mounting location for the Gill 4212	60

Nomenclature

Λ -ratio	Lambda-ratio. See Section 2.3
ν	Kinematic viscosity, see Subsection 3.1.2
Cr_{eq}	Chrome equivalent, see Equation (2.4)
m_{step}	Added particle mass per experiment step, see Section 3.3
Ni_{eq}	Nickel equivalent, see Equation (2.5)
ppm_{step}	Increase in contamination level in ppm per experiment step, see Section 3.3
Q_{pump}	Rated pump flow, see Subsection 3.1.3
$V_{lubricant}$	The amount of lubricant within the lubrication system, see Subsection 3.1.3
V_{step}	Added particle volume per experiment step, see Section 3.3
AGMA	American Gear Manufacturers Association
AISI	American Iron and Steel Institute
ASA	Acrylonitrile styrene acrylate
ASM	American Society for Materials
ASTM	American Society for Testing and Materials
BHN	Brinell hardness number
BSPP	British Standard Pipe Parallel
DAQ	Data acquisition
EIS	Electrochemical impedance spectroscopy
FTIR	Fourier transform infrared spectroscopy
HSS	High-speed steel
HV	Vickers pyramid Number
MWDS	Metal Wear Debris Sensor
n	Number of particles before the cleanliness level is exceeded, see Section 3.3
OPC	Optical particle counter
PMI	Positive material identification
ppm	Parts per million
SAE	Society of Automotive Engineers
SS	Stainless steel
UNCTAD	United Nations Conference on Trade and Development
UNF	Unified fine thread
XRF	X-ray fluorescence

1. Introduction

1.1. Background

For over 2 millenniums there has been a requirement for speed- and torque-conversions from one device to another, and the transmission has therefore served an important purpose[1]. The gearbox is used in everything from precision instruments like clocks to transportation vehicles like ships.

The global market relies on the latter, and a report from UNCTAD shows that 80% of the global trade is carried by sea[2, p.91]. At the beginning of 2019, there was a total of 95,402 ships in the world fleet[2, p.28].

Many of these ships use reduction gearboxes to convert the thrust of the engine to a lower speed for the propeller. It is therefore important that the gearbox is working and reliable to prevent huge losses in terms of repair- and tug-costs and loss of income because of unplanned downtime.

According to the insurance company Gard AS, repair- and tug-costs for a ship with gearbox failures have a mean expense of US\$ 528,000 with a US\$ 1,400,000 standard deviation and with time loss mean expense of US\$ 316,000 with a standard deviation of US\$ 340,000. This results in a mean expense of US\$ 844,000. A system that is able to predict breakdowns of the ships ahead of time could, therefore, save millions of US\$ for the maritime industry.

1.2. History of Oil Condition Monitoring

Most mechanisms operating with oil can be monitored by wear debris analysis. Based on the size, concentration and material of these particles, a lot can be known about the state of the machinery. There has therefore been much development within the field of condition monitoring and failure prediction over the years.

Means of measuring magnetic particles suspended in fluids started in the 1930s and 40's with the development of sensors being able to warn about possible failures on oiling systems in power plants and engines[3, 4, 5, 6]. Systems being able to detect non-magnetic particles also existed, but it required a lot of time and laboratory equipment to conduct the tests[7].

During the 1950s, easier methods of measuring magnetic particles using magnetic sensors were developed, and not long after, during the 1960s, people were also able to measure non-magnetic particles suspended in fluids using electrical conductance[8, 9]. Around this period, companies also figured how to measure the water contamination within a lubricant[10, 11].

By the end of the 1970s and beginning of the 1980s, the interest for oil condition monitoring accelerated with several patents being filed[12, 13, 14, 15, 16, 17, 18].

1.3. State-of-the-Art

A lot of industries require methods for condition monitoring, which has resulted in many companies developing sensors for detecting and measuring water and particle debris contamination within lubrication systems.

There are several major companies leading the development of condition monitoring for lubrication systems. Eaton, Parker Kittiwake, Poseidon, and Stauff all offer several market-leading methods for detecting contamination in lubrication systems.

There are several methods for detecting water and particle debris contamination. The most used method is to measure a change in electromagnetic properties as conductivity, inductivity, and the dielectric constant. The electromagnetic properties of the lubricant change when subjected to water or particle debris.

The most used method for measuring water contamination, real-time, is capacitive sensing. These sensors are, however, limited to measure the relative humidity in the lubrication. Several companies are offering these types of water-in-oil sensors, such as Eaton, Kongsberg, and Pall[21, 22, 23]. There are however, sensors that can measure free water content, such as the Kytola OILAN Water In Oil Analyzer, seen in Figure 1.1[19]. Another reliable method for measuring water and other types of contamination is Fourier transform infrared spectroscopy (FTIR), which could map all molecules within the lubricant based on wavelength radiation of the different molecules[24]. This has traditionally been done in laboratories, but later development by Foster-Miller has allowed the same technology to be used real-time[25].



Figure 1.1.: Kytola OILAN A4[19]



Figure 1.2.: Parker MWDS[20]

Using electrical conductance and inductance is the Parker Metal Wear Debris Sensor, seen in Figure 1.2, which can count ferrous and non-ferrous particles with a large detection range, either in- or on-line.

Measuring the dielectric constant is a robust method of measuring the oil condition and contamination within a lubricant. Stauff has, however, developed a sensor that is supposed to be 60 times more sensitive than dielectric sensors on increasing contamination[26]. The sensor can be seen in Figure 1.4 (a). As the lubricant get contaminated or degraded, the dielectric constant changes. A measurement of the dielectric constant could therefore be used as a guide of reference for the oil condition.

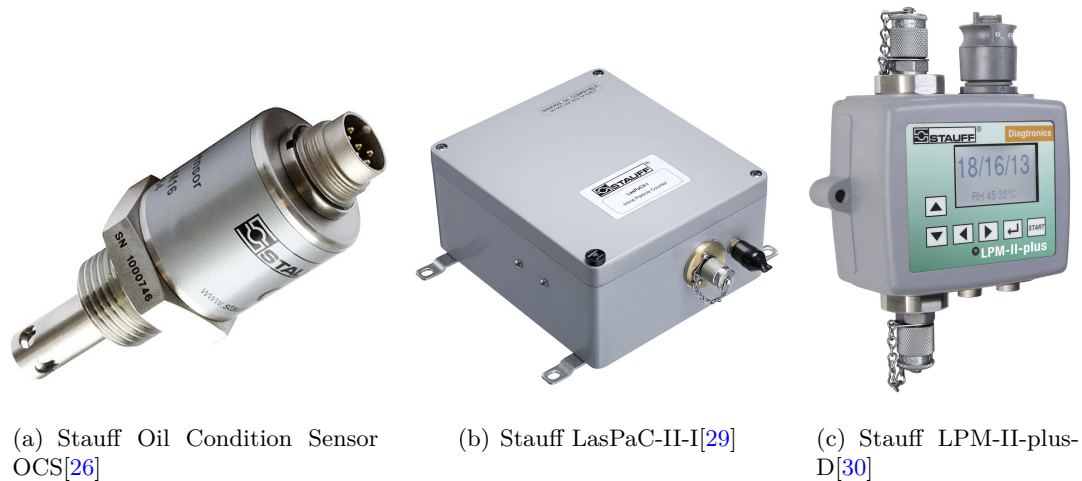
Another method for detecting particle debris contamination is with the help of lasers. This method will work with in- or on-line monitoring as a laser will shine through the fluid. A photodiode will receive the light and detect particles based on the intensity of the received light[27]. Both Eaton and Stauff are selling sensors using this technology, seen in Figures 1.3 and 1.4 (b) [28][29].

A method which is similar to the laser sensors, is the optical sensors. They use a collimated precision LED as the light source which shines on a photo diode[30]. The reduction in light intensity as a particle flows through the sensor will deduce the particle size, the same as with the laser sensor. Stauff is selling the optical sensors as well[30]. This can be seen in Figure 1.4 (c).

The advantage with the mentioned laser and optical sensors is that they are configured to send ISO cleanliness levels out of the box in addition to some larger particle sizes. ISO cleanliness levels are discussed later in Section 2.5. Another advantage is that they will detect all kinds of particle debris, independent of what material the particle consists of.



Figure 1.3.: Eaton CCT 01 transmitter and PFS 01 laser sensor[28]



(a) Stauff Oil Condition Sensor OCS[26] (b) Stauff LasPaC-II-I[29] (c) Stauff LPM-II-plus-D[30]

Figure 1.4.: Stauff offers a lot of sensors to measure lubricant contamination

To figure out the specific material that is contaminating the lubricant, an x-ray fluorescence (XRF) analysis can be used. Parker Kittiwake has developed a portable tool to analyze the lubricant and find the specific contamination content, seen in Figure 1.5. This is, however, for the moment, just an off-line method, and requires samples of the lubricant to be analysed[31]. The XRF method is the same technology used in positive material identification (PMI). It can determine the chemical content, which could be useful to determine the origin of the contamination. The Pacific Northwest National Laboratory is, however, developing a way to do this kind of analysis in real-time[25]. Real-time lubrication analyses using XRF and FTIR technology in-line with lubrication systems could be on the way and will probably revolutionize the oil condition monitoring.



Figure 1.5.: Parker XRF Analyser[31]

A lot of companies like Eaton, Poseidon, and Stauff are now offering complete packages for detecting all kinds of lubricant contamination, including particle debris, water, and fuel contamination. This, combined with the ISO cleanliness level indicator, is very user friendly as all the user needs to do is installing the sensor package and mount the cleanliness level indicator. The sensor packages can be used for many applications.

It is hard to come by information on each of these sensors, as the companies selling them are quite secretive.

1.4. Problem

With big equipment comes the requirement of being able to handle high loads. When high loads are applied, there is a significant increase in the risk of failure. Engineers have, through experience, learned to design gearboxes according to the application by calculation, but there is always an unknown, such as the factor of lubrication, which is difficult to predict.

Often in lubrication analysis, off-line samples (see Figure 2.10) have been used to monitor the condition of the lubrication, and thereby the condition of the gearbox. The problem with off-line monitoring is that it is slow and costly since it requires technicians to sample the lubricant and then to send the samples to laboratories to have them analyzed. In addition to the problem with time and costs, 50% of the tests show no problems with the oil at all, while 45% indicate imminent problems that require

further testing, and just 5% shows serious problems that might have been detected too late in the first place[32].

Sensors for monitoring the condition of the lubrication, including water- and particle-contamination, in real-time, is therefore not just sensible, but might be critical to prevent failures in time.

1.5. Objective

By testing three sensors, each with their own working principle, the goal is to determine the benefits and weaknesses with each sensor. To do that, each sensor will be reviewed and tested. Several experiments will be conducted in order to test each sensors ability to detect materials with different electromagnetic properties. The experiments will also be designed to test how sensitive and accurate each sensor is to changes.

The results will then be evaluated to determine which sensor or sensors that would be best fitted for use to reduce the failure rates and expensive repair costs for marine reduction gearboxes. All sensors will then be weighed up against each other to find a cost efficient setup that will monitor all crucial contamination levels.

1.6. Thesis Structure

This thesis is composed of 6 chapters: Introduction, theory, methods, analysis, discussions and conclusions. There will also be an appendix at the end including drawings and data sheets.

The introduction contains a background of oil condition monitoring and the history of it. It will also contain a state-of-the-art study and a description of the problem that needs to be solved with an objective of what is going to be in focus in this thesis. The theory will describe all relevant theory that is needed to conduct the tests and making a valid conclusion. The methods chapter will describe how the task is executed and puts the theory in practice. The analysis chapter will be about analysing the results received from the tests done in the methods chapter. The discussion chapter discusses the results from the analysis chapter based on the theory. The final chapter, conclusion, will summarize the thesis and a conclusion will be drawn based on what is learned.

2. Theory

2.1. Gear Materials

In gearboxes subjected to high loads, the teeth have to be tough enough, so they do not bend or fracture. In addition to that, they also need a hard teeth surface to resist wear and Hertzian fatigue. That usually requires molybdenum steels such as AISI 41xx-series, nickel-molybdenum steels such as AISI 46xx-series or nickel-chromium-molybdenum steels such as the AISI 86xx-series. These hard steels are usually martensitic steels after their adequate heat treatments.

The steels will go through a case-hardening process to form a hard surface[34, p.268]. There are several methods used to case-harden a steel, and is usually based on the carbon content of the material. The most used case-hardening processes are induction hardening, carburizing and nitriding. Induction hardening heats and quenches the material. The carburizing and nitriding process however diffuses the part with carbon or nitrogen followed by quenching to make the carbon or nitrogen atoms be interstitially locked in the steel lattice, which forms martensite. Martensite is a very hard structure and gives the teeth surface the desirable properties. Figure 2.1 shows how the changes in hardness values from the surface towards the center of a case-hardened AISI 4140 gear. Figure 2.1 also shows a maximum Vickers hardness value of about 650 HV which equals to about 550 BHN.

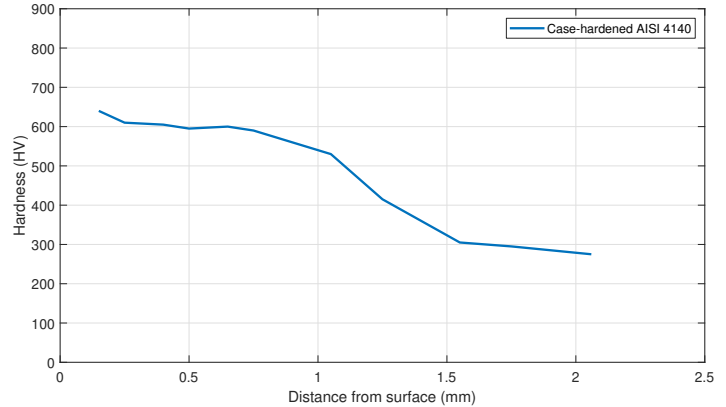


Figure 2.1.: Hardness profile of a case-hardened AISI 4140 specimen[33]

The shape of hardness profile varies based on the case-hardening method used, from nitriding having the steepest slope, to induction hardening having the most gentle slope.

To establish which materials have certain properties to resist surface fatigue, American Gear Manufacturers Association (AGMA) has created a material property which are used for estimating the lifetime of gears before subjected to surface fatigue. This property is called surface-endurance strength, derived in Equation (2.1). The surface-endurance strength does however need to be corrected before used together with the surface stress, discussed later in Section 2.4. A list of surface-endurance strengths for different materials can be found in *Machine Design: An Integrated Approach*[35, Table 12-21].

$$S_{fc} = \frac{C_L C_H}{C_T C_R} S_{fc'} \quad (2.1)$$

where

- S_{fc} = Corrected surface-endurance strength
- C_L = Life factor
- C_H = Hardness factor
- C_T = Temperature factor
- C_R = Reliability factor
- $S_{fc'}$ = Uncorrected surface-endurance strength

All factors are described in detail in *Machine Design: An Integrated Approach*[35, p.724-729].

2.2. Oil Debris Prediction

Wear is classified as a process of mass loss over time. There will always be mass loss in a tribological system, and for a gearbox, a lot of research has been conducted to see how the debris generation happens over time. The debris generation rate has been predicted to follow a bathtub curve, as shown in Figure 2.2.

When a gearbox is ran for the first time, it will always go through a run-in period. This allow the gear teeth to mate properly and to reduce the teeth surface roughness, and thereby increasing the specific film thickness[36, p.1100]. During the run-in period, adhesion wear and scuffing damage is the biggest fears. The failure modes will be described in Section 2.3. To keep these failure modes under control, American Society for Materials (ASM) recommends running in new gearsets at half load the first 10 hours[36, p.1100]. The run-in process will generate a lot of very fine debris, around $10\ \mu\text{m}$ or smaller, and it is therefore recommended to change the lubricant after the first 50 hours[37, p.309][36, p.1101].

After the run-in period, there will be a stable period with a stable debris generation. This period will also only generate very fine particles as a result of wear. The debris generated during this period has a maximum size of $15\ \mu\text{m}$ with a mean size of $2\ \mu\text{m}$ [38, p.132]. During this period, there will be a stable wear process, and if something were to go wrong, it would be a random failure based on several independent factors. Common for both these cases are the wear is benign and is in principle not harmful.

After the stable period, the debris generation will increase. This is mainly because of Hertzian fatigue, discussed later in Section 2.3. The debris generation will increase when it exceeds a certain time as Hertzian fatigue don't have any endurance limit[36, p.1098]. At this point, bigger particles, up to around $150\ \mu\text{m}$ starts to break apart from the tooth surface, which will accelerate the debris generation rate until the gearbox reaches failure[38, p.132].

The clearest indication that a gearbox is onset of failure is a rapid increase of wear rate. So if a sensor were to measure the number of particles contaminating the oil, the clearest indicator would be the derivative of the number of particles.

Figure 2.3 shows the bathtub curve and the sizes of debris that can be expected for each stages in the lifespan of a gearbox.

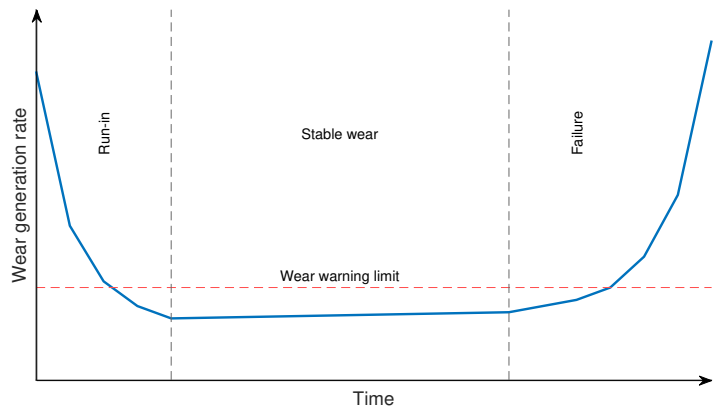


Figure 2.2.: Bathtub curve indicating the stages of wear rates

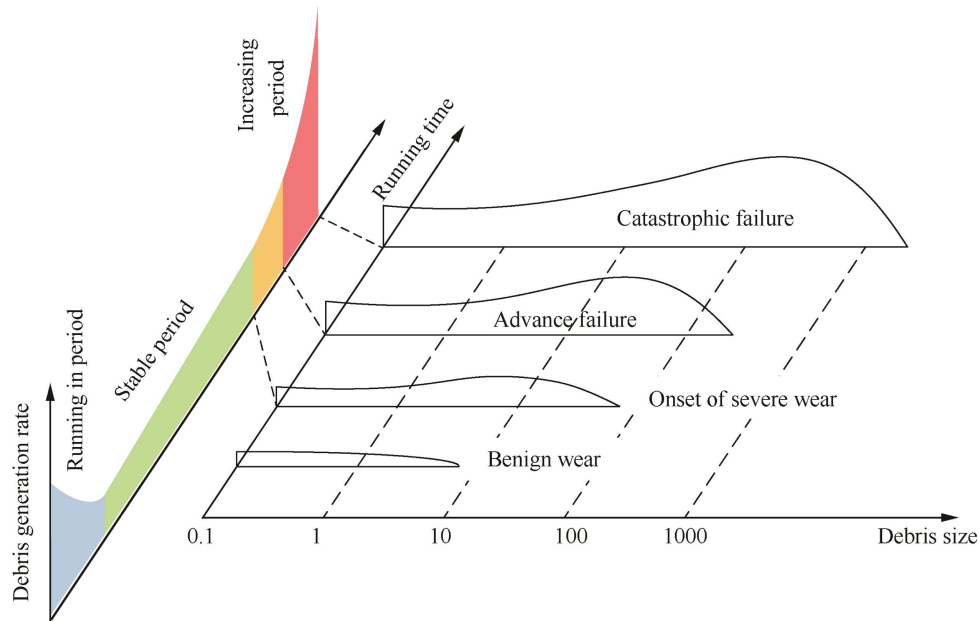


Figure 2.3.: Debris generation and wear process in a gearbox[39]

2.3. Gearbox Failure Modes

The failure modes of a gearbox can be split into 2 categories, non-lubrication-related failures and lubrication-related failures. The lubrication-related failure modes can again be split into 3 common categories, all which have distinct features[36, p.1098]. The 3 common failures are (Figure 2.4):

- Hertzian fatigue (pitting and micropitting)
- Wear (adhesion, abrasion and polishing)
- Scuffing

The stresses that appears when two teeth surfaces mate are very complex and usually consists of dynamic Hertzian fatigue in combination with rolling and sliding[35]. These stresses can cause several types of failures that will be discussed.

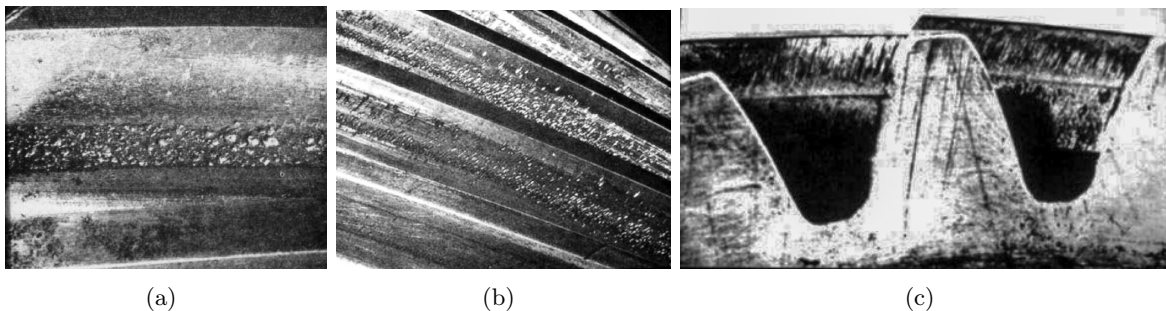


Figure 2.4.: Examples of how the different failure modes can look like. (a) Hertzian fatigue(Pitting), (b) Wear(Abrasion) and (c) Scuffing[40]

Hertzian fatigue or surface fatigue is when the contact stress exceeds a certain stress level for many cycles, which results in small particles detaching from the surface of the gear teeth[36, p.1098-1099]. The failure often starts as a crack, which propagates over a large number of cycles until they finally break apart from the tooth itself[36, p.1098-1099]. Unlike bending fatigue, there is no endurance limit

for Hertzian fatigue, which means that pitting will be a problem eventually, even though the gearbox is designed for an infinitely high stress and infinitely high number of cycles[36, p.1098-1099]. As seen in Figure 2.5, the stress limit for Hertzian fatigue goes towards zero over a large number of stress cycles, which means that it will eventually be a problem.

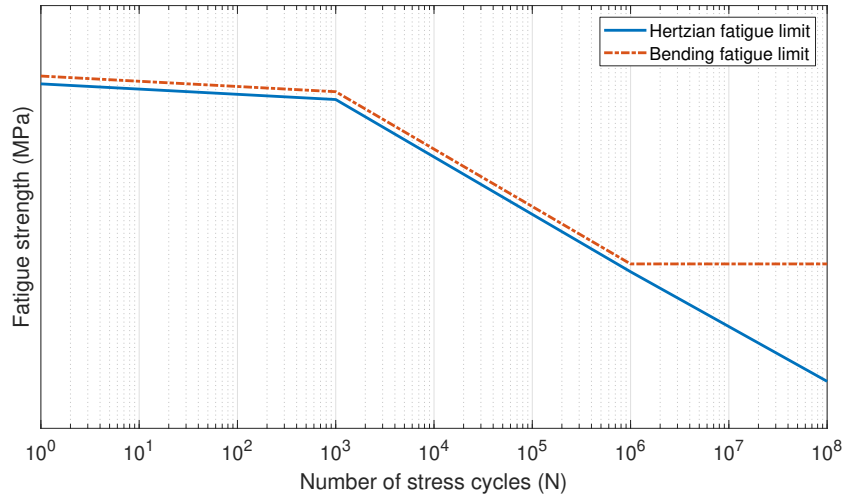


Figure 2.5.: Typical shapes for bending and Hertzian fatigue endurance limits for steels plotted in an S-N curve

Water contamination in the lubricant may also cause pitting because of hydrogen embrittlement in the teeth surface. Hertzian fatigue is usually split into pitting and micropitting. The difference between pitting and micropitting is the size of the pits. Micropits usually have a size of $5 - 10 \mu m$ while regular pits is about ten times larger[36, p.1098-1099][41]. Micropitting itself is not necessarily considered destructive but might grow into pitting. It is usually only observed in gear operating under the Λ -ratio. There are several ways to extend the pitting and micropitting life of the gears, and one of them is to keep the Λ -ratio as high as possible.

Λ -ratio is the ratio between the lubricant film thickness to the composite surface roughness, also called specific film thickness. This has proven to be a good method to determine safe operating conditions in a gearbox. A very low Λ -ratio will not give adequate lubrication as the lubricant will be squished inside the small pits in the roughness of the surface.

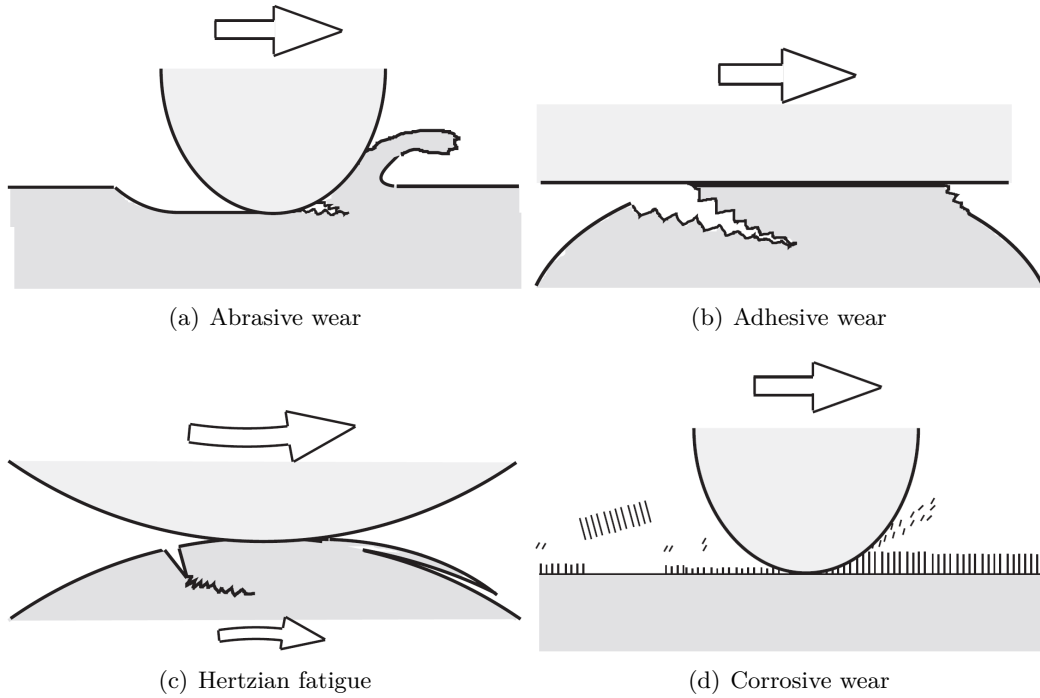


Figure 2.6.: Illustrations for 4 common types of wear in a tribological system[37, p.278]

Wear describes gradual removal of material of the gear tooth surface[34, p.267]. It can be split into several categories, the most common being abrasion, adhesion and corrosive wear.

Abrasive wear is described as gradual removal of material on the gear tooth surface because of sliding contact with hard particles within a contaminated lubricant, shown in Figure 2.6. The hard particles will plough into the tooth surface and remove material[37, p.281]. That is why case hardening of the gears is so important, to increase the hardness ratio between the abraded and abrasive material. A low hardness ratio leads to abrasive wear, while a high hardness ratio leads to deformation of the abrasive particles instead of ploughing of the gear surface, as shown in Figure 2.7[37, p.284]. Abrasive wear will either be a result of foreign particles in a closed gearbox, or an oil supply without adequate filtering[42, p.591].

Adhesive wear is described as gradual removal of material on the gear tooth surface due to the lack of sliding contact. When the two mating gear surfaces has enough adhesive bonding strength to resist relative sliding, particles detach from the surface because of high compression and shearing stresses[37, p.278-279].

Corrosive wear can happen in corrosive liquids when sliding between the two teeth surfaces takes place[37, p.295]. Tribochemical reaction produces a layer on the tooth surface which at the same time is removed by friction between the mating gears[37, p.295].

The wear failure mode will happen if the lubrication is containing debris, is too thin or lacking. Wear

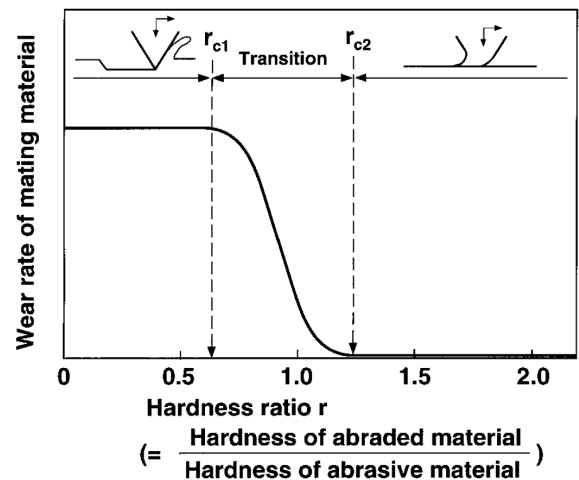


Figure 2.7.: Illustration of the effect of the ratio between the abraded and abrasive hardness on the wear rate from abrasive wear[37, p.284]

can contribute to further pitting by metallic particles indenting the teeth, causing stress concentrations which leads to crack propagation as well as disrupting the lubricant film[36, p.1100-1102]. It should be noted that some wear could be beneficial as it increases the Λ -ratio between the gear sets[34, p.267].

Scuffing failure is defined by ASM as a localized damage caused by two unprotected sliding surfaces resulting in solid-phase welding between the two surfaces[41][36, p.1102-1104]. Unlike Hertzian fatigue and wear, scuffing is a sudden failure that usually happen during the break-in period of the gear teeth[34, p.268]. Reducing the risk of scuffing includes having a high surface hardness on the gear teeth as well as selecting a suitable lubricant[34, p.268].

Table 2.1.: Debris size from the different kinds of failure modes[43]

	Debris size
Abrasive wear	$< 6 \mu m$
Adhesive wear	$< 5 \mu m$
Corrosion wear	$> 100 \mu m$
Micropitting	$3 - 10 \mu m$
Pitting	$40 - 100 \mu m$

What is common for all of these failure modes is that they are lubricant-related and are hard to counteract. What can be done is to take preemptive measures to make sure there are low risks for these failure modes, such as selecting the right lubricant and having a clean lubricant which includes filtering the lubricant and keeping water out. Research done by GILL Sensors & Controls shows that 34.4% of gearbox failures are caused by inadequate lubrication and that 19.6% are because of contamination problems[44].

A Λ -ratio above 2 should be enough to prevent failures such as adhesive, abrasive and corrosive wear, but the ultimate failure mode will be Hertzian fatigue which is impossible to avoid[35, p.718]. The only solution is to increase the pitting resistance.

Table 2.1 shows what kind of debris size that could be expected from the different types of failure modes.

2.4. Surface Stress Estimation

There are methods to estimate the lifetime before Hertzian fatigue occurs. A researcher named Buckingham did a lot a research and found an equation that could estimate the surface stresses between two gear teeth. AGMA adopted the Buckingham equation and now uses it to calculate the pitting resistance for gears[35, p.718].

$$\sigma_c = C_p \sqrt{\frac{W_t}{FId} \frac{C_a C_m}{C_v} C_s C_f} \quad (2.2)$$

where

- σ_c = Surface stress
- C_p = Elastic coefficient
- W_t = Tangential force on gear teeth
- F = Face width
- I = AGMA surface-geometry factor
- d = Pitch diameter
- C_a = Application factor
- C_m = Load-distribution factor
- C_v = Dynamic factor
- C_s = Size factor
- C_f = Surface-finish factor

This surface stress will then be compared to the surface-fatigue strengths, discussed in Section 2.1, to find the safety against surface fatigue. The safety factor against surface fatigue can be calculated as listed in Equation (2.3).

$$N = \left(\frac{S_{fc}}{\sigma_c} \right)^2 \quad (2.3)$$

where

N = Safety factor against surface-fatigue
 S_{fc} = Corrected surface-endurance strength
 σ_c = Surface stress

The safety factor against surface-fatigue has to be greater than 1 for the gear teeth surface to last the amount of time set in the life factor (C_L) in Equation (2.1).

All factors are described in detail in *Machine Design: An Integrated Approach*[35, p.710-731].

2.5. Lubricant Contamination

In this thesis, a number of substances will be added to the lubricant to test the area of usage of three different sensors. This will in theory result in some sensors not being able to detect all of the particles. The following substances, will be added to the lubricant:

- AISI 316L stainless steel
- AISI M2 high-speed steel
- Iron silicate blasting powder
- Water

The solid substances that are going to contaminate the lubricant all have different sizes in order to simulate different failure modes and to check the limitations of each sensor. For the purpose of industrial gearboxes, two cleanliness level were found. A cleanliness level of 17/15/12 is recommended by the book, *Machinery Condition Monitoring - Principles and Practices*[45, p.156]. Eaton however recommends a cleanliness level of 19/15/11 for industrial gearboxes[46, p.6]. The two recommended cleanliness levels is also shown in Table 2.2. The cleanliness level notation is standardized by ISO 4406 and sets an upper limit for the number of particles in a milliliter of fluid over the sizes: $4 \mu m$, $6 \mu m$ and $14 \mu m$ respectively[47]. A cleanliness level of 17/15/12 and 19/15/11 translates to the following number of particles:

Table 2.2.: Oil debris contamination limit for an industrial gearbox following ISO 4406

Cleanliness level	17/15/12			19/15/11		
Particles size	$> 4 \mu m$	$> 6 \mu m$	$> 14 \mu m$	$> 4 \mu m$	$> 6 \mu m$	$> 14 \mu m$
Particles/ml	640 - 1300	160 - 320	20 - 40	2500 - 5000	160 - 320	10 - 20

The lubricant can be contaminated by several substances, such as metallic and non-metallic particles and water, which will be discussed later in this section. A relatively high viscosity grade is needed to keep the lubricant on the surface on the gear teeth surfaces such that there will not be any metal to metal contact under the high loads, as usually seen in a gearbox.

The lubricant has a magnetic relative permeability close to 1, and will not be magnetized by a magnetic field. Magnetic sensors will therefore be able to distinguish between the lubricant and magnetic particles.

Table 2.3.: Oil conductivity for common types of gear oil[48, 49]

Oil type	Electrical conductivity @23°C	Dielectric constant
Mineral oil	$\sim 6 \cdot 10^{-12} S/m$	2.1 – 2.4
Polyalphaolefin	$\sim 24 \cdot 10^{-12} S/m$	2.1 – 2.4
Polyalkylene glycol	$\sim 195\,000 \cdot 10^{-12} S/m$	6.6 – 7.3

As shown in Table 2.3, the viscosity of the lubricant will not determine the electrical conductivity, but rather the type of oil. However, the electrical conductivity is very low for all types of oil, and will be discussed further later in Section 2.6.

There are several physical properties of the substances in a gearbox which can be measured to find the contamination or lubricant quality level. Often these are based on electrical or magnetic properties, as the properties listed below.

Electric conductivity is a materials ability to conduct electricity, which is the inverse of electrical resistivity. This material property is crucial when detecting particles using sensors that register change in conductivity.

Magnetic permeability is a materials ability to be magnetized and is critical in order to be detected by sensors using a magnetic element. When considering the permeability of steels, it depends on the microstructure of the steel. Ferritic and martensitic microstructures are magnetic, while the austenitic microstructure are non-magnetic and will not be detected by magnetic sensors. All steels can however have an austenitic microstructure, but that is over the initial austenizing temperature which generally starts around $300^{\circ}C$ depending on the alloy. That will not be a problem when testing the oil contamination in a gearbox as the temperature of the lubricant will be well below $100^{\circ}C$.

Dielectric constant is a materials ability to transmit electrical potential energy[49]. A way to determine the lubricant quality could be to measure the dielectric constant. During the lifetime of a lubricant, the lubricant will degrade which also reduces the dielectric constant of the lubricant[49]. Measuring a change of the dielectric constant of a substance over time could therefore be a good indication of lubricant quality degradation and particle debris or water contamination. The dielectric constant will be altered if mixing lubricants with different viscosities, acid number or base number as well as mixing additives into the lubricant.

2.5.1. Metallic Debris

Metallic particles are usually contaminating the lubrication from the gear tooth surface following the failure modes described in Section 2.3. This is the kind of particles that are measurable by most oil contamination sensors.

A way to determine if an alloy is magnetic or not at room temperature is to use a constitution diagram like the Schaeffler diagram. The Schaeffler diagram is usually used for stainless steels in welding applications and maps materials based on ferrite- and austenite-promoting elements which gives an indication of the micro-structure within the alloy. To map a material, the chrome- and nickel-equivalent needs to be calculated with the equations given below and then the material is plotted in the Shaeffler diagram based on the results from the equations as shown in Figure 2.8.

$$Cr_{eq} = \%Cr + \%Mo + 1.5 \cdot \%Si + 0.5 \cdot \%Nb \quad (2.4)$$

The chrome equivalent is a value to measure the influence of ferrite-promoting elements.

$$Ni_{eq} = \%Ni + 30 \cdot \%C + 0.5 \cdot \%Mn \quad (2.5)$$

The nickel equivalent is a value to measure the influence of austenite-promoting elements.

As most gear wheels in heavy duty gearboxes are made out of steel, the Schaeffler diagram is a good and simple indicator to use to find out if a magnetic sensor could be used or not. For example the Gill 4212, described later in Subsection 2.6.1.

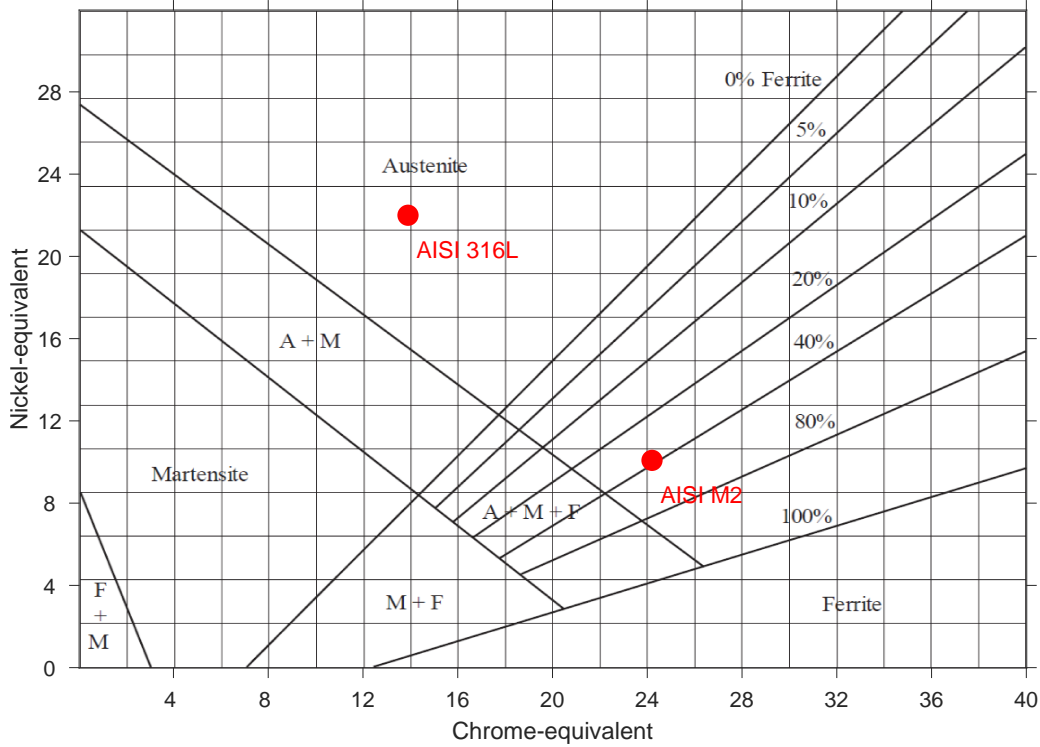


Figure 2.8.: Schaeffler diagram of AISI 316L and AISI M2

To use the Schaeffler diagram, the chrome- and nickel-equivalent of a steel is calculated based on the chemical composition of the steel. The two numbers will then be plotted in the diagram, shown in Figure 2.8. As a rule of thumb, ferrite and martensite are magnetic while austenite is non-magnetic. A mix of the different micro structures can result in a steel that a relative permeability somewhere in between a fully magnetic and a non-magnetic steel.

Table 2.4.: Chrome- and nickel-equivalents for AISI 316L and AISI M2

	AISI 316L	AISI M2
Cr_{eq}	20.6250	9.45
Ni_{eq}	13.9	24.2

Table 2.4 shows the chrome- and nickel-equivalents for the two types of steels described later in Subsection 2.5.1.

AISI 316L stainless steel is an austenitic stainless steel which is often used where there is a use for corrosion resistance. AISI 316L has a high presence of austenite-promoting elements that give the alloy austenitic micro-structure at all times, no matter the temperature or heat treatment.

Tables 2.5 and 2.6 lists the chemical composition and some relevant mechanical and electromagnetic properties of AISI 316L.

Table 2.5.: Chemical composition of AISI 316L stainless steel[50]

Chemical composition of AISI 316L								
C	Mn	Ph	S	Si	Cr	Ni	Mo	N
<0.03%	<2.0%	<0.045%	<0.03%	<0.75%	16.0-18.0%	10.0-14.0%	2.0-3.0%	<0.10%

Table 2.6.: Properties of AISI 316L stainless steel

Properties of AISI 316L			
Hardness Brinell	Relative permeability	Electrical conductivity	Dielectric constant
217 BHN[50]	1.003 – 7[51]	$1.45 \cdot 10^6 S/m$ [52]	∞ [49]

AISI 316L stainless steel with a fully austenitic structure will have a relative permeability of 1 which means that it has the same permeability as free space. Austenitic steel can however form inter-metallic phases when susceptible for temperatures or work hardening, and this could change the permeability some, but not to the extent that it would be magnetic. The anticipated micro-structure of 316L SS is shown in the Shaeffler diagram in Figure 2.8.

As this is a non-magnetic material, this should not be detected by magnetic sensors. It does however have an electrical conductivity which is different from the lubricant, so a sensor measuring the conductivity in the fluid should be able to detect AISI 316L particles.

AISI M2 high-speed steel, is a very hard and brittle steel within tool steels. It is usually used for tools, where high hardness is needed to cut through the softer alloys, for example thread taps.

Tables 2.7 and 2.8 lists the chemical composition and some relevant mechanical and electromagnetic properties of AISI M2.

Table 2.7.: Chemical composition of AISI M2 high-speed steel[53]

Chemical composition of AISI M2								
C	Mn	Ph	S	Si	Cr	Va	W	Mo
0.78-0.88%	0.15-0.40%	<0.03%	<0.03%	0.20-0.45%	3.75-4.50%	1.75-2.20%	5.50-6.75%	4.50-5.50%

Table 2.8.: Properties of AISI M2 high-speed steel

Properties of AISI M2			
Hardness Brinell	Relative permeability	Electrical conductivity	Dielectric constant
248-262 BHN[53]	$10^3 - 10^6$ [54]	$1.85 \cdot 10^6 S/m$ [55]	∞ [49]

The anticipated micro-structure of AISI M2 is shown in the Shaeffler diagram in Figure 2.8. This is a ferromagnetic material and should have no problem being detected by a magnetic sensor. This material also have an electrical conductivity different from the lubricant and should be detected by sensors measuring the conductivity of a fluid.

2.5.2. Non-metallic Debris

To test the limitations for each sensor, there will be added non-metallic debris as it is supposed to be impossible to detect using common oil contamination sensors.

Iron silicate or Fayalite is an iron-rich silicate mineral usually found in rocks and are often used for abrasive blasting.

Tables 2.9 and 2.10 lists the chemical composition and some relevant mechanical and electromagnetic properties of iron silicate.

Table 2.9.: Chemical composition of iron silicate blasting powder[56, Part.no.18-996]

Chemical composition of iron silicate powder					
FeO	SiO2	Al2O3	CaO	MgO	Quartz
42-48%	35-39%	3-6%	2-4%	1-3%	<0.1%

Table 2.10.: Properties of iron silicate

Properties of iron silicate			
Hardness	Relative permeability	Electrical conductivity	Dielectric constant
6 – 7 Mohs[56]	~ 1[57, p.191]	$5 \cdot 10^{-6} S/m$ [58]	~ 8.8[59]

A hardness of 6 Mohs equals a Brinell hardness of 742 BHN. A hardness value this high leads to a high risk of abrasive damage. Iron silicate does not belong in a gearbox, but is used as a non-metallic debris which could be hard to detect depending on which sensors are to be used.

Iron silicate is classified as a paramagnetic material, which means that it has a relative magnetic permeability slightly greater than 1. As the magnetic permeability is very low, it will probably not be detected by magnetic sensors. The electrical conductivity is also very low, which makes it hard for conductance measuring sensors to distinguish iron silicate from water or oil.

The lubricant can also contain non-metallic debris such as particles from gaskets, sealants and other grime. These substances are not magnetic and will not be detected by magnetic sensors. It might also not be detectable by conductive sensors. They should however be detectable by particle counters, such as the Parker MWDS, described in Section 2.6.

Particles from gaskets and sealants are usually not as dangerous as the other particles, as the hardness ratio is very high, see Figure 2.7. They can however contaminate and change the characteristics of the lubricant or clog up filters.

2.5.3. Water

Water can be a huge problem within gearboxes, especially when it is not dissolved in the lubrication, also known as vapourized water. It is therefore important to have control over the saturation limit of water for the type of oil used within the gearbox. Listed in Table 2.11 are the saturation limits for several types of oil in ppm. All though there are centrifuging systems for removing water from a lubricant, often these systems are portable and will only filter out the water if it is detected.

Table 2.11.: Water saturation limits for the different types of oil

Oil type	Saturation limit at 20°C
Synthetic gearoil	~ 200 ppm[60]
Polyalphaolefin	400 – 2000 ppm[61]
Polyalkylene glycol	10000 – 20000 ppm[61]

Table 2.12.: Life extension of the lubricant based on how much the water contamination level in ppm is reduced[62]

Current moisture level	Life extension factor									
	ppm	2	3	4	5	6	7	8	9	10
50 000	12 500	6 500	4 500	3 125	2 500	2 000	1 500	1 000	782	782
25 000	6 250	3 250	2 250	1 563	1 250	1 000	750	500	391	391
10 000	1 500	1 300	900	625	500	400	300	200	156	156
5 000	1 250	650	450	313	250	200	150	100	78	78
2 500	625	325	225	156	125	100	75	50	39	39
1 000	250	130	90	63	50	40	30	20	16	16
500	125	65	45	31	25	20	15	10	8	8
250	63	33	23	16	13	10	8	5	4	4
100	25	13	9	6	5	4	3	2	2	2

The biggest risks of having water in the gearbox is that it will ruin the lubrication film strength, accelerate the aging of the lubricant, lead to corrosive wear and cause hydrogen embrittlement[63]. Table 2.12 shows how the lifetime of the lubricant can be increased by reducing the water contamination. For example, the life time of a lubricant can be tripled by reducing the water contamination from 100 ppm to 13 ppm. Hydrogen embrittlement is caused by hydrogen atoms penetrating the steel surface and locking themselves interstitially between the atoms of the steel, making the steel brittle and prone to breaking.

Table 2.13.: Properties of Water

Properties of water		
Relative permeability	Electrical conductivity	Dielectric constant
0.999902[51]	0.0005 – 0.05 S/m[64]	87.9(0°C) – 55.5(100°C)[49]

As saturated water is harmful, the usual way to measure water content is to measure the water concentration as a percent of saturation level[65]. Even though saturated water is the most dangerous form of water contamination, dissolved water should also be kept to a minimum. The saturation level is however dependent on temperature and oil type, and it is therefore important to know this when measuring the water contamination level within the oil as the water dissolution in the lubricant increases as the temperature of the lubricant increases, as seen in Figure 2.9[65]. Water in oil content is usually measured using humidity sensors which may be integrated into other oil condition monitoring sensors.

The water contamination limit will be set to 100 ppm to reduce the risk of having water related gearbox failures. A 100 ppm contamination limit equals to about 50% water saturation within the lubricant for a standard synthetic gear oil[60].

Water has a dielectric constant distinct from lubricants, and could therefore be used to estimate the amount of water within the lubricant.

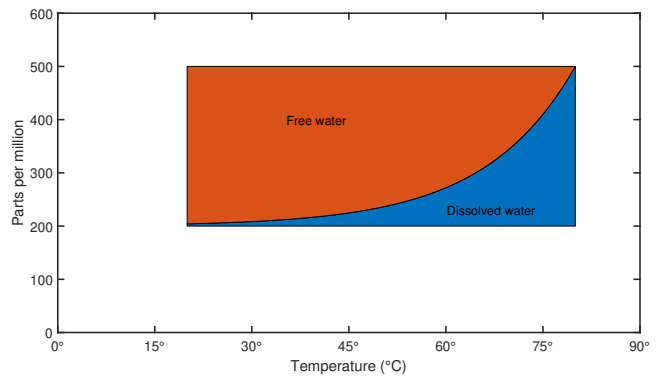


Figure 2.9.: Water dissolution in a common gear oil limit as a function of temperature[60]

2.6. Sensors

When selecting a sensor to monitor a lubricating system, it is important to know which substances the sensor needs to detect. If a sensor can not detect a certain particle, it is not possible to take preemptive measures to ensure that the failure modes connected to that substance will not happen. It might therefore pay off to have several sensors that detects different substances to make sure that all substances are covered.

Table 2.14.: Electromagnetic properties for the different substances, from Section 2.5

Materials	Electrical conductivity	Relative permeability	Dielectric constant
Mineral oil	$6 \cdot 10^{-12} S/m$	~ 1	2.1 – 2.4
AISI 316L	$1.45 \cdot 10^6 S/m$	1.003 – 7	∞
AISI M2	$1.85 \cdot 10^6 S/m$	$10^3 - 10^6$	∞
Iron Silicate	$5 \cdot 10^{-6} S/m$	~ 1	~ 8.8
Water	0.0005 – 0.05 S/m	0.999902	87.9(0°C) – 55.5(100°C)

The sensors can be mounted to the lubrication system in three different ways, in-line (**1**), on-line (**2**) or off-line (**3**). Each method will decide how the lubricant is sampled for the lubricant analysis. In-line monitoring will give the most accurate results as it have a representative lubricant sample than will not differ from the lubricant inside the gearbox. On-line condition monitoring will analyse a portion of the lubricant that is sampled from the main lubricant supply, but is directed in a separate line parallel to the main lubrication system, as shown in Figure 2.10. Off-line condition monitoring is done by taking a sample from the lubrication system, and then analysed. To be able to have an real-time oil analysis, the condition monitoring needs to be either in-line or on-line with the lubrication system. Off-line sensors is not recommended as it will not analyse a representative sample of the lubricant.

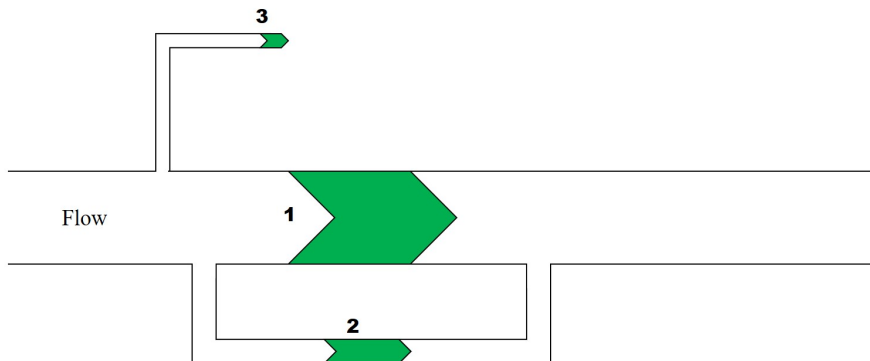


Figure 2.10.: The different options for sensor location. (1) In-line, (2) On-line and (3) Off-line

In this section, the theory of how each of the sensors operate will be explained based on the information that each manufacturer has published in the user manuals for the sensors.

2.6.1. Gill 4212

The Gill 4212 Oil Condition Monitoring Sensor is a sensor that will detect ferrous metal particles in a lubricant using a magnetic element which also collect the particles. The sensor is also equipped with dielectric element which can detect for example change in oil quality or the presence of saturated water over 10%.

The sensor should according to the manufacturer be able to distinguish between fine and coarse metal and report the volume of each of the different particles. The sensor should also be able to measure

the temperature within the oil and a significant change in dielectric value, which could be lack of oil or significant water contamination. Gill does not tell how accurate the sensor can be, but say that the scale can be calibrated by setting the size and quantity of the particles to distinguish between fine and coarse particles. Based on ranges given in the sensor user manual, seen in Tables 2.15 and 2.16, it seems that the difference between fine and coarse particles are between $850\ \mu m$ and $2\ mm$. In general, Gill does not give any specific information on how the sensor works or any limitations regarding the maximum fluid velocity past the sensor. They do however state that more than $0.5\ g$ of debris will overload the sensor. The probe will therefore need to be checked, and all debris removed from the probe when the sensor overloads.

The sensor can be ordered with several methods for reading the outputs and with several different types of threads depending on how the user wants to mount it. The different available outputs for reading the output signal is analog $0 - 10\ V\ DC$ and $4 - 20\ mA$ output and a digital CAN J1939 output. The manufacturer says that it can be mounted in the oil pan, but recommends that it stays in the path of the oil flow. It is therefore useful to be able to order the sensor with the right threads, so that it can replace the drain plug. As seen in Figure 2.11, the sensor needs to be screwed in a place somewhere in the lubrication system. Gill does not state a maximum pressure of which the sensor can operate, but it is assumed $\sim 1\ bar$ as it is supposed to be mounted in a tank or a low pressure system.

The sensor has 3 output signals. Two signals for the fine and coarse readings, which is based on how much debris is on the probe for the different sizes of particles, and one signal which can be used for either the lubricant temperature or reading the lubricant quality, based on a dielectric value (Table 2.17).

For this thesis, the sensor was ordered with $0 - 10\ V$ output with a $M22X1.5$ threads, part number in Table 3.1. The data will be acquired with a DAQ, also specified in Table 3.1. This sensor requires a voltage input of $6 - 36\ V\ DC$ and has a sampling rate of $10\ Hz$.



Figure 2.11.: Gill 4212 Oil Condition Monitoring Sensor[66]

Table 2.15.: Maximum range fine debris[66]

Fine Debris Particle Size	Material Type	Maximum Mass
$1 - 6\ \mu m$	Iron Powder	$0.41\ g$
$60\ \mu m$	Iron Powder	$0.44\ g$
$125 - 300\ \mu m$	Iron Powder	$0.43\ g$
$450\ \mu m$	Iron Fillings	$0.48\ g$
$420 - 850\ \mu m$	Iron Fillings	$0.35\ g$

Table 2.16.: Maximum range coarse debris[66]

Coarse Debris Particle Size	Material Type	Maximum No. Off
$2\ mm$	Chrome Steel Ball Bearing	>20
$3\ mm$	Chrome Steel Ball Bearing	20
$4\ mm$	Chrome Steel Ball Bearing	12
$5\ mm$	Chrome Steel Ball Bearing	10

As the majority of gears in marine reduction gearboxes are made of magnetic alloy steels, the Gill 4212 should be able to detect all particles which originates from the gears.

Table 2.17.: Guideline oil reference number[66]

Reference Media	Alarm State	Raw oil reference number
Air	Green	1 000 – 1 015
Water	Red	860
Oil	Green	990

Table 2.17 shows guidelines to how the oil quality reference number should be interpreted. Since the reference number of the oil is highly dependent of the type of lubricant, the value should be calibrated to the actual system that is used.

Based on the theory in Section 2.5, it is predicted that the Gill 4212 Oil Condition Monitoring Sensor is able to detect AISI M2 HSS particles as it has a high relative permeability, and saturated water above a certain level. It should also be able to detect major changes in the dielectric properties of the lubricant which can be an indicator for the lubricant quality or water content, explained in Section 2.5.

All data in Subsection 2.6.1 is gathered from the Gill 4212 oil condition monitoring sensor user guide[66].

2.6.2. Poseidon Trident QW3100

The Poseidon Trident QW3100 is a sensor that uses electrochemical impedance spectroscopy (EIS) to measure the lubricants health. EIS sends out a sinusoidal signal with a certain magnitude with an increasing frequency, and receives a response correlated to chemical and physical properties which alters the magnitude and phase of the input signal. Based on the frequency response of the lubricant, the inductive, capacitive and resistive properties of the lubricant can be determined and be used for identifying the contamination.

To find the contamination in the lubricant, Poseidon recommends keeping track of the interfacial impedance and see how it changes based on the contamination. As seen in Table 2.14, the electrical conductivity for metallic materials are much greater than for mineral oil. The interfacial impedance should therefore in theory decrease as the lubricant gets more and more contaminated by these particles. Poseidon recommends comparing percentage of the decreasing impedance values over time to relate it to the actual oil condition.

The sensor also integrates a water-in-oil sensor that senses the relative humidity in the lubricant by measuring the dielectric properties, as explained in Section 2.5.

To mount the sensor in the lubricating system, Poseidon recommends placing the sensor in a section of the lubricating system with sufficient flow of a representative lubricant, similar to the Gill 4212. It is mounted in a hole with a -8 SAE O-ring Boss fitting. However, unlike with the Gill 4212, Poseidon does not recommend to mount the Trident QW3100 in the oil sump as the sensor can misinterpret the contamination level because of contamination build-up. They also recommend having a filter in applications with large size debris above $< 500 \mu\text{m}$ as they can short the electrodes in the sensor.



Figure 2.12.: Poseidon Trident QW3100 Oil Condition and Water Contamination Monitor[67]

Poseidon states that the sensor can operate in a pressurized lubrication system up towards 10.3 *bar* but does not specify a upper and lower fluid velocity level.

It sends data with either Modbus RTU RS-485 or CAN J1939, and needs a 10 – 30 *V DC* power input. The signals transferred by the sensor is held by a holding register as the data is updated. The data stored in the holding register is the raw data that is used to interpret the condition of the lubrication fluid. The different signals are the following, listed in Table 2.18.

Table 2.18.: Poseidon Trident QW3100 holding registers as described in the user manual[67]

Register Address	Description
200	% Relative Humidity
201	Sweep Count
202	Interfacial: Temperature Pre Reference
204	Interfacial: Temperature Post Sample
206	Bulk: Temperature Post Sample
208	High Frequency: Temperature Post Sample
210	Interfacial Impedance
212	Bulk Resistance
214	High Frequency Bulk

Based on the theory in Section 2.5, it is predicted that the Poseidon Trident QW3100 is able to detect AISI 316L SS and AISI M2 HSS particles as they have electrical properties that are distinct from that of the lubricant as well as water because of the integrated water-in-oil sensor.

According to Poseidon, the interfacial impedance measurements are very temperature sensitive, and they therefore recommends discarding the measurement if the measured temperature before and after the impedance measurements is not within 1°C of each other. They also recommends setting a operating temperature and discard all the measurements if the temperature is more than $\pm 10^{\circ}\text{C}$ of that operating temperature. This implies that the gearbox on a particular ship should reach its operating temperature before any measurements should be compared against each other. Considering the large variations of speeds and loads in a marine reduction gearbox, this could be an disadvantage as the temperatures could vary quite a bit. The problem could however be countered by only doing measurements in a certain temperature window, even though the oil will not be monitored all the time.

All data in Subsection 2.6.2 is gathered from the Poseidon Trident QW3100 user manual[67].

2.6.3. Parker Kittiwake MWDS

The Parker Kittiwake Metal Wear Debris Sensor will detect both ferrous- and non-ferrous metals. The manufacturer states that the sensor operates using inductive coil technology to measure the electromagnetic properties of the wear debris, including the electrical conductivity and magnetic permeability of the particles.

The MWDS needs to be placed on-line in a closed loop lubrication system as the contaminated lubricant will flow through the sensor, as shown in Figure 2.13. Each hole for each end of the sensor are threaded by $\frac{1}{2}$ " BSP threads. These can be used for various connections, such as hose nipples or hardlines. The sensor is rated for a maximum pressure of 20 *bar*.

The sensor requires an fluid velocity of 0.28 – 1.9 m/s which corresponds to 1.3 – 9 $\frac{\text{l}}{\text{min}}$ to register all particles, so the pump have to be selected according to these values. As all the particles are counted when passing through the sensor, as with an OPC, it is reasonable to think that velocity limit is specified, such that transient or turbulent flow does not occur as this can lead to particles being counted more than once[68].

The sensor can communicate either via Modbus RTU (RS-485 or TCP/IP) or CANopen protocol. To operate it needs a $18 - 32V DC$ power input. The sensor will report the particle count, particles per minute and mass per hours in bins based on particle size and if the particle is ferrous or non-ferrous. The different bins that the sensor reports in are listed in Table 2.19. All in all, the sensor has 60 output signals. The particles per minute signal has a refresh rate of 10 seconds and the mass per hour signal has a refresh rate of 5 minutes.



Figure 2.13.: Parker Kittiwake Metal Wear Debris Sensor[20]

The software that comes with the sensor has inbuilt particle limits that gives out a warning or alarm if particles per minute or mass of particles per hour exceeds a certain limit. Per default, these limits are set to 5 for warning and 10 for the alarm. These will have to be adjusted according to the fluid cleanliness level, discussed in Section 2.5, and fluid volume in the lubrication system.

Parker recommends that the sensor is mounted before any filtration and that it is fed with a lubrication supply which is representative of the main lubrication flow.

Table 2.19.: The different bins for classification of different particles[20]

Bin	Ferrous ranges	Non-ferrous ranges
	Minimum value (μm)	Minimum value (μm)
A	40	135
B	70	200
C	100	300
D	150	400
E	200	500
F	300	600
G	400	700
H	600	800
I	800	900
J	>1000	>1000

Based on the theory in Section 2.5, it is predicted that the MWDS is able to detect AISI 316L SS and AISI M2 HSS particles as they have electromagnetic properties that are distinct from that of the lubricant. Even though it is divided by ferrous and non-ferrous, it is anticipated that martensitic particle falls under the ferrous category.

All data in Subsection 2.6.3 is gathered from the Parker Kittiwake MWDS instruction manual[20].

2.7. Hypothesis

Based on the theory discussed in Chapter 2, the following hypothesis is made. The hypothesis will be a prediction of what is going to happen with the different tests, described in Section 3.3. Table 2.20 shows what is expected when it comes to which sensors are able to detect which substances. These contaminants are a good choice as they covers most combinations of electromagnetic properties. Being both magnetic and non-magnetic, and conductive and non-conductive.

It is believed that the Gill 4212 are able to detect AISI M2, because of its magnetic properties as well as vaporized water. It is also believed that it can detect significant oil quality degradation that has a

big influence on the dielectric constant of the lubricant. The sensor should be able to measure particle debris up to a total mass of 0.44 g of the supplied particle debris, described in Table 3.6.

Table 2.20.: Substance detectability prediction for the different sensors. Cells marked with (x) indicates detectability

	Gill	Poseidon	Parker
AISI 316L		x	x
AISI M2	x	x	x
Iron silicate			
Water (vaporized)		x	
Water (saturated)	x	x	

The Poseidon Trident QW3100 should however in theory be able to detect all substances listed in Table 2.20, excluding the iron silicate because of the dielectric constant being pretty similar to that of the lubricant itself. The sensor does not have any limitations to how much contamination it can measure, but it does has its limitations when it comes to accuracy of the of the readings. The way it measures contamination makes it for example impossible to use on an application were it is required to have the ISO cleanliness level as an output. The interfacial impedance and bulk resistance should based on the total conductivity decrease as the contaminants are added, except for the iron silicate.

The Parker MWDS is believed to only have the ability to measure materials with electromagnetic properties different from the lubricant, such as conductivity or magnetic permeability. It should therefore only be able to detect the AISI 316L from 135 μm and above and the AISI M2 particles from 40 μm and above

3. Methods

This chapter contains an overview and explanation of all the parts used to conduct the objectives explained in Section 1.5 including the plumbing and wiring of the testing rig. The chapter will also include a description of the experiments that will be done, based on the theory reviewed in Chapter 2.

3.1. Setup

To conduct the oil condition monitoring, the three sensors had to be installed on a closed loop lubrication system on the gearbox that need to be tested. The gearbox is a part of an already existing rig situated at the university, seen in Figure 3.2, and assembled by personnel working there. The three different sensors were already bought by the university, but the other parts needed to conduct the research had to be ordered. A list of all the items, excluding the already existing gearbox rig can be seen in Table 3.1. All the necessary components needed to conduct the experiment is shown in Figure 3.1 and is described further in this chapter. A complete plumbing diagram can also be seen in Appendix B.

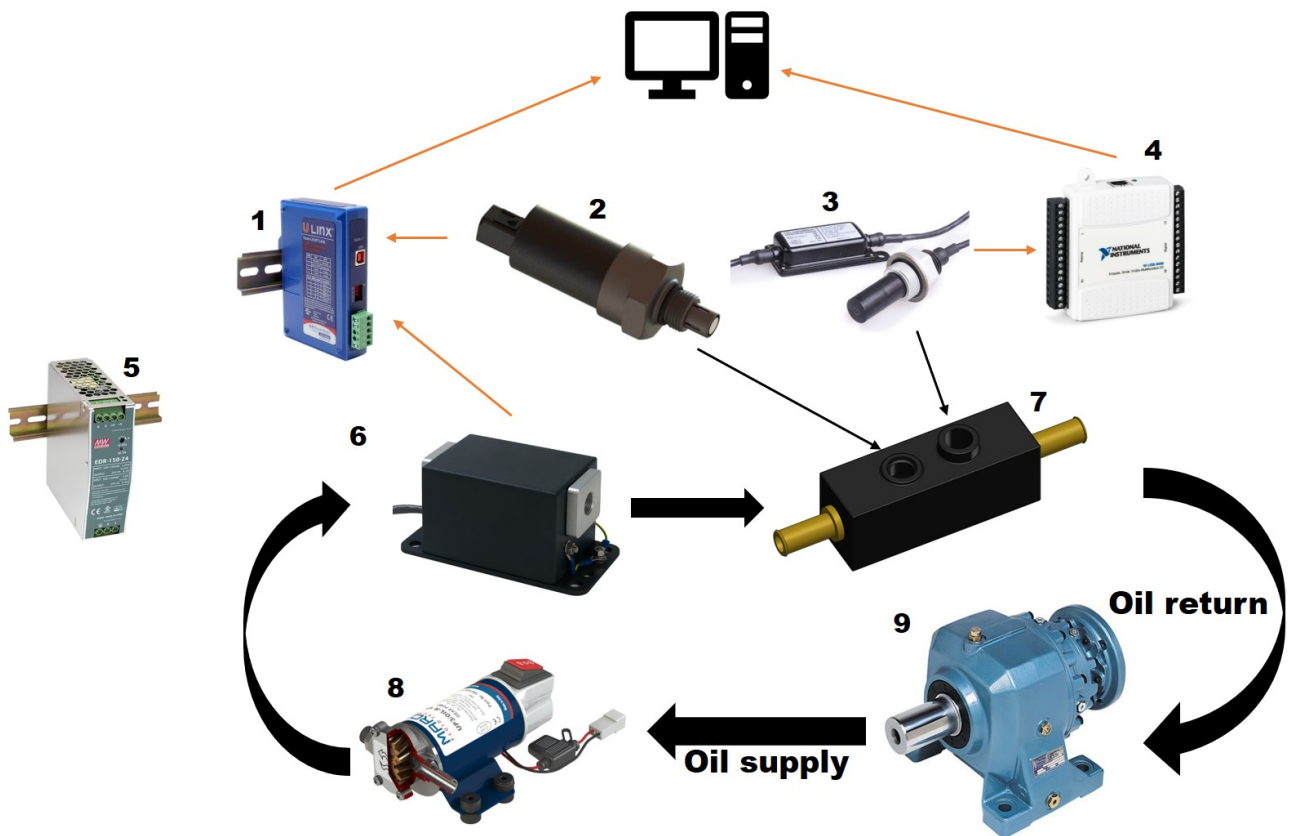


Figure 3.1.: Overview of the setup. (1)USB to RS-485 Adapter, (2)Poseidon Trident QW3100, (3)Gill 4212, (4)NI USB DAQ, (5)Power Supply, (6)Parker MWDS, (7)Sensor block, (8)Oil pump, (9)Gearbox

Table 3.1.: Bill of materials

Bill of materials		
Manufacturer	Part no.	Product description
Gill	4212-00-038	4212 Oil condition sensor
Poseidon	PS-0113-0200	Trident QW3100 Oil condition and water contamination monitor
Parker	AS-K19551-KW	Metallic Wear Debris Sensor
Advantech	BB-USOPTL4DR	USB to RS-422/485 Converter
Marco	164 022 12	UP3/OIL-R 12V Low Speed Reversible Pump 5.5l/min
Mean Well	EDR-150-24	DIN Rail Power Supply 24V 6.5A
Mean Well	EDR-150-12	DIN Rail Power Supply 12V 10A
National Instruments	USB-6008	Multifunction I/O Device
Bosch Rexroth	R928019459	Oil filter

3.1.1. Test Rig

The tests were performed on a rig used for testing condition monitoring algorithms on electric motors and gearboxes. The rig consists of two industrial gearboxes in between two 3-phase squirrel cage motors. Seen in Figure 3.2, one ABB induction motor (1) is connected to a Brevini two-stage planetary gearbox (2), which is connected to a Brevini two-stage bevel planetary gearbox (3) via a one-to-one geared connection. An ABB brake motor (4) is placed on the output shaft of the bevel planetary gearbox (3) to add resistance in the gear-sets.

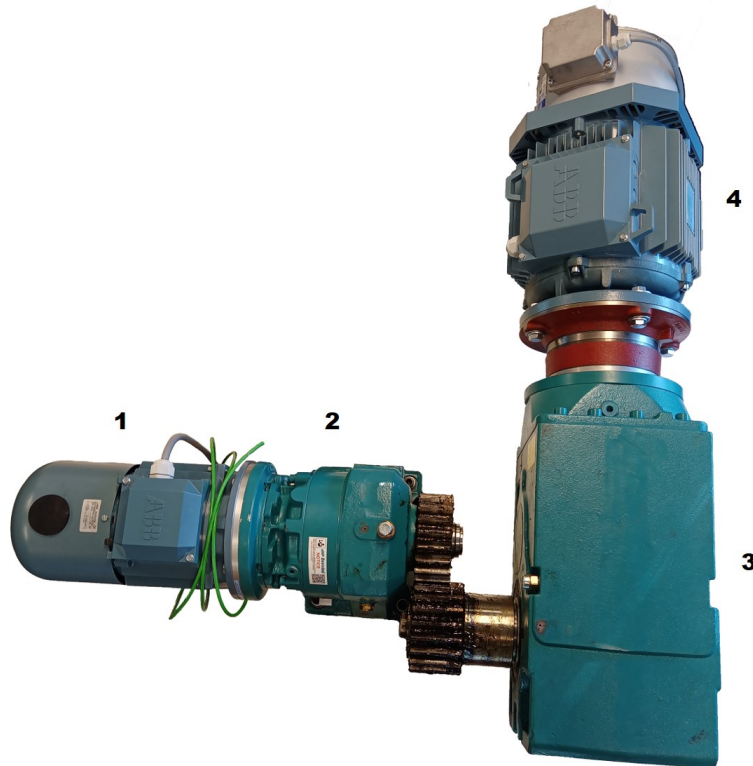


Figure 3.2.: Gearbox test rig setup. (1)ABB M3ARF 090S 4 , (2)Brevini PD2010, (3)Brevini BPH213, (4)ABB M3AA 132M 8

3.1.2. Gearbox

The gearbox used for the oil condition monitoring testing is a two-stage Brevini PD2010 industrial planetary gearbox(2), shown in Figure 3.2. Without a circulation system, the gearbox has a lubrication capacity of 1.3 liters[69, p.256]. The gear-set were changed to a new gear-set prior to the experiments.

Even though the gearbox could be run without a lubrication system, Brevini recommends having a system to circulate the oil. This system will filter out any particles contaminating the lubricant as well as stabilizing the lubricant temperature. Having a lubrication system on the gearbox will greatly increase the lifetime of the gearbox.



Figure 3.3.: Magnetic and non-magnetic drain plug

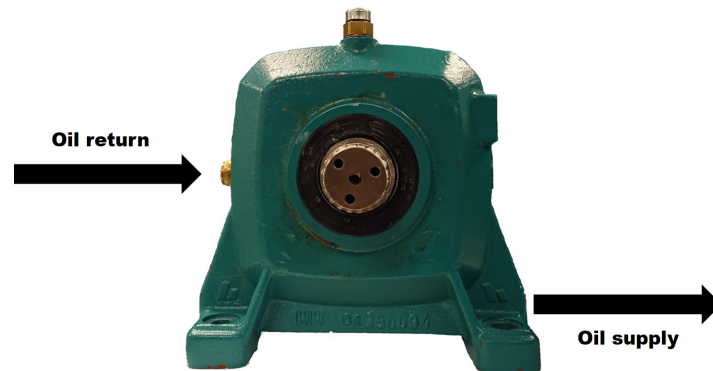


Figure 3.4.: Brevini PD2010

Brevini recommends a lubricant with ISO VG 150 classification for output speed over 20 rpm and temperatures below 50°C [69, p.242]. This is what is used in the lubrication system. An ISO VG 150 lubricant has a kinematic viscosity of $\nu = 150\text{ cSt}$ [70].

The gearbox has 5 holes distributed around itself. Two holes on the bottom of the gearbox are used for drain plugs. Two holes on level with the input and output shaft are used as lubricant level indicators. The last hole is located on the top of the gearbox and is used for filling the lubricant and is fitted with a breather plug. All holes are threaded with $\frac{3}{8}$ " BSPP threads.

Seen in Figure 3.4, one of the holes on the bottom of the gearbox will be used as the supply line for the pump. This is beneficial as the gravity will push the lubricant to the pump, such that the pump do not have to suck the lubricant from the gearbox, and thereby reducing its lifetime. The oil return will go through one of the holes located on the mid-plane of the gearbox, this is so the breather plug can have its intended location. The oil level sight glass will be placed on the opposite side of the oil return hose nipple.



Figure 3.5.: Bosch Rexroth oil filter

The Brevini gearboxes comes standard with a magnetic drain plug to attract all magnetic particles in the oil. However, for the purpose of this thesis, the magnetic drain plug will be replaced with a non-magnetic drain plug, seen in Figure 3.3, to make sure that all the artificially added particles will go through the lubrication system and pass the different sensors.

3.1.3. Lubrication System

To test the sensors, a closed loop lubrication system is mounted to the two-stage industrial planetary gearbox (2), which sits between the brake motor (1) and the bevel planetary helical gearbox (3), seen in Figure 3.2.



Figure 3.6.: Hose nipple used for plumbing[56]

On the oil supply and oil return hole, shown in Figure 3.4, there are mounted two $\frac{3}{8} \times \frac{1}{2}$ " BSPP hose nipples. These allow a 12 mm hose to be connected to the gearbox (Figure 3.6). From the oil supply output from the gearbox, the hose is connected to a UP3/OIL-R [71] gear pump (Figure 3.7 and (8), shown in Figure 3.1). From the pump, the hose is connecting all the sensors together before it returns to the gearbox again which closes the loop of the lubrication system. To make sure that all the sensors have a reading that is representative of the lubrication inside the gearbox, a filter will not be added onto the lubrication system as it will remove most of the particle contamination.

The Marco pump was chosen because of the flow rate of $5.5 \frac{L}{min}$, which is within the flow limit of the Parker MWDS, described in Subsection 2.6.3. The pump also has suitable fittings that has the same size as the Parker MWDS fittings. The pump will be supplied with a 12 V DC power supply rated at 10 A. The manufacturer states that the pump has a consumption of 5 A, so a 10 A power supply should be more than enough to drive the pump[71]. The pump has a 7.5 A fuse in case of shorts or possible overloads as a result of too high pressures in the lubrication system.

According to Marco, the pump should not be operated above a system pressure of 2 bar, which makes the pump the weakest part in the lubrication system[71]. It will therefore be beneficial to have the lubrication system without any tight orifices. Marco also suggests a lubricant viscosity under 350 cSt, which complies with what Brevini recommends for their planetary gearbox[72].

To reduce the oil usage, the experiments with particle debris will be followed by a lubricant filtering to filter out all the particle from the experiment, seen in Figure 3.5. To do that, an oil filter is installed between the pump and the Parker MWDS. To eliminate the need of having to install and remove the filter between each experiment, two 3-way ball valves will be installed on each side of the filter. This makes it possible to completely bypass the valve during the experiments. The installment of the filter was done after experiment no. 1 was conducted, seen in Section 4.4.

The hose used in the system is a transparent 12 mm hose. The transparency allows for watching the lubricant as it flows through the system. An inner diameter of 12 mm was chosen as it fits with $\frac{1}{2}$ " size fittings which is the fittings used on both on the Parker MWDS and the Marco gear pump.

To make sure that the readings from the sensors are correct, the Reynolds number will be calculated for the flow to make sure the flow is laminar. If the flow is not laminar, the lubricant will swirl inside the lubrication system which can make the sensor readings flutter or make the particles being counted more than once, as discussed in Subsection 2.6.3. The Reynolds number in the Parker MWDS will give a good indication of the flow pattern elsewhere in the system as the restriction is biggest through the Parker MWDS. To calculate the Reynolds number, the fluid velocity are needed.



Figure 3.7.: Marco UP3/OIL-R gear pump[71]

$$v_{parker} = \frac{Q_{pump}}{A_{parker}} = \frac{5.5 \frac{L}{min}}{\pi \cdot \left(\frac{10 mm}{2}\right)^2} = 1.16 \frac{m}{s} \quad (3.1)$$

where

v_{parker} = Fluid velocity through the Parker MWDS
 A_{parker} = Parker MWDS crosssectional area

From Equation (3.1), the fluid within the Parker MWDS will have a velocity of $1.16 \frac{m}{s}$. This results in laminar flow, since the Reynolds number (Equation (3.2)) is lower than 2300.

$$Re = \frac{v_{parker} \cdot d_{parker}}{\nu} = \frac{1.16 \frac{m}{s} \cdot 10 mm}{150 cSt} = 77.8 \quad (3.2)$$

where

Re = Reynold number of the fluid within Parker MWDS
 v_{parker} = Fluid velocity through the Parker MWDS
 d_{parker} = Parker MWDS hole diameter

The volume of the gearbox including the lubrication system was measured to be 1.5 liters. This will be used later during the tests to determine the concentration of the contamination within the lubricant.

3.1.4. Sensor Location

Based on theory in Chapter 2, it is decided that all the sensors will be installed on-line in the lubrication system. The Gill 4212 could have been mounted in the gearbox case itself, but as it is threaded by $M22X1.5$ threads, it is easier to mount it in the lubrication loop. This removes the need of having to drill and tap the gearbox case to be able to install the Gill 4212.

As the Parker MWDS is made for being installed on-line in a lubrication system, the sensor is designed around a pipe section. Each end of the sensor is threaded by $\frac{1}{2}$ " BSPP threads which makes it easy to install on the lubrication loop. To fit the $12 mm$ hose, $\frac{1}{2}$ "x $\frac{1}{2}$ " hose nipples are installed at each end of the Parker MWDS.

The Gill 4212 and Poseidon Trident QW3100 however are installed by threaded connection, so some kind of a block for mounting the sensors within the lubrication loop is therefore needed. The approach for designing the mounting block is described in Subsection 3.1.5.

3.1.5. Design of Sensor Block

The easiest way to install the sensors with a threaded installation was to make a block that is added to the lubrication loop. Before designing the sensor block, a few requirements had to be established to make sure that everything would work the first time, and thereby eliminating the need of altering the design of the block. The requirements are:

1. Having space for mounting both the Gill 4212 and Poseidon Trident QW3100
2. Not being magnetic to not disturb the readings from the Gill 4212 sensor
3. Can endure some abuse without being destroyed
4. The material has to be threaded
5. Be cheap, easy and quick to produce

6. Be tight to prevent the lubricant leaking through
7. Be mineral oil resistant
8. Be able to be connected to the lubrication system with a 12 mm hose
9. The inside has to have smooth transitions to induce laminar flow of the lubricant

To fulfill the first requirement was easy as there were no limitations of how big the block could be. The block ended up being 55mm x 55mm x 150mm big which would fit both sensors by a good margin.

To fulfill requirement 2-7 several material were considered as useful. At first, steel, aluminium and 3D-printed plastic were considered, but steel was quickly abandoned for being both magnetic and hard to produce. That left aluminium and plastic, both suitable as they are non-magnetic materials, they can endure some abuse and both materials can be threaded. By 3D-printing the sensor block, the block could be made a lot quicker and cheaper. However, the choice of 3D print filament is important as some may be more resistant to lubricant leak.

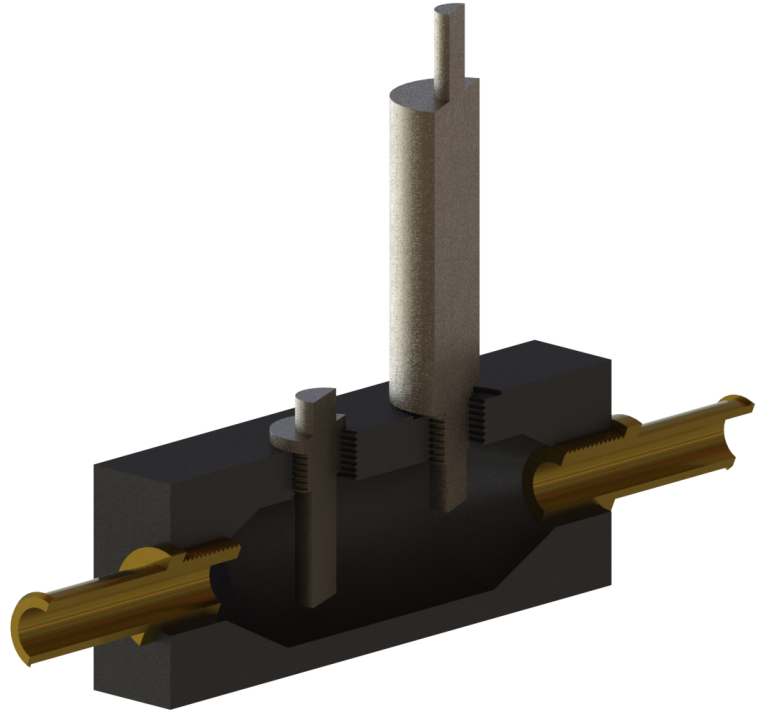


Figure 3.8.: Section view of the assembled sensor block

To fulfill requirement number 8, the easiest way was to make threaded holes, and then install hose nipples, instead of machining or 3D-printing hose nipples. Threaded connections are much stronger, and can be replaced if destroyed, unlike if the hose nipples was 3D-printed into the sensor block.

The last requirement made plastic the preferred material, as a 3D-printing allows for a hollow section within the sensor block. Machining the sensor block out of aluminium with regular tools would never had been able to get the smooth transitions inside the block, as seen in Figure 3.8.

It was still unknown which 3D-printing filament was suitable for the application. The university, had some ASA filament in stock which could be used, as it is stated to be "suited for outdoors use". The sensor block ended up being printed with the ASA filament.

The 3D-printer used to print the sensor block, uses one filament for the print itself in addition to one filament dedicated to the support material. The filament for the support material is volatile against a certain detergent which lets the support material being washed away. This allows for the smooth surface and hollow section within the sensor block. When the 3D-printing of the sensor block was finished, the part was submerged into the detergent to remove the support material. Figure 3.9 shows a rendered image of how the sensor block looks like without support material.



Figure 3.9.: Sensor block

When the support material was removed, the sensor block was ready to be threaded according to the fittings and sensors that were to be mounted. The two holes on each side of the sensor block was threaded with a $\frac{1}{2}$ " BSPP thread tap to allow for the mounting of the two $\frac{1}{2}$ "x $\frac{1}{2}$ " hose nipples. The hole for the Gill 4212 sensor was threaded by a $M22X1.5$ tap and the Poseidon Trident QW3100 was threaded with a -8 SAE O-ring Boss fitting.

The -8 SAE O-ring Boss fitting is not a type of thread, but a hydraulic fitting specified as a threaded connection in addition to grooves to make a solid and tight connection[73]. The connection was as a result of this modeled as a hole with a chamfer, and then threaded with a $\frac{3}{4}$ – 16 UNF tap when the 3D-print was done, according to the SAE standard for that type of hydraulic fitting[73].

The drawing of the sensor block can be seen in Appendix C.

For the tests where the removal of the Gill 4212 is needed, there is a need for a plug to prevent the oil from escaping the lubrication system. The solution was to 3D-print a plug with the same threads as the Gill 4212, $M22X1.5$ threads, that could be screwed in place of the Gill 4212. A rendered illustration of the plug can be seen in Figure 3.10. A drawing of the plug can be seen in Appendix D.

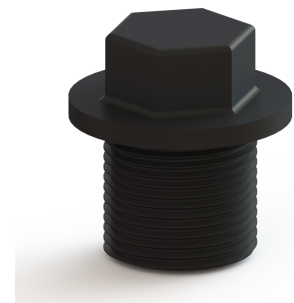


Figure 3.10.: M22x1.5 plug to replace the Gill 4212

3.2. Sensor Wiring and Setting up the Software

To acquire data from all the sensors, they had to be wired up according to the user manuals from each manufacturer. The Gill 4212 was wired up to a DAQ that can receive 0 – 10 V inputs and the Poseidon Trident QW3100 and Parker MWDS was wired up to a RS-485 to USB adapter. A complete wiring diagram can be seen in Appendix A.

Each sensor has its own software to calibrate and collect the data, supplied by the manufacturers. In the case of Gill 4212 which sends data through the National Instruments DAQ, it is the simplest to make a MATLAB-script that interpret the data as MATLAB has comprehensive tools to make the data processing easy and adaptive.

3.2.1. Gill 4212

As shown in Table 3.2, the sensor has three output signals, fine particles, coarse particles and oil condition or oil temperature. The three output signals will be connected to the analog input ports AI 0, AI 4 and AI 1 on the DAQ respectively. The power and power ground will be connected to the positive and negative terminal on the 24V DC power supply. The clear wire is used to reduce the noise in the system and will be connected to a common ground. Figure 3.11 shows an illustration of the DAQ used to process the 0 – 10 V signals from the sensor.

To process the inputs from the DAQ, MATLAB will be used with a Data Acquisition tool (Figure 3.12) to log the data from all each of the DAQ input channels listed in Table 3.2[75]. The logged data will then be analysed and shown graphically in MATLAB.



Figure 3.11.: National Instruments USB-6008 DAQ[74]

Table 3.2.: Wire color codes for the Gill 4212[66]

Wire Color	Designation	Connection terminal
White	Fine	AI 0 on DAQ
Green	Coarse	AI 4 on DAQ
Orange	Oil/Temp	AI 1 on DAQ
Black	Power Gnd (V-)	GND on power supply
Red	Power (V+)	+24V on power supply
Blue	(Not Connected)	-
Clear	Screen	GND on power supply

After the data is logged in the data acquisition app, the data is saved to a MATLAB Data file (.mat). The MATLAB Data file will then be imported in a MATLAB script. The MATLAB will convert all the voltage data to usable values according the Gill 4212 user manual and then plotted to have a graphical representation[66]. The MATLAB script to convert and plot the sensor data can be seen in Appendix E.1.

Shown in Table 2.15, 0.43 – 0.44 g is supposed to give a sensor reading on the fine signal of 10 V or 100% with the AISI M2 metal powder used in these experiments. To confirm this, 0.43 g of powder will be collected in a sample glass. The probe will then be put up to the sample glass, and the sensor signals will be checked to confirm that the results match the given information from the Gill 4212 user manual. If the signal is off, Equation (3.3) will be altered such that the signal matches the collected debris.

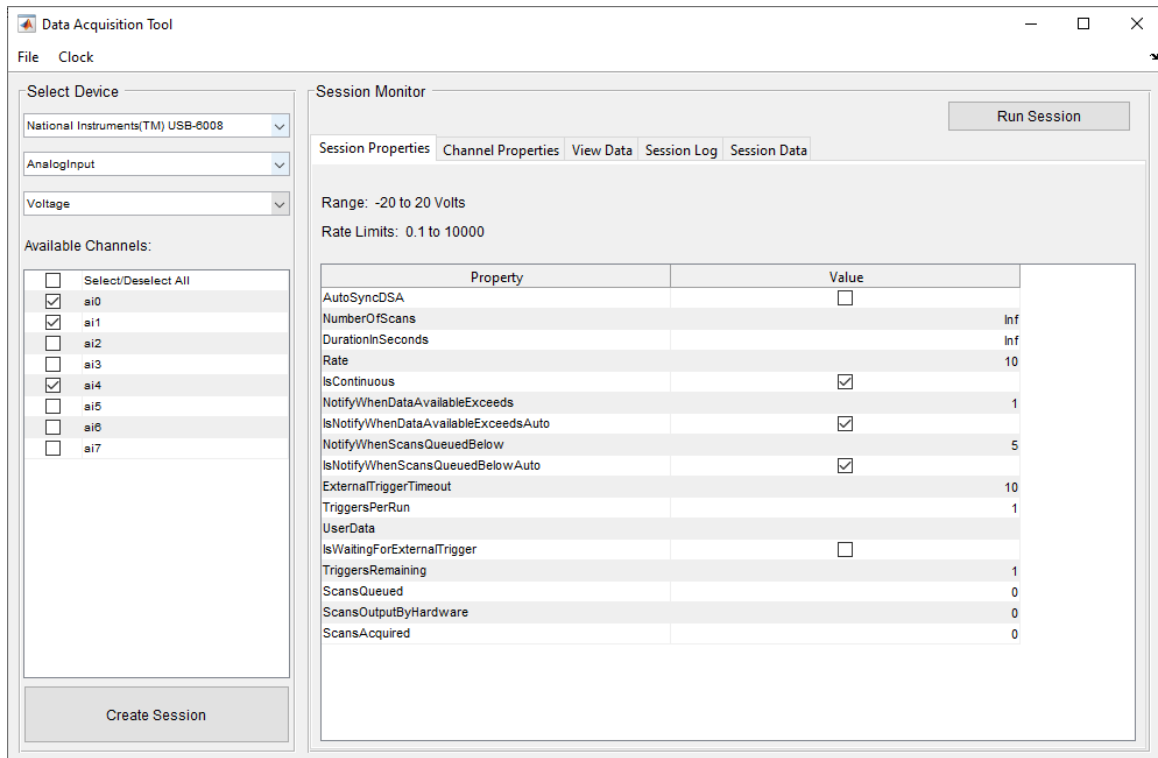


Figure 3.12.: Overview of the Data Acquisition Tool to log the data from the Gill 4212 sensor [75]

As the DAQ receives voltage signals from the sensor, the signals has to be mapped to a signal that is easy to interpret. For the fine and coarse debris signals, the values should be mapped to a value between 0 and 100%, where a signal of 100% means that the probe is full of debris. The sensor is first calibrated in the calibration software supplied by Gill according to the user manual (Figure 3.13). To map the voltage signals from the Gill 4212, the following equation (Equation (3.3)) is used. The sensor calibration is described in Section 4.2 and the Equation (3.3) is adapted accordingly.

$$d(t) = V(t) \cdot \frac{G}{10V} + O \quad (3.3)$$

where

$d(t)$ = Debris signal

$V(t)$ = Input voltage signal

G = Gain

O = Offset

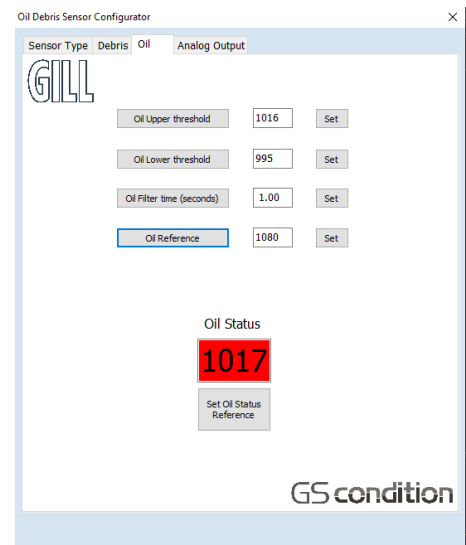


Figure 3.13.: Gill Sensor Configuration Tool

The oil quality signal is according to Gill a non-linear dielectric signal that should be calibrated. To set the oil reference value, the probe should be submerged into fresh oil. The acquired signal should be set to 1000. The lower and upper alarm threshold should be set by respectively having the probe in oil with 10% water and no oil (air). The oil quality is calibrated with the calibration software from Gill. Once calibrated, the oil condition output signal will either send out a 0 V output or a full scale output based on if the threshold is exceeded or not.

3.2.2. Poseidon Trident QW3100

The Poseidon Trident QW3100 communicates with the computer via the RS-485 protocol. For it to work, the sensor has to be wired correctly to the RS-485 adapter according to the QW3100 user manual and the RS-485 adapter user manual.

The sensor has several different signals, all transferred through the RS-485 wire pair. The RS-485 positive and negative terminals will therefore be connected to the A and B terminals on the RS-485 adapter respectively. The wire marked as RS-485 0V ref is connected to the ground terminal on the power supply which is connected to a common ground. To power the sensor, the positive and negative terminals is connected to the positive and negative terminals on the 24 V power supply. Table 3.4 shows all the colored wires and their respective signals.

Table 3.3.: The RS-485 configurations for the Poseidon Trident QW3100

Configuration	
Baud rate	115 200
Data bits	8
Parity	No
Stop bits	1
Slave address	1



Figure 3.14.: Advantech B+B SmartWorx Isolated USB to RS-422/485 Converter[76]

To use the RS-485 adapter, it had to be setup correctly in order to be used for 2-wire RS-485 protocol. Switch 1, 2, 3 and 4 all had to be switched ON in order for the adapter to read the sensor data correctly.

To ping the holding registers seen in Table 2.18, the modbus connection had to pinged with the configuration seen in Table 3.3. The signals will be logged using the MATLAB script in Appendix E.4 and plotted using the MATLAB script in Appendix E.2.

Table 3.4.: Wire color codes for the Poseidon Trident QW3100[67]. *Colors in parenthesis are striped on the wires




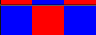
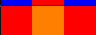









Wire Color	Designation	Connection terminal
Orange	Power (V+)	+24V on power supply
Orange(White)	Power Gnd (V-)	GND on power supply
Green	RS-485 -	B terminal on RS-485 adapter
Green(White)	RS-485 +	A terminal on RS-485 adapter
Blue	RS-485 0V ref	GND on power supply
Blue(White)	CAN GND	-
Brown	CAN HI	-
Brown(White)	CAN LOW	-

3.2.3. Parker Kittiwake MWDS

As with the Poseidon Trident QW3100, the Parker Kittiwake MWDS can use the RS-485 protocol to communicate with the computer. The Parker however requires other settings than the Poseidon. Also, the Parker MWDS is configured from factory using the TCP/IP configuration. To use the TCP/IP connection, an Ethernet cable was spliced with the Parker MWDS in a T-568B configuration. The RJ45 on the Ethernet cable were then connected to an extra network adapter in the laboratory computer.

The power supply were connected to the sensor as listed in Table 3.5.

Table 3.5.: Wire color codes for the Parker MWDS[20]. *Colors in parenthesis are striped on the wires

Wire Color	Designation	Connection terminal
	White(Blue)	Power (V+)
	Blue(White)	Power Gnd (V-) & RS-485/CAN 0V ref
	Red(Blue)	(Not Connected)
	Blue(Red)	(Not Connected)
	Red(Orange)	(Not Connected)
	Orange(Red)	(Not Connected)
	White(Grey)	Alarm in
	Grey(White)	Alarm out
	White(Green)	TCP/IP Tx+
	Green(White)	TCP/IP Tx-
	Orange(White)	TCP/IP Rx-
	White(Orange)	TCP/IP Rx+
	Brown(White)	RS-485 -
	White(Brown)	RS-485 +
		+24V on power supply
		GND on power supply
		-
		-
		-
		-
		RJ45 Pin 3
		RJ45 Pin 6
		RJ45 Pin 2
		RJ45 Pin 1
		A terminal on RS-485 adapter
		B terminal on RS-485 adapter

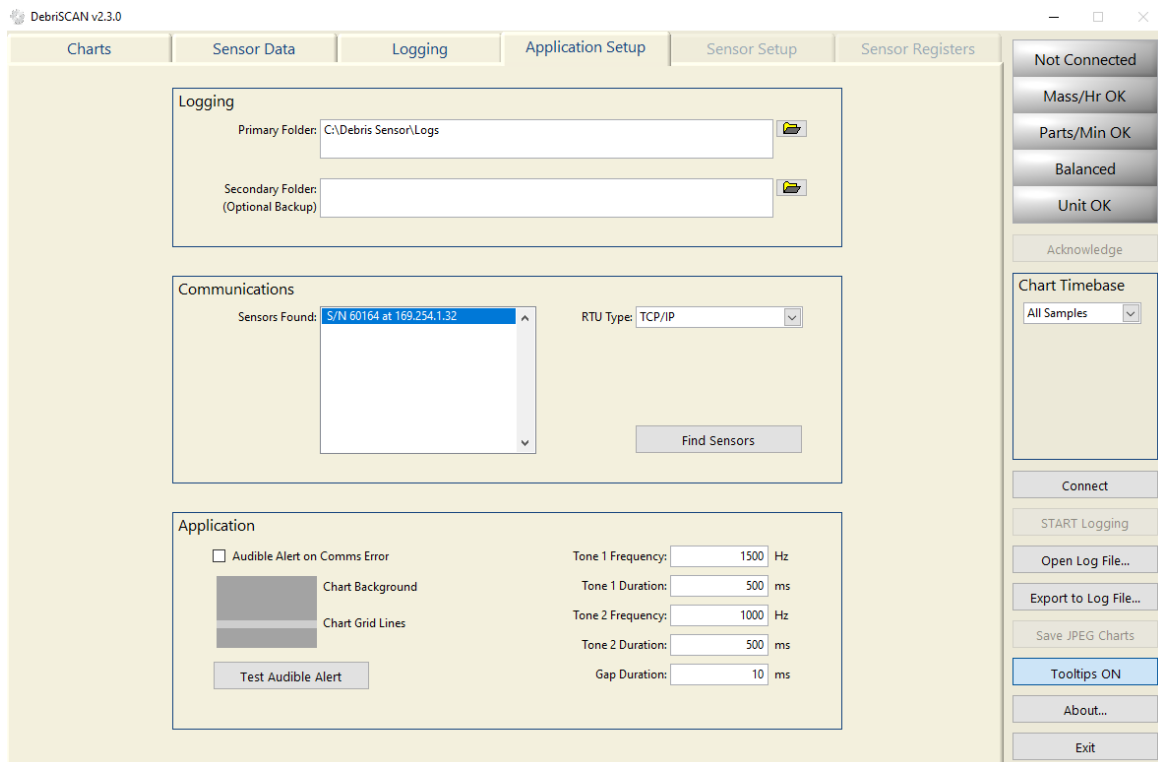


Figure 3.15.: Screenshot of the Parker DebrisSCAN sensor connecting tab

To log all the sensor data, the Parker DebrisSCAN (Figures 3.15 and 3.16) is used. After the experiments are done, DebrisSCAN exports all the log data to a database file. The database file is then imported to MATLAB (Appendix E.3), where the measurement are plotted to a graphically nice and representative graphs.

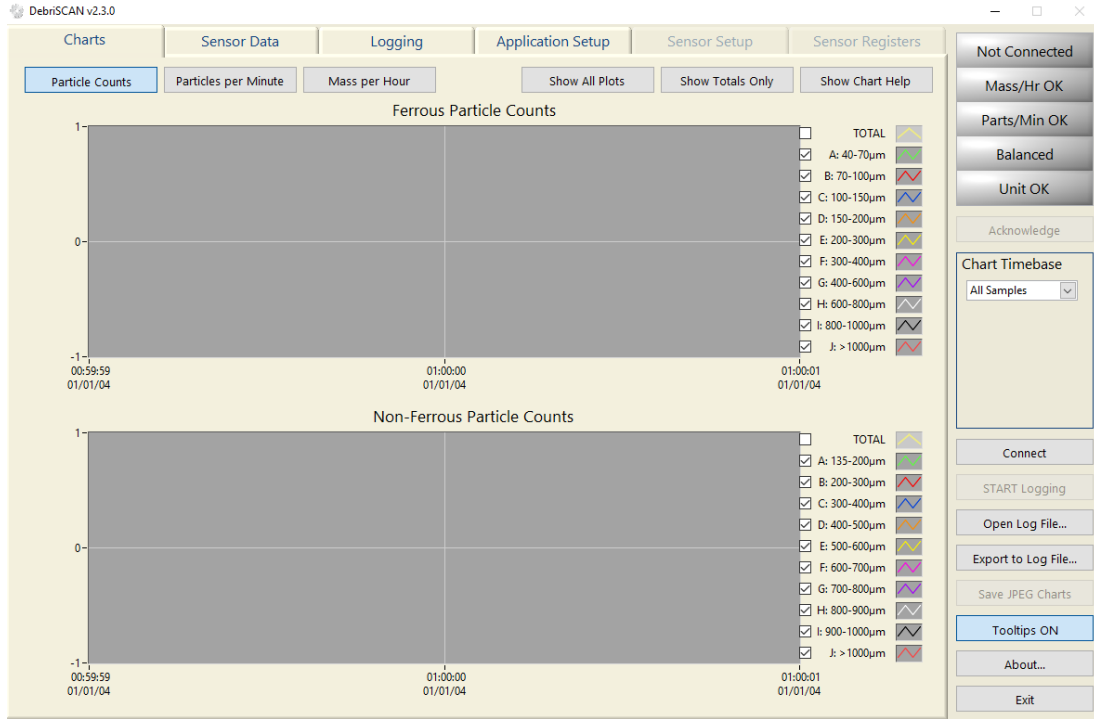


Figure 3.16.: Screenshot of the Parker DebrisSCAN sensor graphical interface tab

3.3. Design of Experiments

To test each sensors ability to detect substances that may be within a gearbox and the sensitivity of each sensor, a number of experiments have to be generated.

An experiment will be generated for each substance listed in Section 2.5. For each experiment, the amount of substance will be gradually added in small quantities to make sure the amount of substance is always known. This in addition to the lubrication volume of the lubrication system will then be used to calculate the substance density in ppm and checked against the cleanliness level, described in Section 2.5. To improve the statistical data and remove inaccuracies that may come during an experiment, all experiments will be done 3 times each.

This section describes all the experiments being conducted listed in Table 3.6. As the Gill 4212 will attract all magnetic particles, the experiment with AISI M2 will have to be done twice. One experiment with the Gill sensor mounted in the system, and one without the Gill sensor mounted.

Table 3.6.: The different experiments being conducted

Experiment no.	Substance	Size	Total amount
1	Water	-	2 mL
2	AISI 316L	46 – 105 μm	0.4 g
3	AISI M2 w/ Gill 4212	45 – 106 μm	0.5 g
4	AISI M2 w/o Gill 4212	45 – 106 μm	0.5 g
5	Iron silicate	200 – 700 μm	20 g

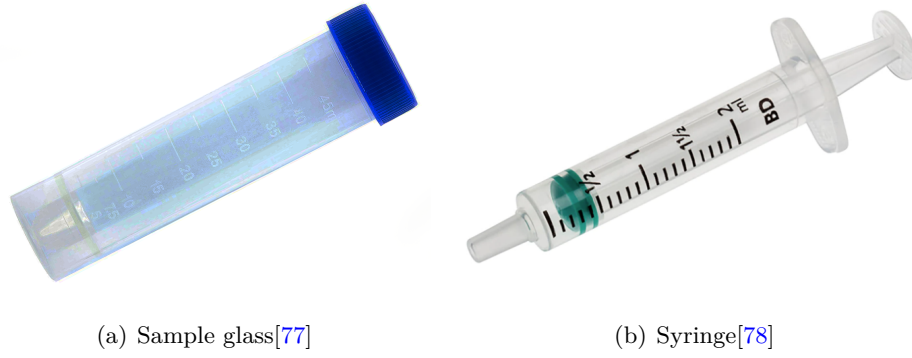


Figure 3.17.: Sample glass and syringe used for adding the contamination

In general metal debris from wear will not have a spherical geometry, but for simplification, spherical metal powder is used as it is easier to obtain.

Each experiment will start with a lubrication system with a new and clean oil so there is no contamination present. The contamination substance will thereby be added gradually to test the sensors ability to detect that certain substance and the sensitivity by checking the rate of change of the sensor data. This will not simulate a real life gearbox debris generation curve, described in Section 2.2, but it is not a concern since the purpose of these tests are to test that the sensors give quick and accurate readings. All particle debris will be carefully weighed and collected in sample glasses and water contamination will be carefully measured and added with the use of a syringe, as shown in Figure 3.17. All experiments could be altered in order to evoke a reaction from a sensor.

In regards to the oil temperature, before each experiment started, the gearbox and pump were run until the oil temperature converges. Considering the temperature sensitive readings of the Poseidon Trident QW3100, seen in Subsection 2.6.2.

Using a cleanliness level of 17/15/12, from Section 2.5, the maximum number of particles above $14 \mu m$ is calculated to find the upper contamination limit (Equation (3.4)).

$$n = 40 \frac{1}{10^{-3}L} \cdot V_{lubricant} = 40 \frac{1}{10^{-3}L} \cdot 1.5 L = 60\,000 \quad (3.4)$$

where

n = Number of particles before the cleanliness level is exceeded
 $V_{lubricant}$ = The amount of lubricant within the lubrication system

A maximum of 40 particles per millilitre results in an upper limit of 60 000 particles, and it will therefore be set as an upper contamination limit for particles above $14 \mu m$ in diameter. Between each test with particle debris, the lubricant will be rerouted through the filter at least 6 minutes, so for each test, the lubricant will be clean.

For the Parker MWDS, each particle will be counted more than once, since it does not measure the particle density, but rather counts each particle that flow through the sensor. To find the particle density, the pump flow can be used to calculate the amount of time needed to run through all the oil in the lubrication system. Based on the calculation in Equation (3.5), it is estimated that a duration of 2 minutes between each sediment is added, is sufficient time to let the contaminants blend with the lubricant.

$$\tau_{parker} = \frac{V_{lubrication}}{Q_{pump}} = \frac{1.5 L}{5.5 \frac{L}{min}} \approx 0.2727 min \approx 16.4 s \quad (3.5)$$

where

$\tau_{ParkerMWDS}$ = Time before all the oil has been circulated through the lubrication system

3.3.1. Adding Water

The first test will cover the sensors abilities to detect water. The water will be added gradually until the water contamination is well above the range of dissolved water. The water will therefore be added up to a limit of 1 300 ppm, this will ensure the water getting saturated in the lubricant. A 1 300 ppm limit equals a water volume of 2.0 mL (Equation (3.6)).

$$V_{water} = \frac{ppm_{water}}{1\,000\,000} \cdot V_{lubricant} = \frac{1\,300}{1\,000\,000} \cdot 1.5 L = 2.0 mL \quad (3.6)$$

where

V_{water} = Water volume based on maximum ppm limit

ppm_{water} = Maximum water contamination to be tested in ppm

Table 3.7.: Steps for adding water

Step	Add	Description
1	Nothing	Start testing with a clean oil
2	0.25 mL	0.25 mL/~ 150 ppm total contamination
3	0.25 mL	0.50 mL/~ 350 ppm total contamination This is around the area where the water starts to saturate at 20°C
4	0.25 mL	0.75 mL/~ 500 ppm total contamination
5	0.25 mL	1.00 mL/~ 650 ppm total contamination
6	0.25 mL	1.25 mL/~ 800 ppm total contamination
7	0.25 mL	1.50 mL/~ 1 000 ppm total contamination
8	0.25 mL	1.75 mL/~ 1 150 ppm total contamination
9	0.25 mL	2.00 mL/~ 1 300 ppm total contamination

To measure the sensitivity for each sensors, the water will be added in portions of 0.25 mL by a plastic syringe. The water used in the testing is regular tap water as it is easy accessible. The test will be done following the steps listed in Table 3.7.

3.3.2. Adding AISI 316L

The second test will be done inserting the AISI 316L powder into the gearbox. The powder will be added gradually until the contamination level is well above the recommended cleanliness level. The powder will be added in portions of 50 mg until it reaches 0.4 g.

Considering the powder is spherical, and estimating the mean diameter being the mean value of between 46 – 105 μm, the volume can be estimated to:

$$V_{316L} = \frac{4}{3}\pi \left(\frac{d_{316L}}{2}\right)^3 = \frac{4}{3}\pi \left(\frac{75\ \mu m}{2}\right)^3 = 2.20 \cdot 10^5\ \mu m^3 \quad (3.7)$$

where

V_{316L} = Mean volume of an AISI 316L particle
 d_{316L} = Mean diameter of an AISI 316L particle

Which can be used further to calculate the upper cleanliness level in ppm.

$$ppm_{316L} = \frac{V_{316L} \cdot n}{V_{lubricant}} = \frac{2.20 \cdot 10^5\ \mu m^3 \cdot 60\ 000}{1.5\ L} \approx 9.0 \quad (3.8)$$

where

ppm_{316L} = Contamination limit for AISI 316L
 V_{316L} = Mean volume of an AISI 316L particle

By using the mass density of AISI 316L with the volume of a AISI 316L particle in Equation (3.9), an increase of 50 mg is the same as an increase of 4.2 ppm.

$$ppm_{step} = \frac{V_{step}}{V_{lubrication}} = \frac{\frac{m_{step}}{\rho_{316L}}}{V_{lubrication}} = \frac{\frac{0.05\ g}{8\ 000\ \frac{kg}{m^3}}}{1.5\ L} \approx 4.2 \quad (3.9)$$

where

ρ_{316L} = Mass density of AISI 316L (=8 000 $\frac{kg}{m^3}$)[79]

Table 3.8.: Steps for adding AISI 316L stainless steel

Step	Add	Description
1	Nothing	Start testing with a clean oil
2	50 mg	50 mg/∼ 4.2 ppm total contamination
3	50 mg	100 mg/∼ 8.8 ppm total contamination Approximately the limit according to the cleanliness level (9.0 ppm)
4	50 mg	150 mg/∼ 12.6 ppm total contamination
5	50 mg	200 mg/∼ 16.8 ppm total contamination
6	50 mg	250 mg/∼ 21.0 ppm total contamination
7	50 mg	300 mg/∼ 25.2 ppm total contamination
8	50 mg	350 mg/∼ 29.4 ppm total contamination
9	50 mg	400 mg/∼ 33.6 ppm total contamination

3.3.3. Adding AISI M2

The third test will be done inserting the AISI M2 powder into the gearbox. The powder will be added gradually until the contamination level is well above the recommended cleanliness level. The powder will be added in portions of 50 mg until it reaches 0.5 g which is slightly above the maximum mass that the Gill 4212 can read, shown in Table 2.15.

Considering the powder is spherical, and estimating the mean diameter being the mean value of between 45 – 106 μm, the volume can be estimated to:

$$V_{M2} = \frac{4}{3}\pi \left(\frac{d_{M2}}{2}\right)^3 = \frac{4}{3}\pi \left(\frac{75.5 \mu m}{2}\right)^3 = 2.25 \cdot 10^5 \mu m^3 \quad (3.10)$$

where

V_{M2} = Mean volume of an AISI M2 particle
 d_{M2} = Mean diameter of an AISI M2 particle

Which can be used further to calculate the upper cleanliness level in ppm.

$$ppm_{M2} = \frac{V_{M2} \cdot n}{V_{lubricant}} = \frac{2.25 \cdot 10^5 \mu m^3 \cdot 60\,000}{1.5 L} \approx 9.0 \quad (3.11)$$

where

ppm_{M2} = Contamination limit for AISI M2
 V_{M2} = Mean volume of an AISI M2 particle

By using the mass density of AISI M2 with the volume of a AISI M2 particle in Equation (3.12), an increase of 50 mg is the same as an increase of 4.1 ppm.

$$ppm_{step} = \frac{V_{step}}{V_{lubrication}} = \frac{\frac{m_{step}}{\rho_{M2}}}{V_{lubrication}} = \frac{\frac{0.05 g}{8\,140 \frac{kg}{m^3}}}{1.5 L} \approx 4.1 \quad (3.12)$$

where

ρ_{M2} = Mass density of AISI M2 (=8 140 $\frac{kg}{m^3}$)[55]

Table 3.9.: Steps for adding AISI M2 high-speed steel

Step	Add	Description
1	Nothing	Start testing with a clean oil
2	50 mg	50 mg/~ 4.1 ppm total contamination
3	50 mg	100 mg/~ 8.2 ppm total contamination The limit according to the cleanliness level (9.0 ppm)
4	50 mg	150 mg/~ 12.3 ppm total contamination
5	50 mg	200 mg/~ 16.4 ppm total contamination
6	50 mg	250 mg/~ 20.5 ppm total contamination
7	50 mg	300 mg/~ 24.6 ppm total contamination
8	50 mg	350 mg/~ 28.7 ppm total contamination
9	50 mg	400 mg/~ 32.8 ppm total contamination
10	50 mg	450 mg/~ 36.9 ppm total contamination The maximum sensor readings for Gill 4212
11	50 mg	500 mg/~ 41 ppm total contamination

3.3.4. Adding Iron Silicate

The last test will be done inserting the iron silicate powder into the gearbox. The powder will be added gradually until the contamination level is well above the recommended cleanliness level. The powder will be added in portions of 1.5 g until it reaches 12.0 g

Considering the powder is spherical, and estimating the mean diameter being the mean value of between 200 – 700 μm , the volume can be estimated to:

$$V_{Ironsilicate} = \frac{4}{3}\pi \left(\frac{d_{Ironsilicate}}{2} \right)^3 = \frac{4}{3}\pi \left(\frac{450 \mu m}{2} \right)^3 = 4.77 \cdot 10^7 \mu m^3 \quad (3.13)$$

where

$V_{Ironsilicate}$ = Mean volume of an iron silicate particle
 $d_{Ironsilicate}$ = Mean diameter of an iron silicate particle

Which can be used further to calculate the upper cleanliness level in ppm.

$$ppm_{Ironsilicate} = \frac{V_{Ironsilicate} \cdot n}{V_{lubricant}} = \frac{4.77 \cdot 10^7 \mu m^3 \cdot 60\,000}{1.5 L} = \sim 1\,908 \quad (3.14)$$

where

$ppm_{Ironsilicate}$ = Contamination limit for iron silicate
 $V_{Ironsilicate}$ = Mean volume of an iron silicate particle

By using the bulk density of iron silicate with the volume of a iron silicate particle in Equation (3.15), an increase of 1.5 g is the same as an increase of ~ 590 ppm.

$$ppm_{step} = \frac{V_{step}}{V_{lubrication}} = \frac{\frac{m_{step}}{\rho_{Ironsilicate}}}{V_{lubrication}} = \frac{\frac{1.5 g}{1\,700 \frac{kg}{m^3}}}{1.5 L} = \sim 440 \quad (3.15)$$

where

$\rho_{Ironsilicate}$ = Bulk density of iron silicate (=1 700 $\frac{kg}{m^3}$)[56, Part.no.18-996]

Table 3.10.: Steps for adding iron silicate

Step	Add	Description
1	Nothing	Start testing with a clean oil
2	1.5 g	1.5 g/ ~ 590 ppm total contamination
3	1.5 g	3.0 g/ $\sim 1\,180$ ppm total contamination
4	1.5 g	4.5 g/ $\sim 1\,770$ ppm total contamination Approximately the limit according to the cleanliness level
5	1.5 g	6.0 g/ $\sim 2\,360$ ppm total contamination
6	1.5 g	7.5 g/ $\sim 2\,950$ ppm total contamination
7	1.5 g	9.0 g/ $\sim 3\,540$ ppm total contamination
8	1.5 g	10.5 g/ $\sim 4\,130$ ppm total contamination
9	1.5 g	12.0 g/ $\sim 4\,720$ ppm total contamination

3.4. Sensor Calibration

Before the experiments are conducted, the sensors has to be calibrated, to give accurate results. All the sensors are pre-calibrated from the manufacturer, so very little work has to be done regarding this. However, since the Gill 4212 gives out a percentage reading based on the debris mass on the end of the probe, the reading should be double checked as the reading may vary based on the debris size.

4. Analysis

This chapter contains information about how the experiments was conducted and the results. Graphical view of the sensor data for each test can be found in Appendix F.

4.1. Temperature

Since the sensor readings in general are temperature dependent. A test was conducted to find out what the steady state temperature is and how long it takes before the gearbox reaches the steady state temperature. The temperature readings were done using the Gill 4212.

When conducting the test, the induction motor ((1) in Figure 3.2) was set to 600 rpm. With a cold gearbox, that resulted in a load on the motor of about 60% of the rated torque.

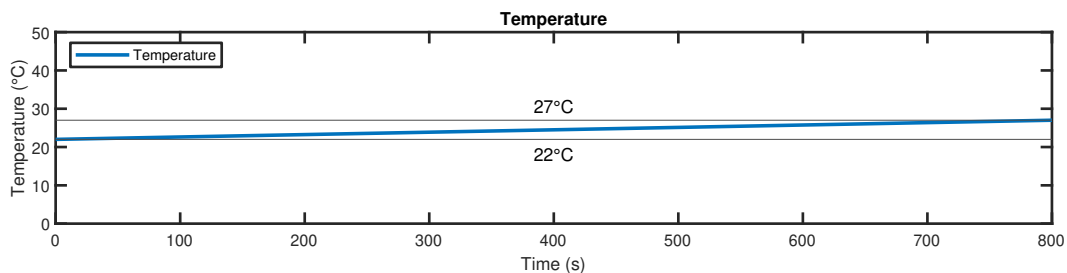


Figure 4.1.: Steady state temperature of the gearbox

As seen in Figure 4.1 the temperature during the testing did increase, but only by 1 °C every 2-3 minutes. The change in temperature was evaluated to not being critical in order to have proper sensor readings during the experiments. The cause to that is believed to be the big oil reservoir of the gearbox and that the load on the gearbox is quite low.

4.2. Calibration

4.2.1. Gill 4212

As explained in Subsection 3.2.1, the fine debris was measured and added in a sample glass, as seen in Figure 4.2. The calibration procedure from the Gill user manual was followed[66]. As the probe showed 0% debris in the calibration when the probe was not subjected to any particles, only the maximum limit had to be set. This was done using the "set" function in the calibration software when the probe was subjected to the sample glass with the metal powder. The calibration were double checked to make sure that the probe went from 0% to 100% when the probe was subjected to the sample glass. As the sensor signals is measured by the DAQ, the MATLAB scripts also has to take a separate calibration into consideration. The signals where also therefore logged with MATLAB during the calibration process. This lead to the values shown in Equation (4.1). Equation (4.1) takes the voltage input signals from the DAQ and maps them to a signal between 0 and 100%. The input voltage to the DAQ was correct, and the input signal did not need to be adjusted.



Figure 4.2.: Fine debris calibration with the Gill 4212

$$d(t) = V(t) \cdot \frac{100}{10V} \quad (4.1)$$

where

$d(t)$ = Debris signal

$V(t)$ = Input voltage signal

G = Gain

O = Offset

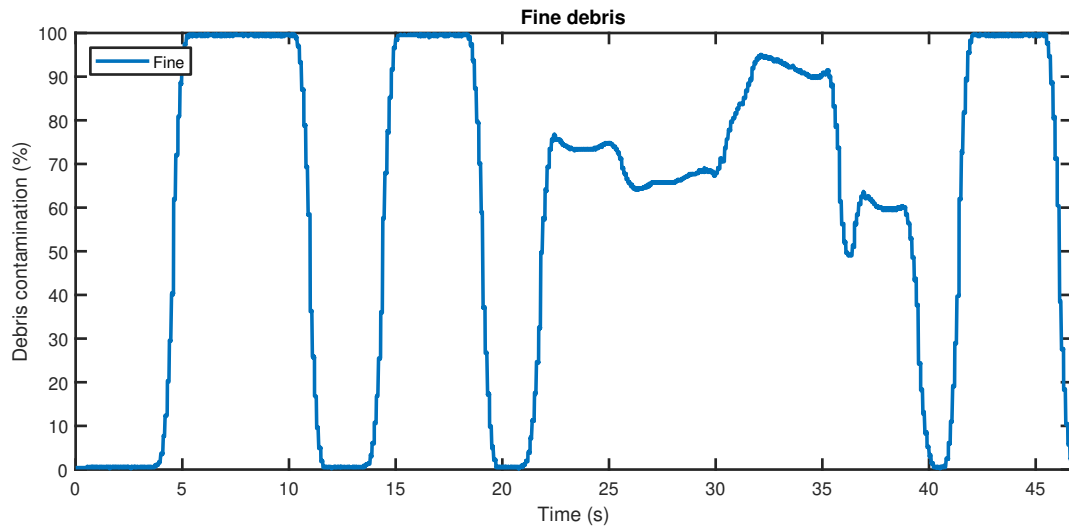


Figure 4.3.: Fine debris calibration testing with the Gill 4212

The channel for measuring coarse debris will not be calibrated, but will be active so that the signal can be logged.

To calibrate the oil condition channel, the reference signal was first set as the sensor was plugged in the system with fresh oil and the oil pump running, as seen in Figure 4.4 (a).



(a) Setting the reference in fresh oil



(b) Setting upper alarm threshold



(c) Setting lower alarm threshold

Figure 4.4.: Gill 4212 oil condition calibration process

The upper alarm threshold were set while the sensor probe was held in the air, as seen in Figure 4.4 (b). The last lower threshold were set while the probe was subjected into an oil with 10% water mixture (Figure 4.4 (c)).

4.3. Initial Testing

Before the experiments were conducted, some baselines were made to have something to compare the sensor data from the experiments with. This is especially important considering the Poseidon measurements. The Poseidon baseline in addition to the information about how much contamination that is added, is used to interpret the sensor signals. If the sensor readings has decreased significantly from the baseline during adding of contamination, the sensor values will be evaluated as being an indication of a bad lubricant. After experiment no. 1, when the filter was installed, another baseline were done in order to have a baseline where there were zero particles in the lubricant.

4.3.1. Gill 4212

To test the data acquisition for the Gill 4212, an initial start up test where done to check if the sensor values change based on the operating conditions.

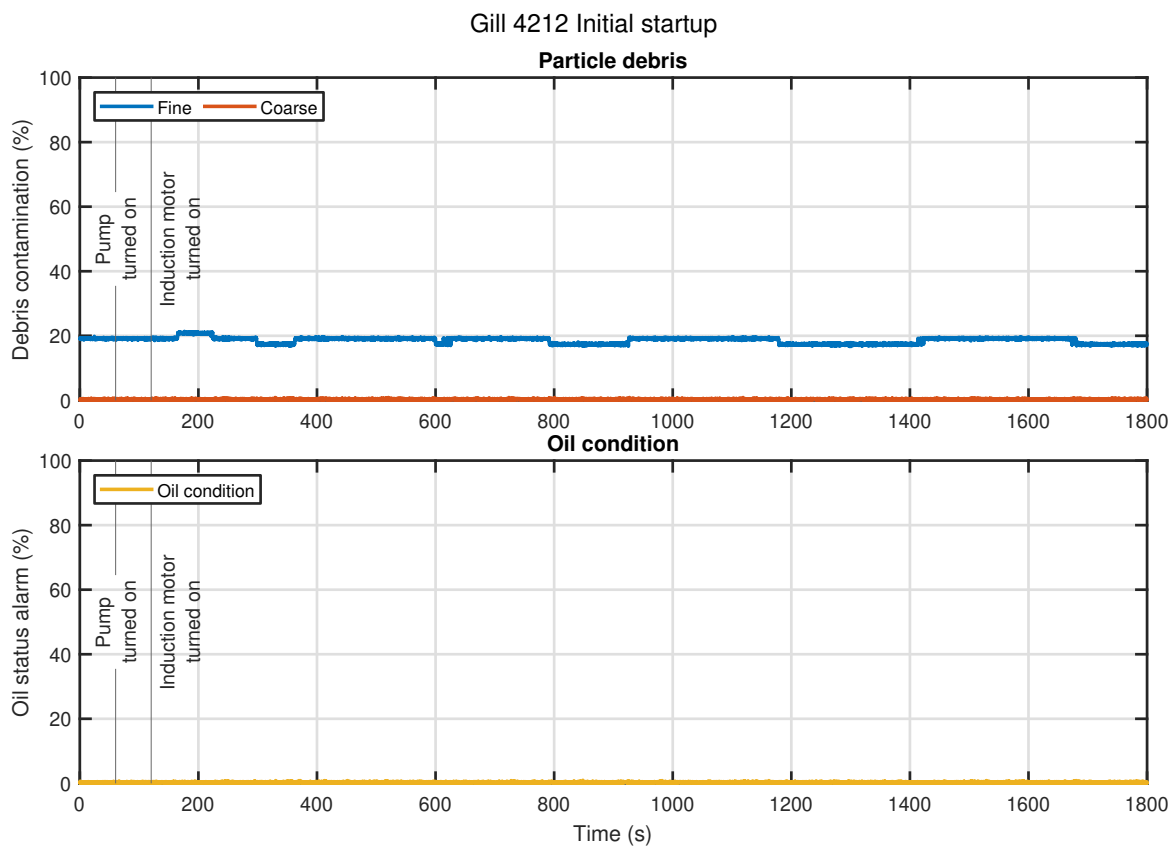


Figure 4.5.: Initial data acquisition with the Gill 4212

As seen in Figure 4.5, there are different milestones indicating when the sensor, pump and induction motors are turned on and how the sensor values changes accordingly. To time the milestones with the tests, the signal logging in MATLAB was started simultaneously as the stopwatch. When milestones such as starting the pump was done, measurements were done on the stopwatch such that the milestones could be added into the graphical representations in MATLAB.

4.3.2. Poseidon Trident QW3100

An initial startup were done to check the steady state values of the holding registers to the Poseidon sensor. As there are little supplied information on how to interpret the signals from this sensor, this

test was important to set the baseline signals with the fresh lubricant. During this test, it was found that the holding registers of the Poseidon sensor updates every 100 seconds.

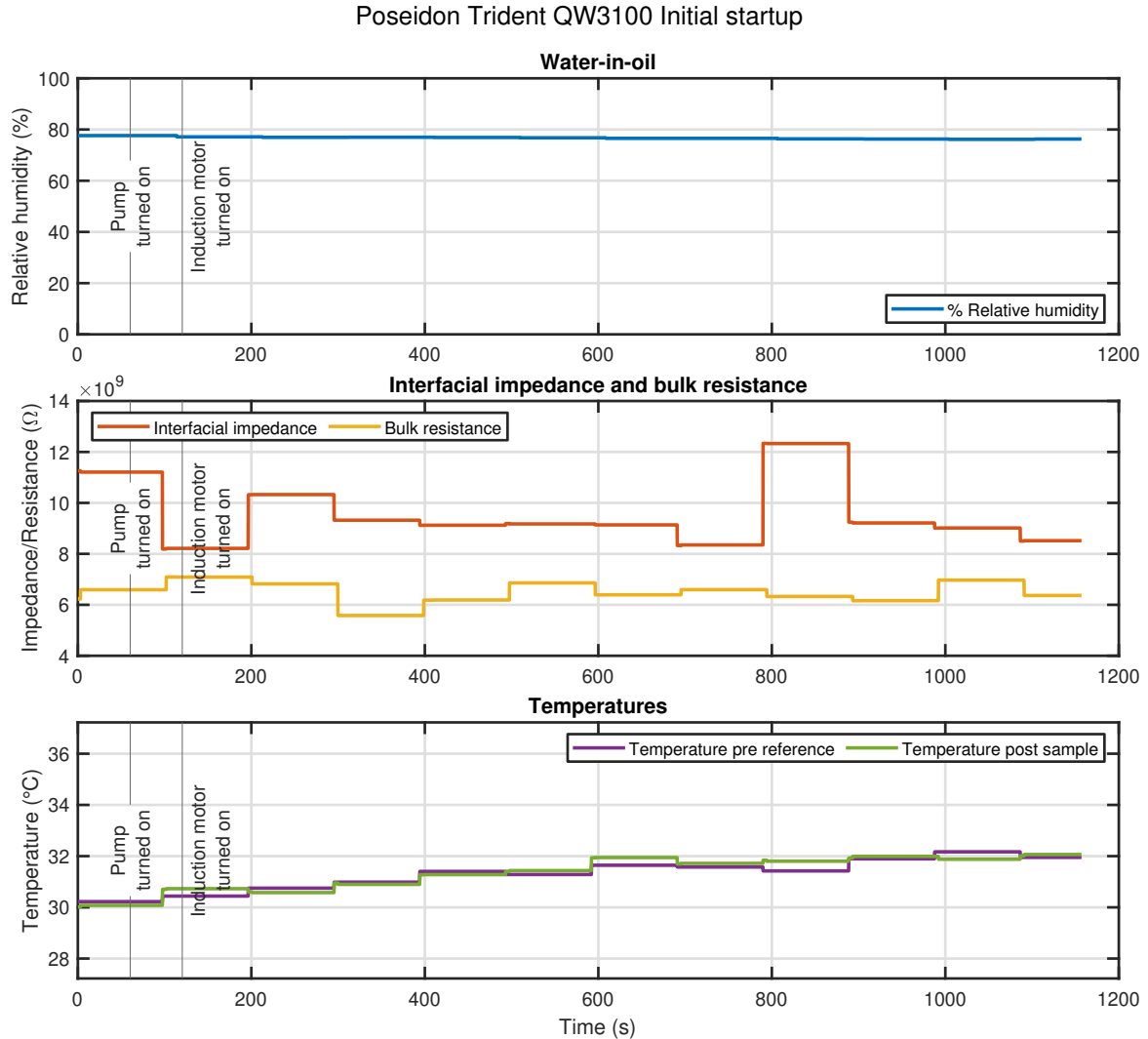


Figure 4.6.: Initial data acquisition with the Poseidon Trident QW3100

Figure 4.6 shows that the relative humidity and temperature stays pretty much at a constant level, but that the interfacial impedance and bulk resistance changes when there is activity in the oil. The interfacial impedance does peak during the run, but it is unknown why the value changes so drastically.

4.3.3. Parker Kittiwake MWDS

The initial startup with the Parker MWDS showed that the supposedly fresh oil was not as clean as anticipated. The debris is probably originating from the new gear-set.

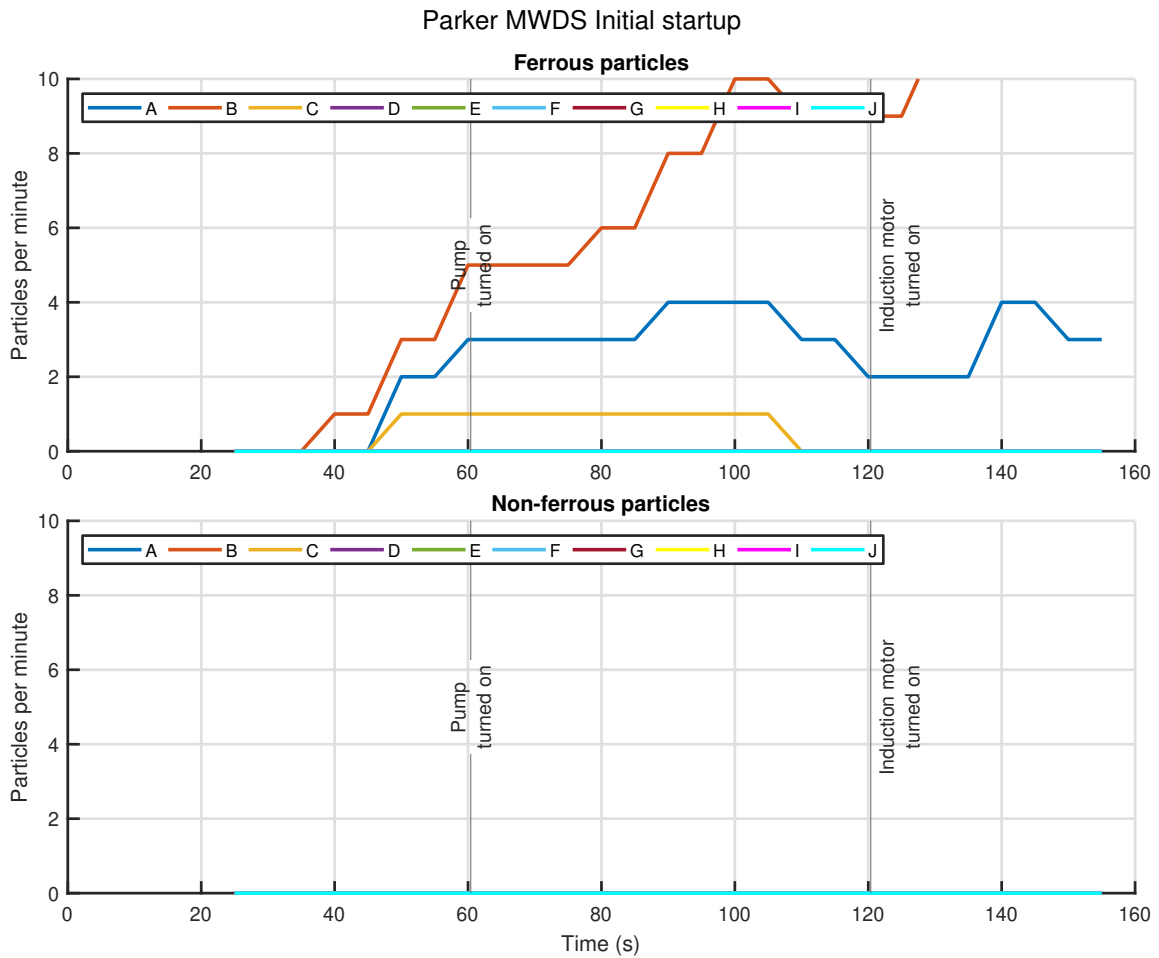


Figure 4.7.: Initial data acquisition with the Parker Kittiwake MWDS

Figure 4.7 shows that the gearbox contains several particles, all below $100\ \mu\text{m}$ (See Table 2.19 for bin ranges). Considering it takes $16.4\ \text{s}$ to run all the oil through the lubrication system, this results in a total of about ~ 5 particles in the whole lubrication system. This is a very small amount and could be neglected.

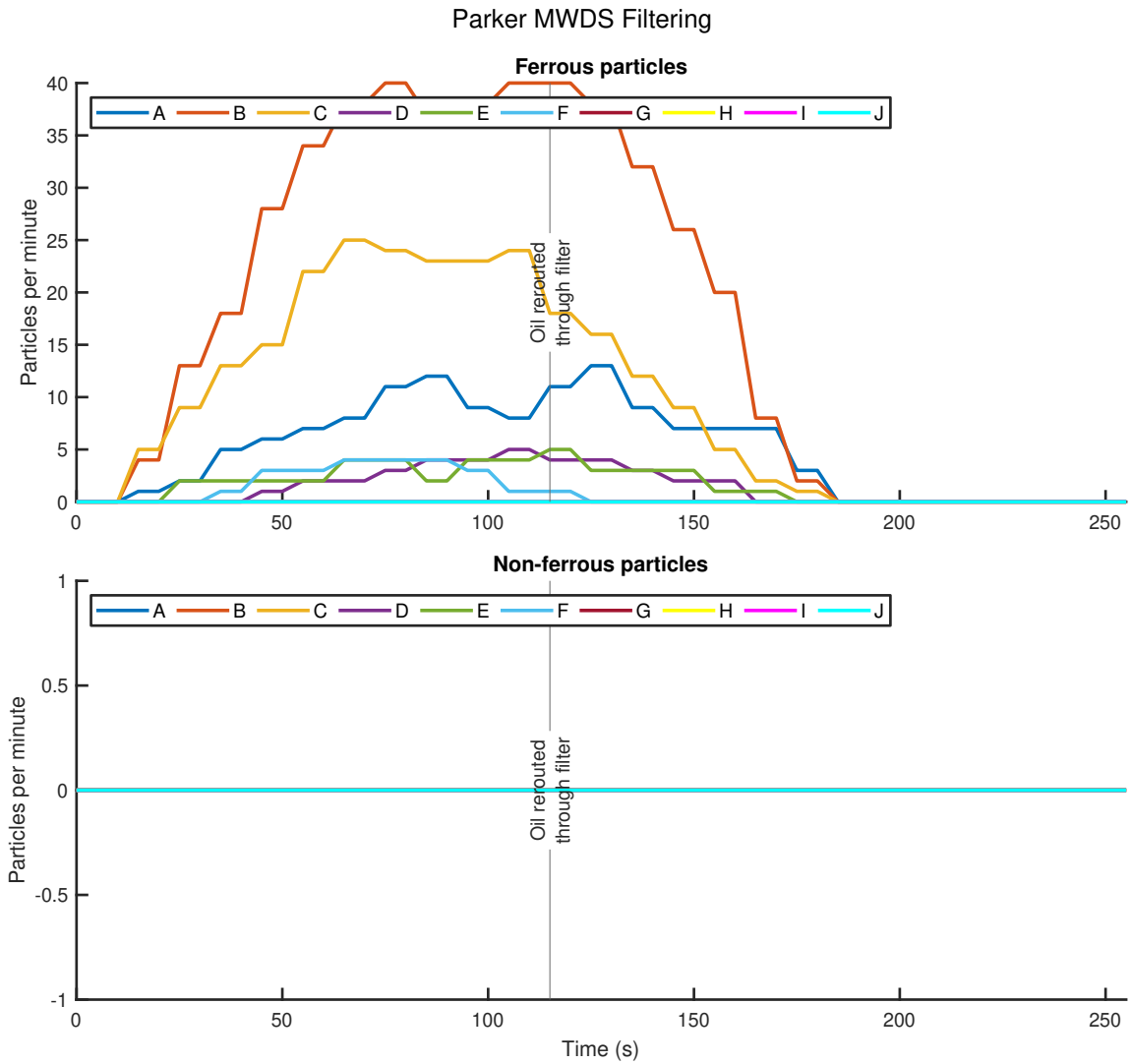


Figure 4.8.: Parker MWDS results on particle filtering

To clean up the particle debris, the oil was run through the oil filter. Figure 4.8 shows how effective the filter was at filtering out the particle debris. The logging was started with the pump switched off. As the logging goes on, the particle debris per minute signal goes to zero which tells us that the filter has filtered out all the particle debris.

4.4. Experiment no. 1

Experiment no. 1 is the experiment being conducted with added water contamination. It was done 3 times, with each time starting as planned in Section 3.3. Each time however, the test was altered to get the desired results, such as to trigger the alarm threshold on the Gill 4212.

4.4.1. Run no. 1

Figures F.1, F.2 and F.3 shows the results from the first run of experiment no. 1. A total of 2.25 mL was added which is about 1500 ppm.

The fine channel measured $\sim 20\%$ contamination on the probe. This is probably from some leftover debris in the gearbox, as this gearbox has never been run with a filter. The oil condition channel alarm did not set of.

The Poseidon showed increasing relative humidity level in the oil as the water was added. The relative humidity started at $\sim 55\%$ and increased to $\sim 90\%$. Even though the water was added at a steady pace, the humidity reading did not start to increase until the test where only halfway done. The interfacial impedance and bulk resistance signals moved, but does not show any signs of increasing or decreasing levels. Based on the signals, it looks like the holding registers are updated once every 100 s.

4.4.2. Run no.2

Figures F.4, F.5 and F.6 shows the results from the second run of experiment no. 1. A total of 6.0 mL was added which is about 4000 ppm.

As with the first run, the Gill did not seem to respond any different, even though the water content was more than doubled.

This time, the relative humidity maxed out, which would result in saturated water. The interfacial impedance and bulk resistance did decrease as stated in Section 2.7.

The Parker measurements are not very relevant in this experiment, but the particles per minute readings did increase from the first to the second run, which would imply that the particle debris contamination were increased from the first run. This would probably be break-in debris from the new gear-set.

It is also interesting to see that the sensor counts a non-ferrous particle at regular intervals. Maybe it could be that there is the same non-ferrous that is counted several times during the test. In that case, it could be interesting to see why it is counted once every 500 s and not once every 16.4 s as the pump flow predicts.

4.4.3. Run no. 3

Figures F.7, F.8 and F.9 shows the results from the third and last run of experiment no. 1. The goal of this run was to see how much water that was required before the Gill 4212 oil condition alarm went of. A total of 160.0 mL was added which is about 10.6%.

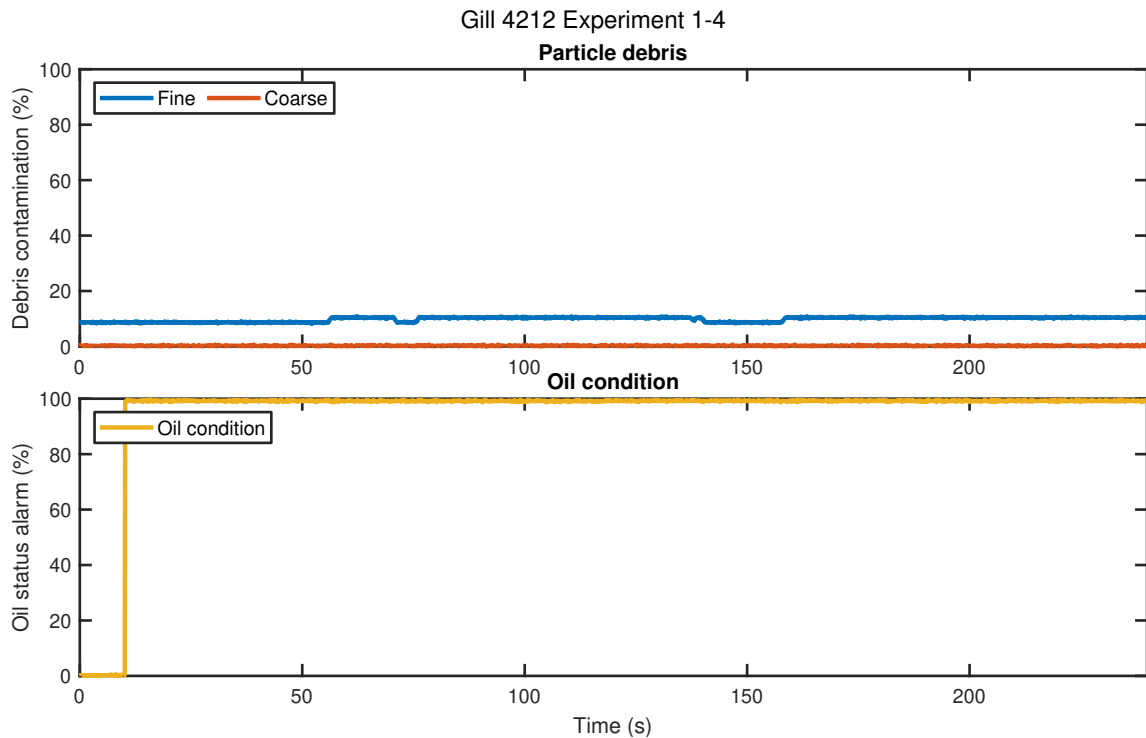


Figure 4.9.: Gill sensor data after experiment no. 1-3

Interpreted from Figure F.9, the pump fuse blew at $t \approx 2300$ s, this made it to hard find out exactly when the Gill oil condition alarm signal were raised. However, when the fuse was changed, the logging were done one more time with that exact water content (See Figure 4.9).

It ended up raising the oil condition alarm, which means that the oil condition alarm were raised with a water content between 100 mL and 160 mL which equals between 6.7% and 10.6% . This sounds reasonable considering the sensor alarm threshold was calibrated with a water content of 10% .

The Poseidon showed high relative humidity content from the start of the test, which could only mean one thing. That the flushing of the gearbox was not done well enough. The interfacial impedance and bulk resistance did seem to decrease some bit during the test, but started to increase again when the pump stopped at $t \approx 2300$ s. The sudden decrease in interfacial impedance at around $t = 100$ s is probably because of a short circuiting of the probe done by maybe a large particle.

The Parker signal did not change much from the second run, except for some larger particles that were counted.

4.4.4. Summary

During experiment no. 1, it was noticed that the relative humidity signal of the Poseidon sensor gave the most relevant signals to use for tests done with water contamination except for last run where the attempt the surpass the Gill oil condition alarm threshold.

It is seen in Figure 4.10 that the starting value of the relative humidity for each run did increase for each time that the experiment was conducted. This is most probably due to the lack of proper flushing of the gearbox. After each run, when the oil is flushed, some amount of free water starts to settle on the bottom of the gear box which is hard to flush.

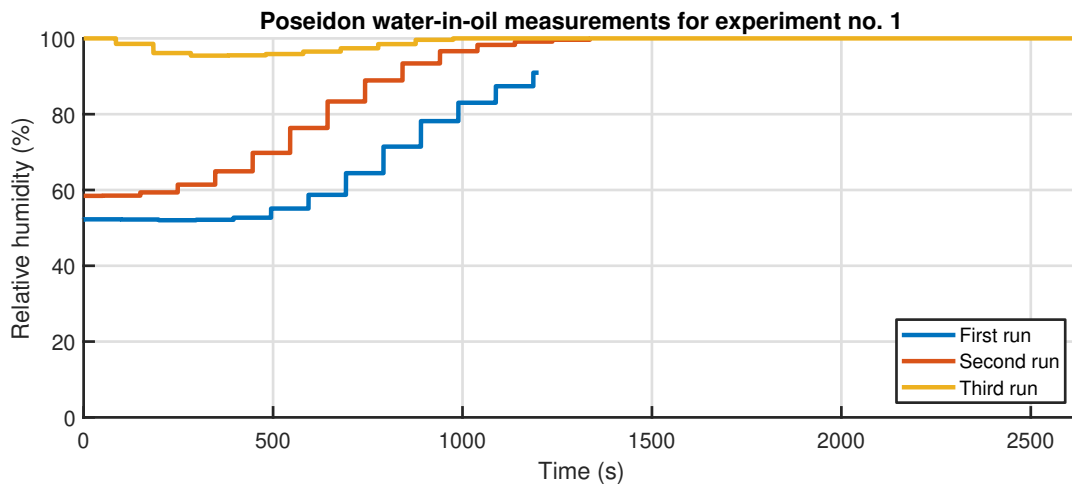


Figure 4.10.: Comparison of the Poseidon water-in-oil sensor data for experiment no. 1

When the new oil is added and the next run is started, the leftover water is then stirred up again into the fresh oil. This makes it impossible to flush out the water from the oil reservoir. The water therefore has to be thinned out until it reaches a low enough level.

It is also interesting to see how the relative humidity level for the first run started at 50%, even though the gearbox was cleaned, with a new gear-set, and with no tests being conducted. Either the oil supplied by the university could have a relative humidity of 50% or the oil got moisturised from the air between when the oil was filled on the gearbox and when the first test was conducted. The university oil drum were almost empty and had probably been that for a long time, which could be the reason.

Based on the incline during the first and second run, the relative humidity seems to rise about 6% in average per 120 seconds. Anyhow, the sensor seem to respond quite quick when adding the water considering that the water has to blend in with the oil.

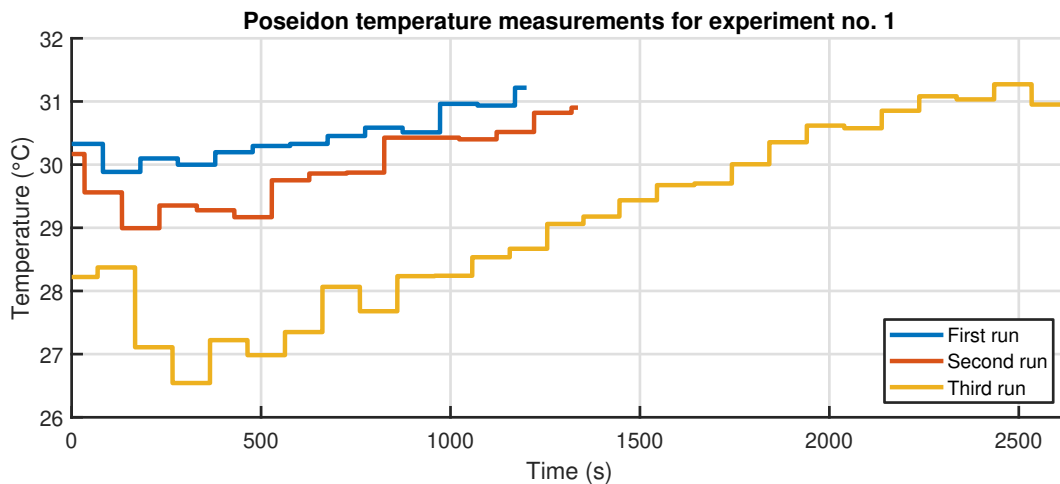


Figure 4.11.: Comparison of the Poseidon temperature sensor data for experiment no. 1

The Gill sensor does seem to respond when adding water up to the set alarm threshold of 10% water.

As seen in Figure 4.11, the temperatures did not differ too much. It is therefore unlikely that the water dissolution limit differed between each run.

After experiment no. 1 was finished, the oil was flushed 4 times to thin out the water content as much

as possible before experiment no. 2 was conducted.

4.5. Experiment no. 2

Experiment no. 2 is the experiment being conducted with added AISI 316L particle contamination.

4.5.1. Run no. 1

Figures F.10, F.11 and F.12 show the results from the first run of experiment no. 2. The first run were done with a total of 400 *mg* of 316L stainless steel debris added. This equals a total contamination of 33.6 ppm.

The Gill did collect some debris, since the fine measurements show a value that is above the baseline in Figure 4.5. This is very interesting since the particles are austenitic and is supposed to be non-magnetic.

The Poseidon relative humidity level is still on 100% which is caused by improper flushing.

After step 3, the ISO cleanliness level should in theory be surpassed. The interfacial impedance was during the test constantly much lower than the baseline signal. However, the signal did not decrease with time as would be expected, and the signal were constant, no matter how much contaminant that were in the oil.

The Parker did see ferrous particle debris, but it is determined that this is a result of the gear-set run-in period. Even though the oil was filtered before this run, it seems like there has been some particle debris that still is left in the system.

4.5.2. Run no. 2

Figures F.13, F.14 and F.15 show the results from the second run of experiment no. 2. The second run were done with a total of 1400 *mg* of 316L stainless steel debris added. This equals a total contamination of 118 ppm. In this run the added debris for each step was increased up to 100 *mg*. There was also added 3 samples at the end of 200 *mg* each to see if there were any drastic changes of the sensor data.

During this run, the interfacial impedance signal did not change much from the baseline signal. Even though the cleanliness level were surpassed, there are no indication from the Poseidon sensor that the oil should be filtered or changed. It could be that it would be easier to figure out a trend based on sensor readings over several hours or days.

The Gill sensor did still not give any relevant information. The Parker gave out a higher particle count than with the first run, but it is still believed to origin from the run-in of the gear-set or growth because of wear caused by the 316L particles.

4.5.3. Run no. 3

Figures F.16, F.17 and F.18 show the results from the third run of experiment no. 2. The third run were done with a total of 2300 *mg* of 316L stainless steel debris added. This equals a total contamination of 194 ppm. In this run the added debris for each step was increased up to 100 *mg*. There was also added 3 samples at the end of 500 *mg* each to see if there were any drastic changes of the sensor data.

The results from the last run were very similar to the second run. There are no major changes between that run and the baseline that would suggest that the oil should be changes because of a large number of stainless steel particles.

The third run were all in all very similar to the second run of experiment no. 2

4.5.4. Summary

Figure 4.12 shows that there were some major changes between the first run, and the second and third run. Also, the baseline signal did not differ from the second and third run. It is very hard to conclude that there were any contamination of the 316L particles based on any of the sensor data.

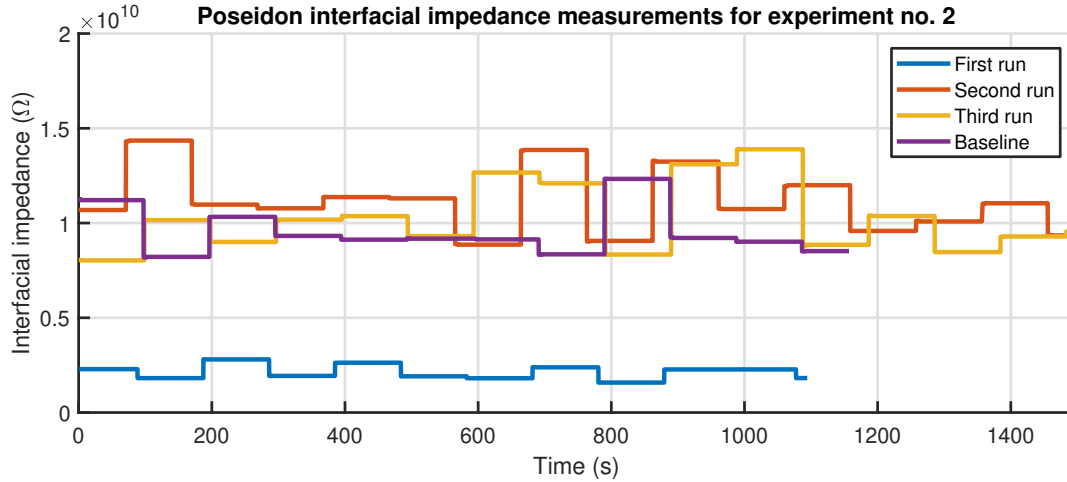


Figure 4.12.: Comparison of the Poseidon interfacial impedance data for experiment no. 2

As stated in Subsection 2.6.3, the Parker MWDS would have been able to detect the 316L particles if they had a size of $135 \mu m$ or bigger.

4.6. Experiment no. 3

Experiment no. 3 is the experiment being conducted with added AISI M2 particle contamination with the Gill 4212. This experiment is designed specifically to test the Gill sensors ability to detect contamination, the readings from the other sensors will therefore not be very relevant. Before each run, the Gill 4212 was checked to see that the probe was clean for particle debris. Before this experiment took place, it was noticed that some contaminant were coming from the gearbox break-in process. It could be that some of the sensor readings may be a result from particles generated by the break-in of the gearbox and not the artificially added debris.

4.6.1. Run no. 1

Figures F.19, F.20 and F.21 show the results from the first run of experiment no. 3. The first run were done with a total of $500 mg$ of M2 high-speed steel debris added. This equals a total contamination of 41 ppm.

Even though the Gill fine channel limit were supposed to be reached, the probe reading did not increase very much from the baseline. This could be a result of a various of reasons. Much of the particle debris could be stuck elsewhere in the lubrication loop, the fluid velocity could be too great for the particles to be able to attach themselves to the probe or the particle could be attached to some other areas on the probe which are not measured with the sensor.

After the test were done, the sensor was removed from the sensor block to be checked and cleaned before the next run. Some small amount of particle debris were found on the probe, but not on the end where the sensor can actually measure the particles.

The Parker did not give out any especially high readings for the first run.

4.6.2. Run no. 2

Figures F.22, F.23 and F.24 show the results from the second run of experiment no. 3. The second run were done with a total of 2000 *mg* of M2 high-speed steel debris added. This time the added particle debris was increased to 200. This equals a total contamination of 164 ppm.

Even though the particle debris was increased by 4 times from the first run, the fine debris signal did not increase. When the probe was later removed from the sensor block, it was seen that the probe was almost free of attached debris.

As with the first run, the Parker did not read any high rate of particle debris passing through the sensor. The Poseidon readings where similar to the baseline readings.

4.6.3. Run no. 3

Figures F.25, F.26 and F.27 show the results from the third and last run of experiment no. 3. The third run were done with a total of 5500 *mg* of M2 high-speed steel debris added. This time the added particle debris was increased to 11 samples with 500 each. This equals a total contamination of 451 ppm.

Only when the amount of added fine debris was increased by 11 times from the original experiment did the sensor readings actually start to respond.

If the Gill and Parker data is compared, it is seen that the Parker measurement increases much faster than the Gill measurements, but that the Parker readings starts to decrease as the particles attaches themselves to the Gill probe.

4.6.4. Summary

Figure 4.13 shows the debris that had attached itself to the Gill 4212 during each run of experiment no. 3. It looks like even though the sensor only can measure about 0.45 *g* of the fine particle debris, the probe can collect several times that amount.

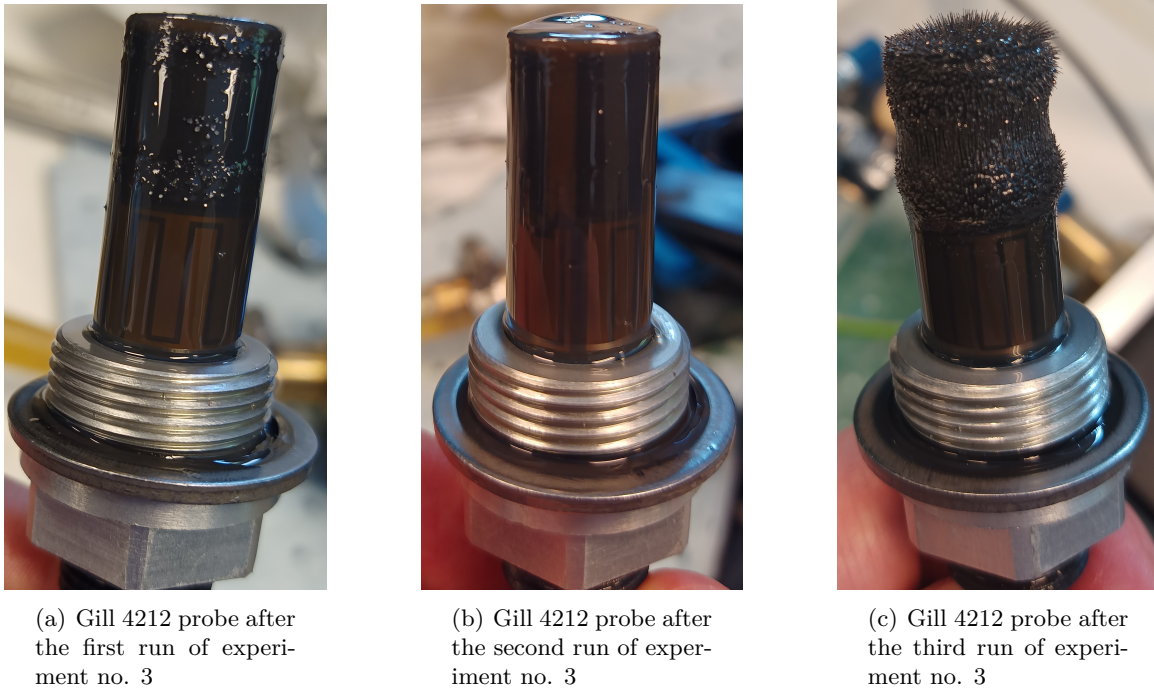


Figure 4.13.: Particle debris on Gill 4212 probe after experiment no. 3

It looks like the Gill is able to collect some of the particle debris, but it is difficult to know how much particle debris that is collected. Because it is impossible to know how much has been attached to the sides of the probe. The sensor should as such be placed carefully in a lubrication system.

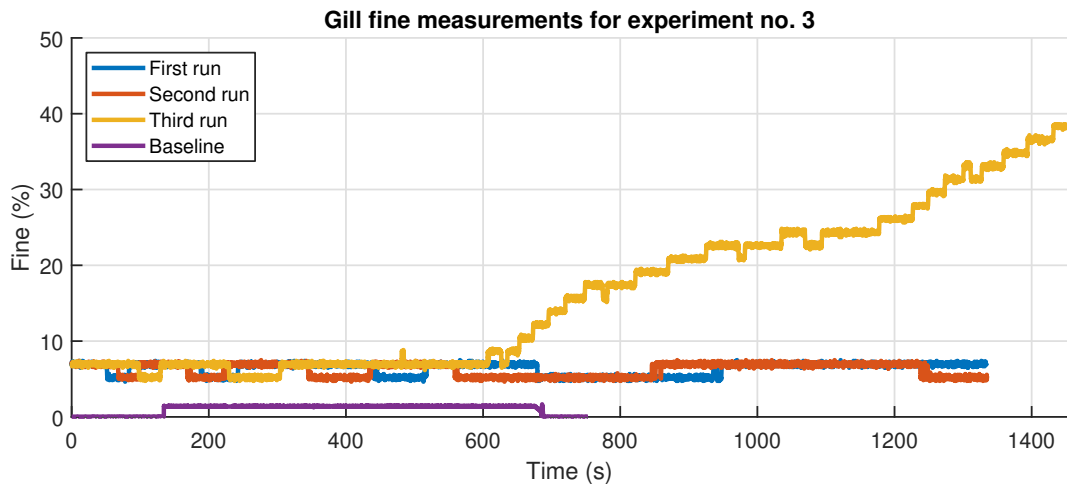


Figure 4.14.: Comparison of the Gill fine particles data for experiment no. 3

Based on the data in Figure 4.14, it looks like the probe does not start to give out any response before the contamination content is above ~ 200 ppm. This is much higher than the cleanliness level stated in Subsection 3.3.3, which is 9 ppm.

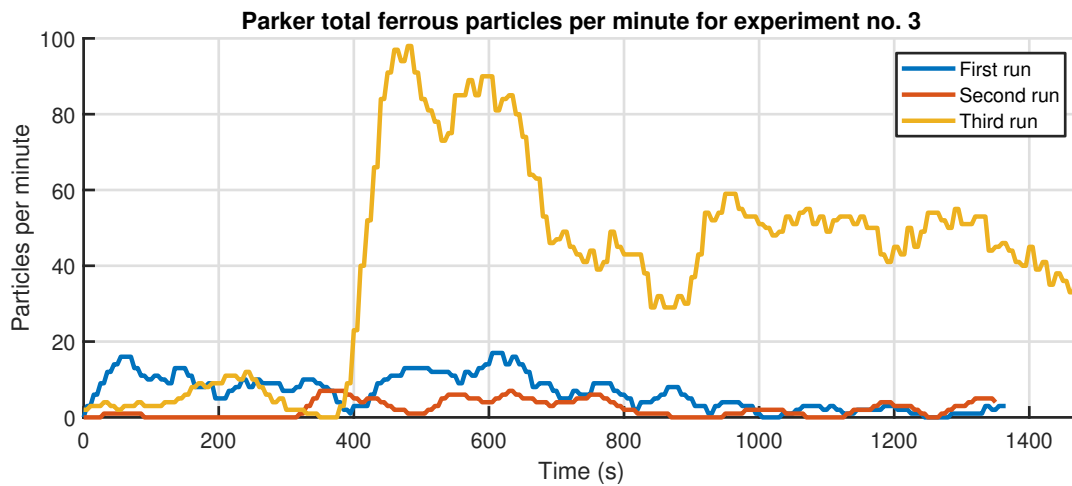


Figure 4.15.: Comparison of the Parker ferrous particle per minute data for experiment no. 3

Figure 4.15 shows how much the particle per minute count suddenly increases for the third run. It is unknown why the sudden change happens, it could be that a sudden turbulent flow results in a lump of particles escapes the gearbox currents and into the lubrication systems that makes it flow through the sensors.

4.7. Experiment no. 4

Experiment no. 4 is the experiment being conducted with added AISI M2 particle contamination without the Gill 4212.

4.7.1. Run no. 1

Figures F.28 and F.29 show the results from the first run of experiment no. 4. The first run were done as stated in Table 3.6, with a total of 500 *mg* of M2 high-speed steel debris added. This equals a total contamination of 41 ppm.

The Poseidon sensor did some strange measurements considering that the logged interfacial impedance was negative for most of the duration of the first run. It was however much lower than the baseline, which is what the signals were supposed to do.

The particles per minute signal of the Parker was much higher for this run than with the baseline. It did not increase linearly as suspected when the additional contamination was added, but the particle per minutes signal converged towards a particle rate of 80 particles per minute. This results in 1.333 particles per second, which is about 22 particles every 16.4 *s*.

4.7.2. Run no. 2

Figures F.30 and F.31 show the results from the second run of experiment no. 4. This run were done with a total of 1 000 *mg* of M2 high-speed steel debris added, 100 *mg* added for each step. This equals a total contamination of 82 ppm.

The Poseidon and Parker measurements for this run were similar as with the first run.

4.7.3. Run no. 3

Figures F.32 and F.33 show the results from the third run of experiment no. 4. This run were done with a total of 5000 mg of M2 high-speed steel debris added, 500 mg added for each step. For this run, the time between each step was increased to 3 minutes. This equals a total contamination of 410 ppm.

The Poseidon and Parker measurements for this run were similar as with the first and second run.

4.7.4. Run no. 4

Figures F.34 and F.35 show the results from the third run of experiment no. 4. Because of the strange measurements from the first 3 runs, it was decided to do another run of experiment no. 4 with the same added contamination as during the second run. This time however, the time between each added sample glass was increased to 5 minutes. The Poseidon sensor was reset in order to fix the issue with negative impedance values. This seemed to be working as the results during this experiment seemed to be sensible. The interfacial impedance did however not decrease as expected, but rather increased. The Parker measurements were very similar to the first 3 runs.

4.7.5. Summary

Even though the amount of particles that was added, was different for each of the first 3 runs, the sensor readings were exactly the same. This is unsatisfactory in the sense that the sensors should be able to distinguish between the different degrees of contamination. Both sensors did however give out readings that were different from the baseline. The fourth step was added later in order to make sense of the first 3 runs. This resulted in more reasonable readings.

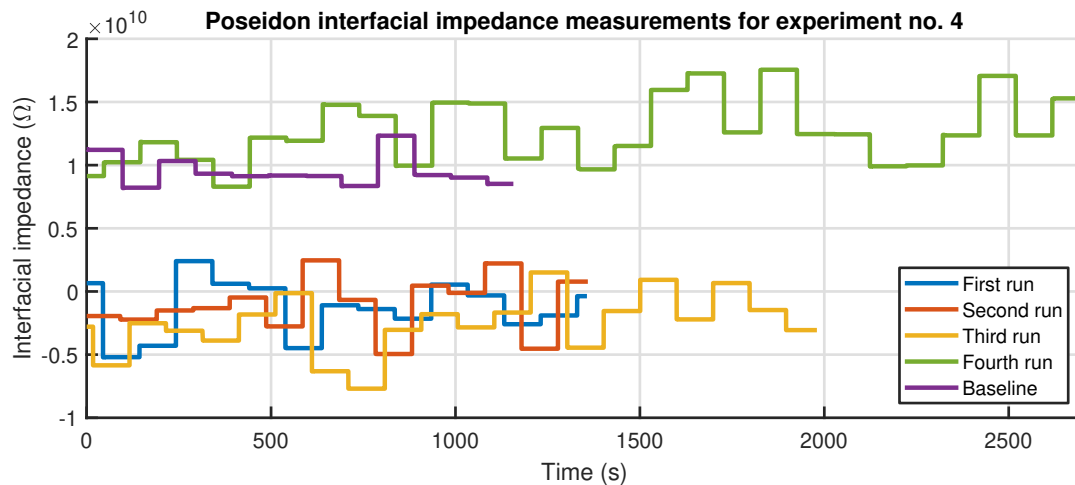


Figure 4.16.: Comparison of the Poseidon interfacial impedance data for experiment no. 4

Figure 4.16 shows the interfacial impedance data for all the runs of experiment no. 4. It was strange that the measurements for the first 3 runs most of the time were below zero and that the signals did not seem to have a negative trend. The results of the fourth run were more reasonable, but it did not decrease the as expected. It rather increased and went above the baseline readings.

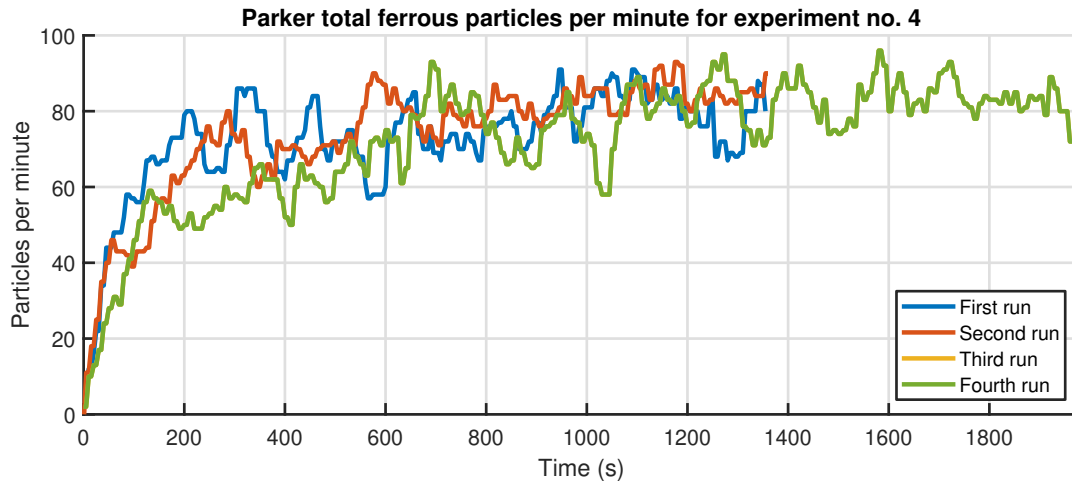


Figure 4.17.: Comparison of the Parker ferrous particle per minute data for experiment no. 4

Figure 4.17 shows the total ferrous particles per minute for all runs of experiment no. 4. It seems that the measurements converge towards ~ 80 particles per minute, when in theory should increase linearly as the debris is added to the lubrication system.

4.8. Experiment no. 5

Experiment no. 5 is the experiment being conducted with added iron silicate particle contamination.

4.8.1. Run no. 1

Figures F.36, F.37 and F.38 shows the results from the first run of experiment no. 5. A total of 12 g of iron silicate powder in 8 equal portions were added. This results in a total contamination of about ~ 4720 ppm.

The Gill sensor did not respond to the iron silicate at all, as expected. The Parker MWDS measured high amount of ferrous debris between 40 and 150 μm . This could either be left over particles from experiment no. 4 or wear because of the addition of iron silicate to the gearbox. Between experiment no. 4 and no. 5, the oil filtering was done over a duration of 15 minutes. It is likely that the contamination comes from the wear caused by the iron silicate particles considering the hardness ratio is smaller than 1 (See Section 2.3). It is probable that the iron silicate experiments has a destructive behavior on the gearbox.

The Poseidon had some interesting measurements. The interfacial impedance went below the interfacial impedance of the baseline, but not as radical as it did during experiment no. 4. Even though the Parker MWDS readings were similar. The reduction in interfacial impedance is most likely due to the generated wear debris, and not the iron silicate itself as the dielectric constant of the iron silicate and the oil itself are very similar. It is believed that this is the result that should have been expected during experiment no. 4.

4.8.2. Run no. 2

Figures F.39, F.40 and F.41 shows the results from the second run of experiment no. 5. The added contamination for this test was done exactly the same as for the first run.

The results for the second run were almost identical with the first run, except for some non-ferrous debris detected by the Parker MWDS. During experiment no. 5, there was abnormal noises coming

from the pump as the iron silicate particles went through it. Considering the high hardness of these particles, it is believed that some of these particles chipped a chuck out of the pump gears, which then got detected by the Parker MWDS.

4.8.3. Run no. 3

Figures F.42, F.43 and F.44 shows the results from the third run of experiment no. 5. The added contamination for this test was done exactly the same as for the first and second run.

The third run gave the results as the first and second run. And as with the second run, there was occurrence of a non-ferrous particle, most likely originating from the pump gears.

4.8.4. Summary

Figure 4.18 shows the total ferrous particles per minute over the duration of the three runs of experiment no. 5. The results for all runs are quite similar.

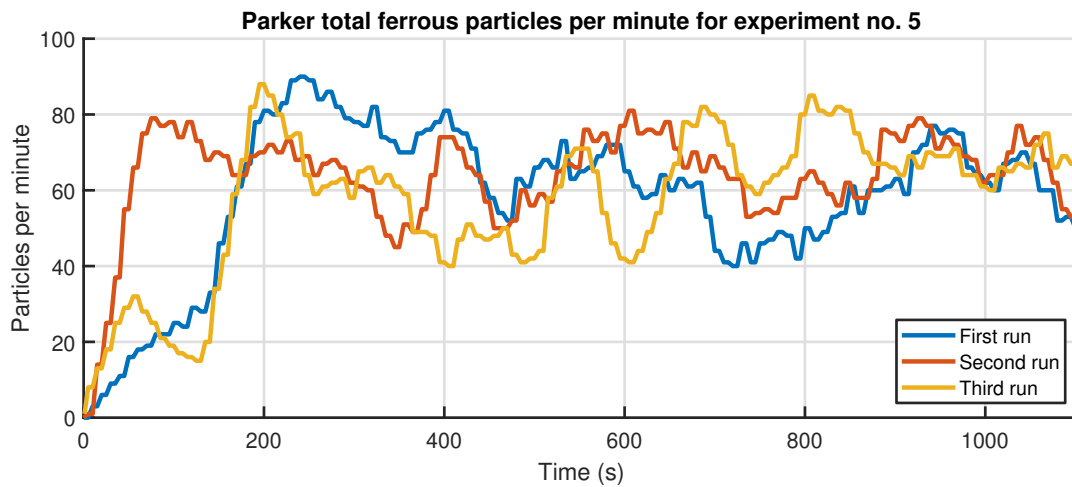


Figure 4.18.: Comparison of the Parker ferrous particle per minute data for experiment no. 5

The Poseidon measurements in Figure 4.19 were pretty consistent, laying slightly below the baseline. Experiments done over a longer time would probably be beneficial in order to have more measurements to take the average over. However, the low impedance level compared to the baseline are most certainly due to the ferrous particles, and not the iron silicate.

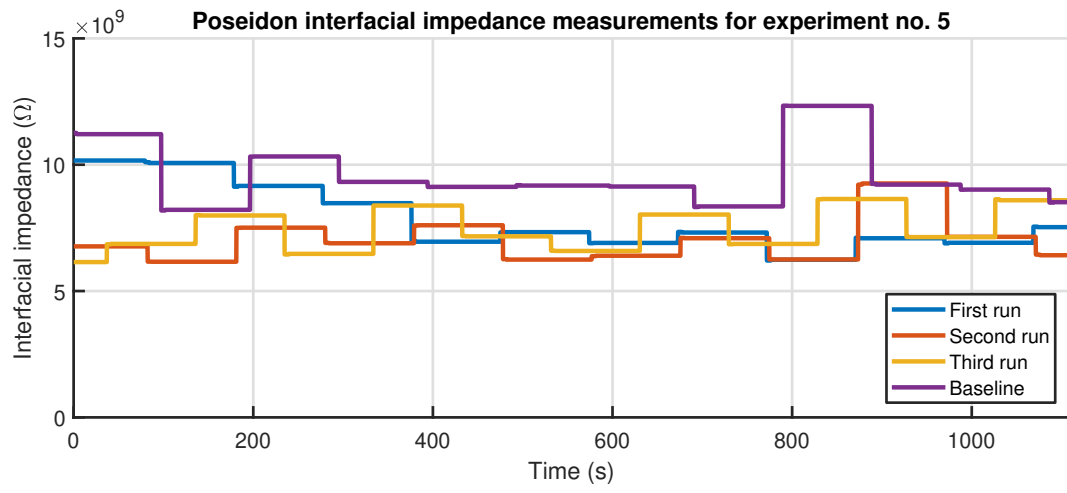


Figure 4.19.: Comparison of the Poseidon interfacial impedance data for experiment no. 5

5. Discussions

5.1. Results of Experiments

The experiments gave a lot of insights on how the particle distribution within the gearbox is. And even though there was a pump to circulate all the oil, many particles did not pass the sensors to be detected. The theory does therefore not match the sensor readings, with the actual contamination within the gearbox being higher than what is indicated by the sensors.

5.1.1. Water

The experiment done with water went as expected, with the relative humidity readings of the Poseidon being very sensitive to the added water. The Gill sensor responded to water with the recommended calibration of 10% water within the oil.

Since the water content should stay below the saturation limit anyway, a relative humidity sensor, such as the water-in-oil sensor on the Poseidon Trident QW3100 is enough. A filter to filter out the water from the oil would also be beneficial in order to increase the lifetime of the oil.

It was learned during the testing, that even with a fresh oil, it was impossible in practice to have the relative humidity content of 0%. The flushing between each run also were very difficult to do because of the lack of proper equipment and oil. The water content in the oil therefore had to be thinned out over several attempts of improper flushing of the gearbox.

All in all, this was a very interesting experiment to do. It is also very relevant to marine reduction gearboxes used in ships, and it would be interesting to do the same experiment, but with sea water and then compare the differences.

5.1.2. AISI 316L

Stainless steels should in theory be detected by both the Poseidon Trident QW3100 and Parker Kittiwake MWDS. The experiment with the AISI 316L ended up being inconclusive. The Parker MWDS did not detect the 316L particles, because the particles were under the stated detectability limit of $135\ \mu m$ or larger. The first run did give some good results, but the results could not be reproduced. It is therefore unknown if the interfacial impedance could be used as a good indicator to detect stainless steels or not.

If there had been more time, the experiment would have been done over a longer period, of maybe a couple of days. There would be easier to see the trends of the signals. The experiment should also have been done with a stainless steel gear set, such that a source of ferritic particle debris would have been eliminated. Although gears made of stainless steels exists, it is usually only used in the food industry.

5.1.3. AISI M2

The two experiments with ferritic steel particles were the ones who gave the most useful results, with two of the sensors being able to detect the particle debris. The Parker MWDS were able to detect the particles, even though the added particle count and measured particle count did not match.

The Poseidon interfacial impedance did decrease for the first 3 runs, but since the impedance level went below zero, it looked like the sensor readings were bugged. The fourth run confirmed this. The results of the fourth run gave sensible impedance readings, but they did not decrease as expected.

The interfacial impedance was higher than the baseline. Based on this, it is hard to believe that this sensor is able to detect particle contamination in the lubricant.

The Gill sensor also did detect particles, but the result was not satisfactory. Only when the contamination was 20 times higher than allowed did the sensor start to collect debris. The probe also collects more debris than the measured amount, and the limit of 0.44 g could therefore not be used as a guide to how much particle debris that has been collected by the Gill 4212. Since the particles has a hard time being attached to the probe, it is believed that the fluid velocity could be too great. The area within the sensor block could then probably be increased in order to slow the fluid velocity down. Another solution could be to mount the sensor in the gearbox, but in the flow path of the oil, as shown in Figure 5.1.

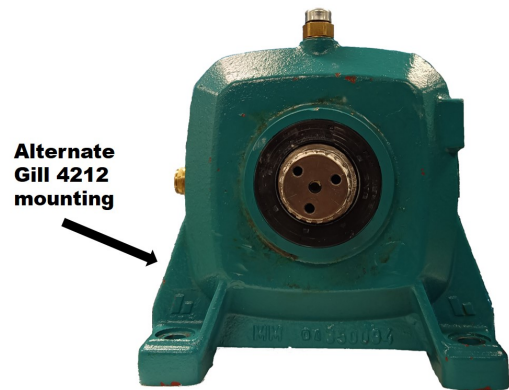


Figure 5.1.: Alternate mounting location for the Gill 4212

This substance is also probably the most relevant substance to test within a gearbox, as ferritic steels are the most commonly found materials within a gearbox.

5.1.4. Iron Silicate

It is almost certain that either of the sensors are unable to detect iron silicate particle. The ferritic particles counted by the Parker MWDS did rise, and the interfacial impedance of the Poseidon sensor did in fact decrease compared to the baseline, but this is an indirect result of the iron silicate particles being added to the gearbox, but not a direct detection of the iron silicate by the sensors. This is due to the low hardness ratio between iron silicate and common gear materials.

An optical or laser sensor would be needed to be able to detect these kind of particles. It is however very unlikely to find these kind of particles in a gearbox. This would be a result of a very dirty environment around the gearbox with improper handling of the gearbox lubrication system.

5.1.5. Contamination for Future Experiments

The experiments were done by contamination substances that were easy to obtain. If the experiments could be done again without any restrictions, the following materials would be used for contaminating the lubricant.

- Case hardened AISI 4130 ($1 - 5\ \mu\text{m}$, resembling wear)
- Case hardened AISI 4130 ($5 - 10\ \mu\text{m}$, resembling micro pitting)
- Case hardened AISI 4130 ($40 - 100\ \mu\text{m}$, resembling pitting)
- ASTM B-23 Grade 2 (Babbitt, resembling a typical plain bearing coating) [80]
- Sea water
- Water
- Sealant sludge

The contaminants would resemble most of the contaminants that could destroy a gearbox. In addition to the added contaminants, there would also be an experiment with degraded oil to see what effect this would have on the dielectric sensor readings. For the test with sealant sludge, crumb rubber from for example a soccer field could be used as an replacement.

5.2. Ease of Installation

Marine reduction gearboxes comes with both splash type and forced lubrication systems, and the ease of installing a sensor is highly dependent on the type of system. As the contamination content will vary throughout the gearbox, it is hard to find one perfect location that either measures or gather all the lubrication contaminants.

Gearboxes with splash type lubrication systems have one possibility of the sensors tested in this thesis, and that is the Gill 4212. It is then important to install the system in such a way that as much as possible of the particle debris will be collected. Normally, the sensor would be installed as a replacement of the oil drain plug in the gearbox. If that is not an option, either the particles does not reach the sensor or the available threads does not match the drain plug threads, the gearbox housing could be drilled and tapped with the right threads.

The Poseidon Trident QW3100 and Parker Kittiwake MWDS requires a closed loop lubrication system to function properly. The Poseidon requires a female -8 SAE O-ring Boss fitting to be installed in the hydraulic loop. The fitting should be located such that the sensor probe in the direct path of the oil.

The Parker MWDS is probably the easiest sensor to install as it has a threaded connection on each end. It is easily installed in lubrication systems with both hoses and pipes. The Parker is the largest of the 3 sensors, which could lead to a problem in tight spaces on ships. Due to the fluid velocity limitation, the sensor also might not fit with the current lubrication system configuration. A solution to this problem could be to run the sensor in parallel with other hydraulic lines rather than in series.

Though it might seem like an unnecessary statement, both the latter mentioned sensors should be installed before the filter in order to measure all particle debris exiting the gearbox.

5.3. Ease of Use

The data from the different sensors had to be collected using several different communication methods. The Gill used a 0 – 10 V output signal for each channel, while the Poseidon and the Parker used the Modbus protocol.

While a voltage output signal is easy to use, it becomes very complex quite fast when the number of readings for each sensor starts to increase. For the Gill sensor, which has 3 output channels, the voltage output is straightforward to use. It is also pre-configured with an alarm relay to work without a computer, if needed.

The Modbus RTU or TCP is also easy to connect, but they require a little more work in order to read the sensor data. The Modbus connection has several holding registers storing all the sensor data, which results in a large number of sensor readings with just 4 wires. As the Poseidon and Parker sensor have several output measurements, the Modbus protocol is a perfect fit.

In regards to being able to interpret the sensor measurements, the sensors are very different. The Gill sensor does what it is calibrated to do, and gives out sensor readings between 0 and 100%. If the sensor is calibrated to give out 100% with 0.1 g of particle debris at the end of the probe, the sensor will give out sensor readings based on that calibration. It should, however, be checked regularly as the amount of debris on the probe could be larger than the sensor readings. It could be a useful tool to

look at the debris collection over time, to see if the debris generation rate in the gearbox has increased or is standing still.

The Poseidon Trident QW3100 does not give the direct measurement to the contamination level, but gives out an impedance reading on the oil. As seen in Chapter 4, the impedance value seems to decrease under high contamination levels, but it is impossible to, for example, check the ISO cleanliness level by using this sensor. It should also be mentioned that it should be calibrated using worn and contaminated oil in order to find the lower impedance threshold. The sensor readings are also highly temperature-dependent, and the internal gearbox temperature should therefore not fluctuate much when doing the impedance measurements. The sensor could be used for measuring pretty much anything contaminating the oil, including having a reference signal on the oil quality, but it is very hard to interpret and should be used in addition to a particle counter as the Parker MWDS.

The Parker MWDS is pre-programmed, and all the useful measurements are already in the holding registers. Both numbers of particles, particles per minute, and mass per hour are stored in the holding registers for all particle sizes, either ferrous or non-ferrous metals. The Parker MWDS does however not have a water-in-oil sensor and should therefore be paired with such a sensor to cover the most crucial sources for gearbox failures.

5.4. Marine Reduction Gearboxes

Since the focus on this thesis is to reduce the occurrence of gearbox failures on ships, there are some areas which are more critical than others. The most relevant and dangerous contaminants are water and hardened steels. The usefulness of the sensors should therefore be considered thereafter.

The Gill 4212 could be a useful tool as it both measures the amount of debris on the probe and collects it. Unlike the Parker MWDS, which only measures particle bigger than $40\ \mu m$, the Gill can detect and collect all particle, no matter the size. The Gill is therefore able to also collect wear particles, as well as micro pitting particles. The important thing to consider is where it is mounted, to make sure that most of the particle debris is actually collected on the probe. The dielectric element is useful, but a capacitive water-in-oil sensor element would be more suitable as it is more sensitive to water.

The Poseidon Trident QW3100 has a broad area of usage, but lacks the accuracy of the Parker MWDS. The interfacial impedance could be a useful tool to measure the contamination level in the oil, but it requires a lot of testing to make sure that data is properly interpreted. The water-in-oil sensor element is a simple yet effective tool to measure the relative humidity level in the lubricant.

The Parker MWDS has the ability to detect the relevant particles with a size over $40\ \mu m$ and is therefore based on Table 2.1 able to detect particles originating from pitting or bigger. A good solution for condition monitoring on ships would be to pair a Parker MWDS with a water-in-oil sensor, such as the one in the Poseidon.

A perfect condition monitoring system on a ship should be able to measure the humidity content and oil degradation as well as detecting all ferrous particle debris originating from wear or bigger particle sizes. I.e. particles of $1\ \mu m$ or bigger. It would also be an advantage to have a sensor that could detect gasket or rubber materials, to indicate degrading or leaking gasket or sealants.

A solution to this could be pairing an optical particle debris counter with a water-in-oil sensor, such as the systems delivered by Eaton and Stauff, mentioned in Section 1.3.

The gearbox lubrication system would also contain a magnetic drain plug as well as a particle and water filtering system.

5.5. Costs

The cost for each sensor varies quite a lot, with the Poseidon being 3 times more expensive than the Gill 4212, and the Parker being 10 times more expensive than the Gill 4212. However, the costs are percentage-wise, very low, considering the total cost of a ship or the costs relating to a gearbox failure, as mentioned in Section 1.1. An introduction of condition monitoring on ships could also maybe lead to cheaper insurance costs in the future.

6. Conclusion

The work connected to this thesis revealed many key aspects of what to consider when monitoring the condition of a marine reduction gearbox.

The costs related to failures in the gearbox of the main propulsion system do results in massive costs, as the tugging and repair costs and loss of revenue could cost the insurance company several million dollars. It is, therefore, beneficial to monitor the lubrication in the gearboxes to prevent expensive failures.

A lot of sensor technology has been developed to monitor these kinds of applications, as Gill 4212, Poseidon Trident QW3100, and Parker Kittiwake MWDS tested in this thesis.

The experiments done in this thesis uncovered the usefulness of each sensor for the specific purpose of monitoring the main propulsion gearbox on a ship. As the sensors only detect contamination based on electromagnetic properties, the sensors do have their limitations to what contamination they can detect.

For marine reduction gearboxes, two kinds of lubricant contamination appear as the most dangerous and reoccurring, water, and particle debris from the gear-set itself.

The Gill 4212 does have the ability to both detect and collect magnetic particle debris, which makes it a good candidate. The particle measurements do not contain much information and should therefore be used with caution. The oil condition measurement does however, appear to be difficult and inaccurate in order to be very useful unless further development is done.

The Poseidon Trident QW3100 can be used for tracking many things, but are not very specific in its measurement. It is, therefore, very hard to interpret the results and make any conclusion about the problem with the lubricant. It can, however, be used as a guide to when a lubricant sample should be further analyzed. The integrated water-in-oil sensor, which measures the relative humidity in the lubricant, is very useful and is a sufficient tool to notify when the gearbox oil requires a change. Further testing should be done to explore all applications for the Poseidon Trident QW3100.

The Parker Kittiwake MWDS is very precise in its detection of particles and is a useful tool to detect particle debris. Even though the sensor was only tested with particles above $45\ \mu m$, it is, in theory, only supposed to detect particles originating from pitting or bigger ($> 40\ \mu m$). So even though this is sufficient to detect the most harmful particle debris, it would be beneficial if it could detect smaller particles as well, like the ones originating from wear and micro pitting. The sensor does not detect water and should, therefore, be paired with a water-in-oil sensor.

A sufficient setup would be the Parker Kittiwake MWDS paired with a water-in-oil sensor, such as the one integrated with the Poseidon Trident QW3100. The sufficient setup is not a perfect setup, and more testing with even more sensors should be done to find a better solution. Even though some of the sensors might be considered expensive, the costs in very small considering the costs of eventual failures.

Table 6.1 sums up the key properties of the tested sensor including advantages and disadvantages. A video of the laboratory setup can be seen here: <https://www.youtube.com/watch?v=HjGachKEtNM>

Table 6.1.: Specifications for the tested sensors

Sensor	Element	Method	Substance detected	Detection range	Advantage	Disadvantage	Cost
Gill 4212	Oil condition	Capacitive	Water and oil degradation	>10% Water	Easy to interpret	Low sensitivity Binary output	1x
	Debris	Inductive	Magnetic particles	NA	Mounts in gearbox housing Collects debris	Does only detect on sensor tip	
Poseidon Trident QW3100	Water-in-oil	Capacitive	Water	0-100% relative humidity	Very sensitive Easy to interpret	Does not read saturated water	3x
	Dielectric constant	Capacitive	All contamination	NA	Should be able to detect all contaminants	Hard to interpret Low sensitivity	
Parker Kittiwake MWDS	Debris	Inductive and capacitive	Ferrous metals	>40 μm	Very sensitive Tracks individual particle	Only detect metallic debris	10x
			Non-ferrous metals	>135 μm	Easy to interpret Detailed information		

6.1. Limitations

All experiments went well, even though some data suffered because of the lack of proper flushing of the gearbox. Proper flushing tools and access to more oil would possibly lead to more reliable data as the gearbox would be cleaner before a new experiment would be performed.

The period during the semester where all the experiments should have been conducted, also got postponed because of the COVID-19 crisis. This resulted in the university, including the laboratories being closed. Because of this, all experiments were delayed by one and a half months, which reduced the extensiveness of them. It also took away the time that should have been used to break in the new gear-set.

6.2. Future Work

Even though much work was done, there is still more testing to do to find the best combination of sensors in oil condition monitoring.

Several other sensors based on different sensor technology should be tested. Optical and laser sensor should be tested as they do not get data based on electromagnetic properties of the measured medium, but rather by light. A water-in-oil sensor measuring the absolute water content would also be interesting to try as the water saturation limit of the lubricant by correlating the data from the relative humidity sensor in the Poseidon Trident QW3100.

As the sensor data did not show a significant increase in contamination as the experiments were done, it would also be beneficial to do the tests with a longer duration between each time contamination was added. This will both allow the contamination to be properly mixed in the lubricant and to let the sensor signals stabilize.

It would also be interesting to do experiments with different materials than the once used in this thesis. Such as gasket or sealant materials, as well as particle debris matching the sizes generated by the different failure modes, explained in Section 2.3.

Bibliography

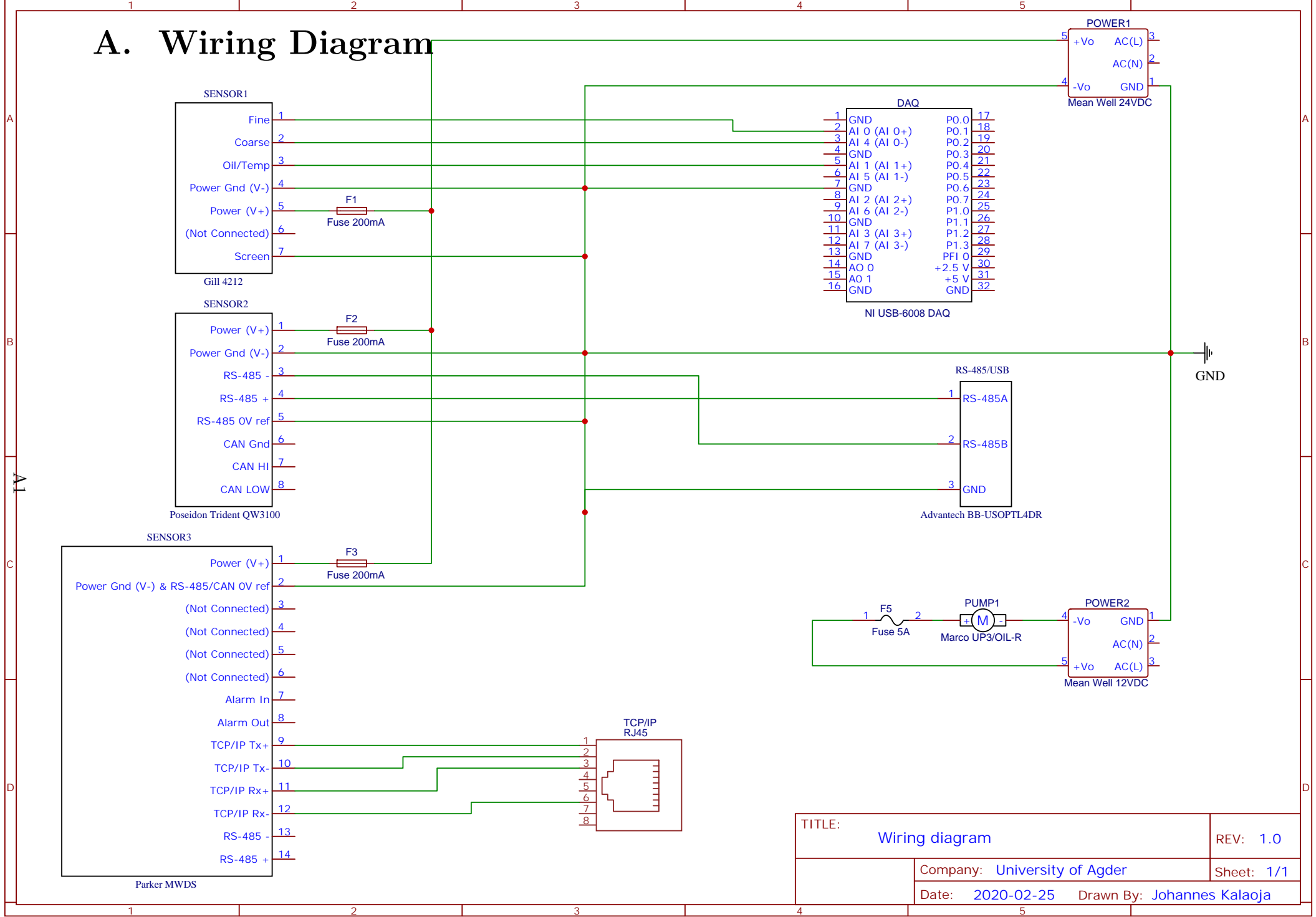
- [1] Apex Dynamics. *Gear History – Where Do Gearboxes Originate?* June 2015. URL: <https://www.apexdyna.nl/en/gear-history/> (visited on 01/13/2020).
- [2] UNCTAD. *Review of Maritime Transport 2019*. 2019. URL: https://unctad.org/en/PublicationsLibrary/rmt2019_en.pdf (visited on 01/15/2020).
- [3] Willem Dirk Van Os. “Device for detecting loose metal parts in the oiling systems of power plants”. U.S. pat. 2252222A. Aug. 12, 1941.
- [4] James C. Booth. “Warning magnetic unit”. U.S. pat. 2462715A. Feb. 22, 1949.
- [5] Edmund W. Bourne Jr. “Engine failure warning device”. U.S. pat. 2429920A. Oct. 28, 1947.
- [6] Edmund W. Bourne Jr. “Signal plug for engine failure warning systems”. U.S. pat. 2450630A. Oct. 5, 1948.
- [7] Wallace H Coulter. “Means for counting particles suspended in a fluid”. U.S. pat. 2656508A. Oct. 20, 1953.
- [8] Dietrich W. Botstiber. “Magnetic chip detector”. U.S. pat. 2936890A. May 17, 1960.
- [9] Dietrich W. Botstiber. “Chip detector for magnetic and non-magnetic conductive particles”. U.S. pat. 3432750A. Mar. 11, 1969.
- [10] Marvin A. Remke and Louis E. Kuntz. “Measuring the water content in oil and water mixtures”. U.S. pat. 3133437A. Phillips Petroleum Co. May 19, 1964.
- [11] David J Chleck. “Method of measuring the water content of liquid hydrocarbons”. U.S. pat. 3539917A. GE Infrastructure Sensing LLC. Nov. 10, 1970.
- [12] Luc Yves Natens and Jean Martha De Gueldre. “Apparatus for detecting metallic particles in a flow of dielectric medium”. U.S. pat. 4004216A. Agfa Gevaert NV. Jan. 18, 1977.
- [13] James R. Hobbie. “Lubricant contamination warning device”. U.S. pat. 4008464A. Eaton Corp. Feb. 15, 1977.
- [14] James H. Magee and Thomas E. Tauber. “Lubricating oil debris monitoring system”. U.S. pat. 4219805A. Vickers Inc. Aug. 26, 1980.
- [15] James H. Magee and Thomas E. Tauber. “Wear particle disintegrator monitor”. U.S. pat. 4302754A. Vickers Inc. Nov. 24, 1981.
- [16] Brian G. McGee and Noel J. Rytter. “Conductive particle sensor using a magnet”. U.S. pat. 5179346A. Caterpillar Inc. Jan. 12, 1993.
- [17] Keith W. Chambers and Clinton A. Waggoner. “Method and apparatus for on-line monitoring of wear in machinery”. U.S. pat. 4651091A. Canada Minister of National Defence. Mar. 17, 1987.
- [18] Paul H. Nielsen. “Device and method for detecting ferrous particles entrained in a fluid.” French pat. 2673290A1. Vickers Inc. Feb. 10, 1995.
- [19] Kytola. *OILAN Water In Oil Analyzer*. Apr. 2020. URL: <https://www.kytola.com/products/oil-analyzers/oilan-water-in-oil-analyzer> (visited on 04/27/2020).
- [20] Parker Kittiwake. *Metallic Wear Debris Sensor Instruction Manual*. 12th ed. Parker Kittiwake. 3 - 6 Thorgate Road Littlehampton West Sussex BN17 7LU United Kingdom, 2019.
- [21] Eaton. *WSPS 05*. Apr. 2020. URL: <https://www.eaton.com/us/en-us/catalog/filters-strainers/wsps-05.html> (visited on 04/27/2020).
- [22] Kongsberg. *WATER IN OIL SENSOR*. Apr. 2020. URL: <https://www.kongsberg.com/maritime/products/engines-engine-room-and-automation-systems/Machinery-Instrumentation/engine-monitoring-systems/water-in-oil-sensor/> (visited on 04/27/2020).

- [23] Pall. *Pall WS12/WS13 Series Water Sensor*. Apr. 2020. URL: <https://shop.pall.com/us/en/industrial-manufacturing/industrial-and-mobile-oem/medium-light-fuel/pall-ws12/ws13-series-water-sensor-zidie4cr54e> (visited on 04/27/2020).
- [24] Jeremy Wright. *Benefits of FTIR Oil Analysis*. Apr. 2020. URL: <https://www.machinerylubrication.com/Read/30205/ftir-oil-analysis> (visited on 04/27/2020).
- [25] Carl S. Byington and David C. Schalcosky. *Advances in Real Time Oil Analysis*. Nov. 2000. URL: <https://www.machinerylubrication.com/Read/138/real-time-oil-analysis> (visited on 03/02/2020).
- [26] Stauff. *Oil Condition Sensor OCS*. Apr. 2020. URL: <https://www.stauff.com/index.php?id=6870%5C&L=1> (visited on 04/26/2020).
- [27] Stauff. *Laser Particle Counter - Inline*. Catalog. 2019.
- [28] Eaton. *CCT 01-set*. Apr. 2020. URL: <https://www.eaton.com/us/en-us/catalog/filters-strainers/cct-01.html> (visited on 04/27/2020).
- [29] Stauff. *Laser Particle Counters LasPaC-II*. Apr. 2020. URL: <https://www.stauff.com/index.php?id=4400%5C&L=1%5C&MP=4398-4399> (visited on 04/26/2020).
- [30] Stauff. *Particle Monitors LPM-II-plus*. Apr. 2020. URL: <https://www.stauff.com/index.php?id=6333%5C&L=1> (visited on 04/26/2020).
- [31] Parker Kittiwake. *XRF Analyser*. Catalog. 2018.
- [32] Bary Wilson et al. "Development of a Modular In-Situ Oil Analysis Prognostic System". In: Jan. 1999.
- [33] Lechun Xie et al. "Effect of Surface Hardening Technique and Case Depth on Rolling Contact Fatigue Behavior of Alloy Steels". In: *Tribology Transactions* 58 (Dec. 2014), pp. 215–224. DOI: [10.1080/10402004.2014.960957](https://doi.org/10.1080/10402004.2014.960957).
- [34] Kenneth C. Ludema and Oyelayo O. Ajayi. *Friction, Wear, Lubrication: A Textbook in Tribology*. second. 6000 Broken Sound Parkway NW, Suite 300: CRC Press, 2019. ISBN: 978-1-4822-1017-0.
- [35] Robert L. Norton. *Machine Design: An Integrated Approach*. fourth. Pearson, 2010. ISBN: 978-0-13-612370-5.
- [36] ASM International. *ASM Handbook: Volume 18: Friction, Lubrication, and Wear Technology*. tenth. Vol. 18. ASM Handbook. ASM International, July 1992. ISBN: 978-0-8717-0380-4.
- [37] Bharat Bhushan. *Modern Tribology Handbook, Two Volume Set*. first. Boca Raton, FL: CRC Press, Dec. 2000. ISBN: 978-0-8493-8403-5.
- [38] Nikolai K. Myshkin and Liubou V. Markova. *On-line Condition Monitoring in Industrial Lubrication and Tribology*. Springer, 2018. ISBN: 978-3-319-61133-4.
- [39] Wei Hong et al. "Mechanical wear debris feature, detection, and diagnosis: A review". In: *Chinese Journal of Aeronautics* 31.5 (2018), pp. 867–882. ISSN: 1000-9361. DOI: <https://doi.org/10.1016/j.cja.2017.11.016>. URL: <http://www.sciencedirect.com/science/article/pii/S1000936117302637>.
- [40] Neale Consulting Engineers. *How To Diagnose Gear Failures*. 2016. URL: <http://www.tribology.co.uk/services/failure-analysis/how-to-diagnose-gear-failures/> (visited on 01/24/2020).
- [41] Lawrence Kren. *Recognizing gear failures*. June 2007. URL: <https://www.machinedesign.com/news/article/21816731/recognizing-gear-failures> (visited on 01/14/2020).
- [42] Robert C. Juvinall and Kurt M. Marshek. *Fundamentals of Machine Component Design*. sixth. John Wiley & Sons Inc, 2017. ISBN: 978-1-118-98768-1.
- [43] *Standard Guide for Microscopic Characterization of Particles from In-Service Lubricants*. Standard ASTM D 7684 - 1. West Conshohocken, PA: ASTM International, 2016.
- [44] Gill Sensors and Controls. *The common causes of gearbox failure*. URL: <https://www.gillsc.com/assets/Uploads/Factsheet-The-common-causes-of-gearbox-failure.pdf> (visited on 01/20/2020).
- [45] Amiya R. Mohanty. *Machinery Condition Monitoring: Principles and Practices*. CRC Press, 2019. ISBN: 978-1-4665-9305-3.

- [46] Eaton. *Condition monitoring and analysis of hydraulic and lubrication fluids*. Catalog. Mar. 2018.
- [47] *Hydraulic fluid power — Fluids — Method for coding the level of contamination by solid particles*. Standard ISO 4406:2017. Geneva, CH: International Organization for Standardization, Aug. 2017.
- [48] Wolfgang Bock. “Industrial Gear Oils”. In: *Encyclopedia of Lubricants and Lubrication*. Ed. by Theo Mang. Berlin, Heidelberg: Springer Berlin Heidelberg, 2014, pp. 977–994. ISBN: 978-3-6422-2647-2. DOI: [10.1007/978-3-642-22647-2_282](https://doi.org/10.1007/978-3-642-22647-2_282). URL: https://doi.org/10.1007/978-3-642-22647-2_282.
- [49] A. A. Carey and A. J. Hayzen. *Dielectric Constant and Oil Analysis*. Sept. 2001. URL: <https://www.machinerylubrication.com/Read/226/dielectric-constant-oil-analysis> (visited on 02/10/2020).
- [50] *Standard Specification for Chromium and Chromium-Nickel Stainless Steel Plate, Sheet, and Strip for Pressure Vessels and for General Applications*. Standard ASTM A 240 - 16a. West Conshohocken, PA: ASTM International, Dec. 2016.
- [51] Engineering ToolBox. *Permeability*. 2016. URL: https://www.engineeringtoolbox.com/permeability-d_1923.html (visited on 02/05/2020).
- [52] ASM International. *ASM Handbook: Volume 1: Properties and Selection: Irons, Steels, and High-Performance Alloys*. tenth. Vol. 1. ASM Handbook. ASM International, July 1990. ISBN: 978-0-8717-0377-4.
- [53] *Standard Specification for Tool Steel High Speed*. Standard ASTM A 600 - 92a. West Conshohocken, PA: ASTM International, 2016.
- [54] Yonghui Wei et al. “Magnetic-field tribological behaviors of aluminum-alloy and steel”. In: *AIP Advances* 8.11 (2018), p. 115014. DOI: [10.1063/1.5049877](https://doi.org/10.1063/1.5049877).
- [55] MatWeb. *AISI Type M2 Molybdenum High Speed Tool Steel (UNS T11302)*. 2020. URL: <http://www.matweb.com/search/datasheet.aspx?matguid=28fdb77f07524170ab825dff9fda8a84> (visited on 02/06/2020).
- [56] Biltema. *Biltema*. URL: <https://www.biltema.no/> (visited on 02/17/2020).
- [57] Thomas J. Ahrens. *Rock Physics & Phase Relations: A Handbook of Physical Constants*. Vol. 3. AGU Reference Shelf Series. American Geophysical Union, 1995. ISBN: 978-0-8759-0853-3.
- [58] Q. Williams et al. “Structural and electronic properties of Fe₂SiO₄-fayalite at ultrahigh pressures: Amorphization and gap closure”. In: *Journal of Geophysical Research: Solid Earth* 95.B13 (1990), pp. 21549–21563. DOI: [10.1029/JB095iB13p21549](https://doi.org/10.1029/JB095iB13p21549).
- [59] R. D. Shannon et al. “Dielectric constants of tephroite, fayalite and olivine and the oxide additivity rule”. In: *Physics and Chemistry of Minerals* 18.1 (July 1991), pp. 1–6. DOI: [10.1007/BF00199037](https://doi.org/10.1007/BF00199037).
- [60] Pall. *Measuring Water Content As Percent Of Saturation*. URL: <https://www.pall.com/en/solutions/water-content.html> (visited on 03/03/2020).
- [61] Hendrik Karl and Steffen Bots. *Humidity Saturation Limits of Hydraulic and Lubrication Fluids*. URL: <https://www.machinerylubrication.com/Read/28697/humidity-saturation-limits> (visited on 03/03/2020).
- [62] Marianne Duncanson. *Detecting and Controlling Water in Oil*. Sept. 2005. URL: <https://www.machinerylubrication.com/Read/787/detecting-water-in-oil> (visited on 03/04/2020).
- [63] Noria Corporation. *Water In Oil Contamination*. July 2001. URL: <https://www.machinerylubrication.com/Read/192/water-contaminant-oil> (visited on 02/09/2020).
- [64] Engineering ToolBox. *Electrical Conductivity of common Materials*. 2008. URL: https://www.engineeringtoolbox.com/conductors-d_1381.html (visited on 02/06/2020).
- [65] Machinery Lubrication. *Online Sensor Measures Dissolved Water in Lubricating Oils and Hydraulic Fluids*. Jan. 2003. URL: <https://www.machinerylubrication.com/Read/434/dissolved-water-oil-sensor> (visited on 02/09/2020).

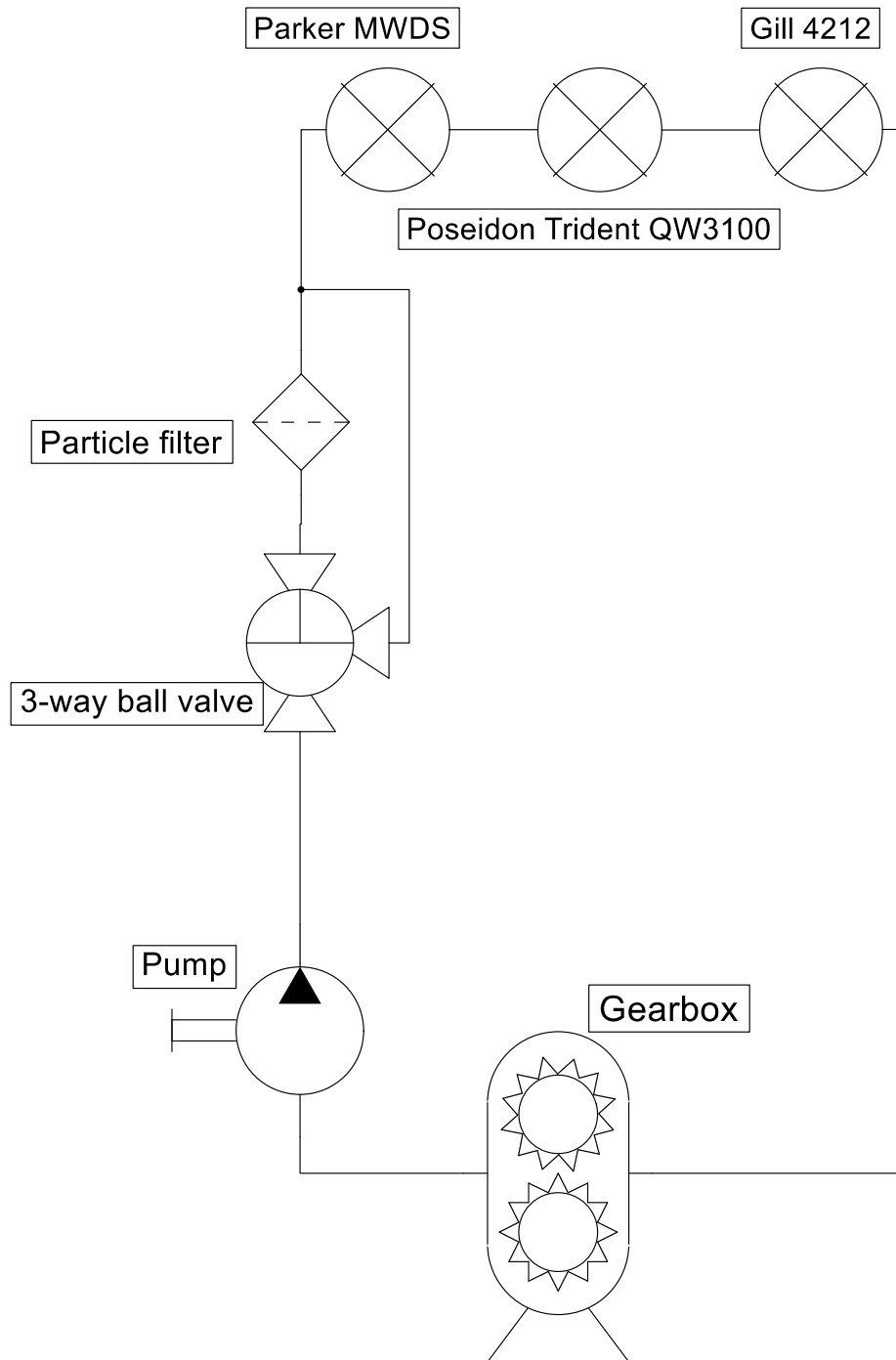
- [66] Gill Sensors & Controls Limited. *Oil Condition Monitoring Sensor User Manual*. 5th ed. Gill Sensors & Controls Limited. Unit 600, Ampress Park, Lymington, Hampshire, SO41 8LW, UK, Apr. 2018.
- [67] LLC Poseidon Systems. *Trident QM3100™/QW3100™ User's Manual*. C. Poseidon Systems, LLC. 200 Canal View Blvd. Rochester, NY 14623, May 2018.
- [68] Ray Garvey. *The Effects of Viscosity on Optical Particle Counting*. May 2007. URL: <https://www.machinerylubrication.com/Read/1029/viscosity-effects> (visited on 02/24/2020).
- [69] Brevini. *Brevini® Planetary Gearboxes Industrial Series*. Catalog. July 2019.
- [70] *Industrial liquid lubricants - ISO viscosity classification*. Standard ISO 3448:1992. Geneva, CH: International Organization for Standardization, Sept. 1992.
- [71] MARCO s.p.a. *UP3/OIL-R Revers. pump lubricating oil + integr.on/off switch*. Feb. 2020. URL: <https://items.marco.it/en/up3-oil-r-revers-pump-lubricating-oil-integr-on-off-switch.html> (visited on 02/24/2020).
- [72] MARCO s.p.a. *Self-Priming Electric Pump for Transferring Various Liquids*. 3rd ed. MARCO s.p.a. Via Mameli 10 - 25014 Castenedolo (Brescia) – Italy, May 2016.
- [73] *Connections for General Use and Fluid Power - Ports and Stud Ends with ASME B1.1 Threads and O-Ring Sealing - Part 1: Threaded Port with O-Ring Seal in Truncated Housing*. Standard SAE J1926/1. 400 Commonwealth Drive, Warrendale, PA 15096: SAE International, 2016.
- [74] National Instruments. *USB-6008*. 2020. URL: <https://www.ni.com/en-no/support/model-usb-6008.html> (visited on 03/06/2020).
- [75] Isaac Noh. *Data Acquisition*. MATLAB Central File Exchange. Mar. 2020. URL: <https://www.mathworks.com/matlabcentral/fileexchange/44234-data-acquisition>.
- [76] Advantech B+B SmartWorx. *Isolated USB to RS-422/485 Converters*. Advantech. 707 Dayton Road, PO Box 1040 Ottawa, IL 61350 USA, July 2019.
- [77] Ølbrygging. *Sterilt prøveglass, 50 ml*. Apr. 2020. URL: <https://www.olbrygging.no/m%C3%A5leutstyr-og-tilbeh%C3%B8r/100171/sterilt-pr%C3%B8veglass-50-ml> (visited on 04/22/2020).
- [78] Farmasiet. *BD Emerald sprøyte 2ml luer sentrert*. Apr. 2020. URL: <https://www.farmasiet.no/product/1120747/hjelpemidler-og-utstyr/injeksjonsutstyr/bd-emerald-sproeyte-2ml-luer-sentrert> (visited on 04/22/2020).
- [79] MatWeb. *AISI Type 316L Stainless Steel, annealed sheet*. 2020. URL: <http://www.matweb.com/search/DataSheet.aspx?MatGUID=1336be6d0c594b55afb5ca8bf1f3e042> (visited on 03/03/2020).
- [80] William Rowland Ltd. *BABBITT METAL - WHAT IS IT AND WHAT DO WE USE IT FOR?* June 2016. URL: <https://www.william-rowland.com/news/item/babbitt-metal-we-use-it-for> (visited on 05/21/2020).

A. Wiring Diagram

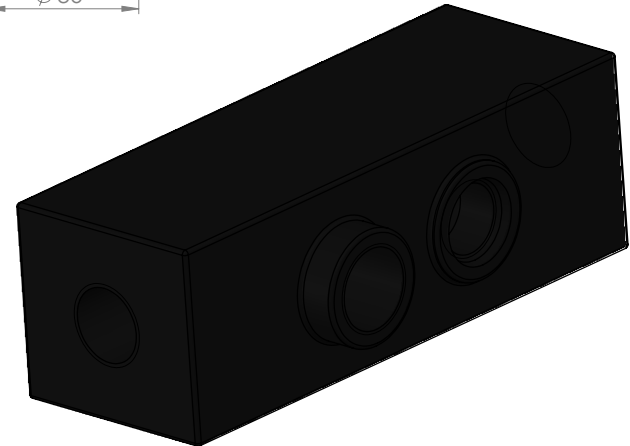
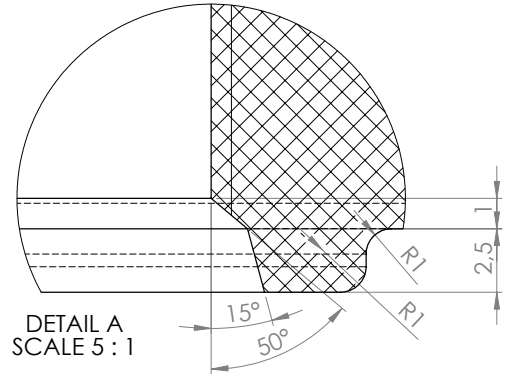
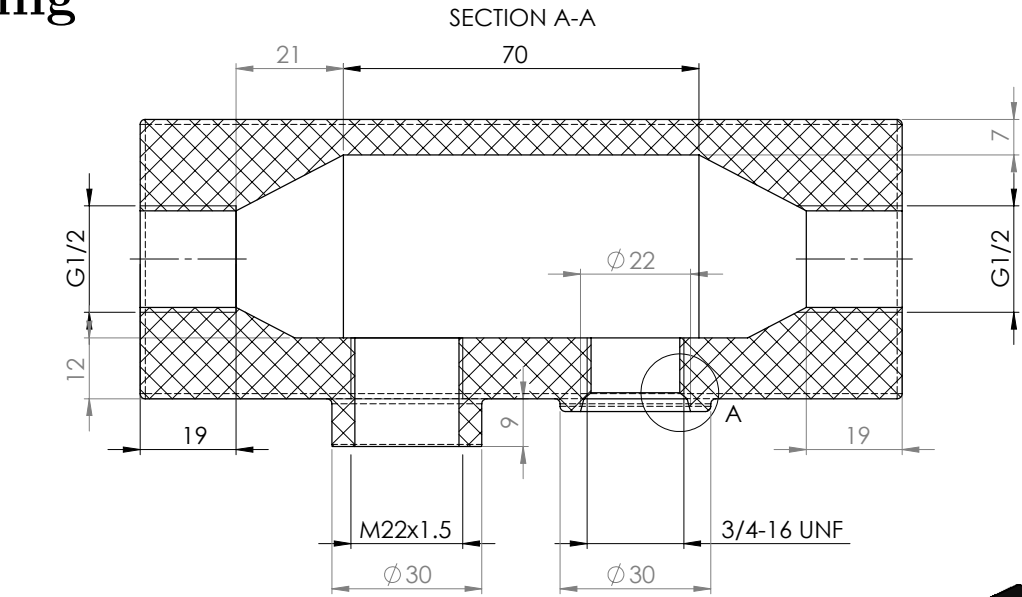
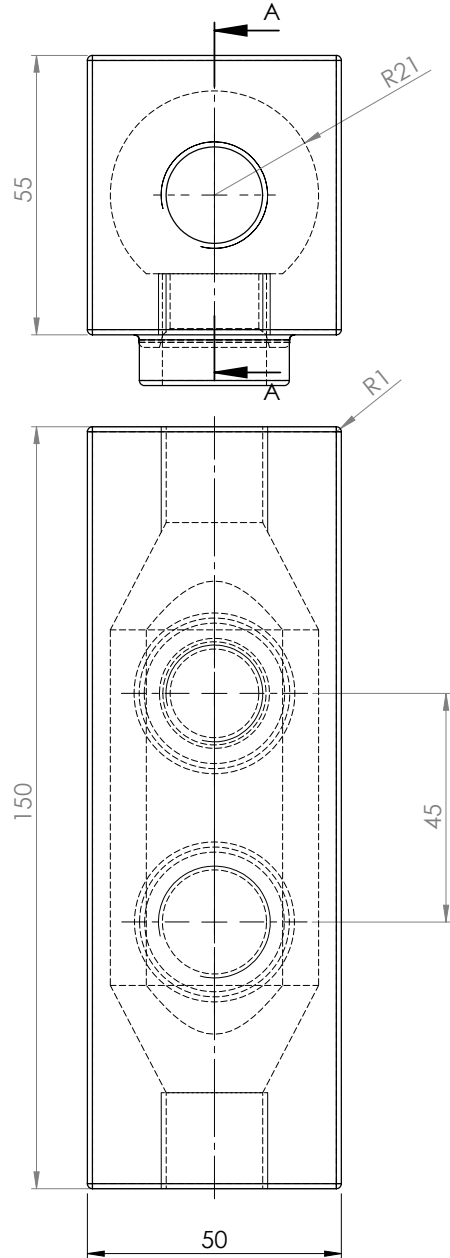


TITLE: Wiring diagram		REV: 1.0
Company: University of Agder		Sheet: 1/1
Date: 2020-02-25	Drawn By: Johannes Kalaoja	

B. Plumbing diagram

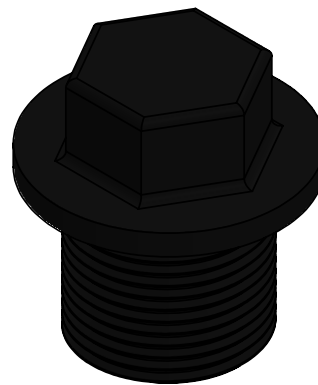
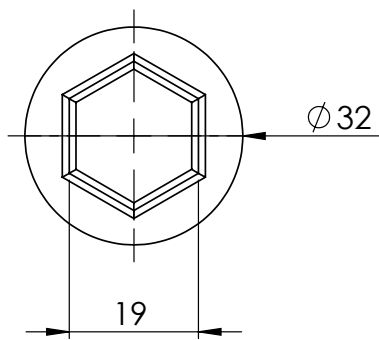
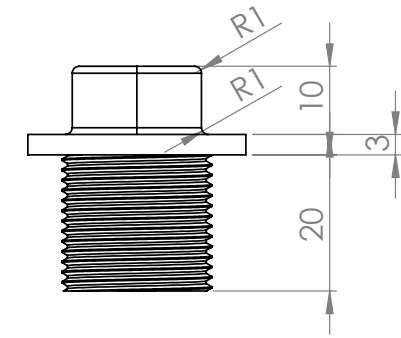


C. Sensor Block Drawing



UNLESS OTHERWISE SPECIFIED: DIMENSIONS ARE IN MILLIMETERS			FINISH:		DEBURR AND BREAK SHARP EDGES		DO NOT SCALE DRAWING		REVISION	
SURFACE FINISH:										
TOLERANCES:										
LINEAR:										
ANGULAR:										
DRAWN		NAME	SIGNATURE	DATE				TITLE: Sensor block		
CHK'D										
APP'VD										
MFG										
Q.A					MATERIAL: ASA		DWG NO. sensorblock		A3	
					WEIGHT: 0.3		SCALE: 1:1		SHEET 1 OF 1	

D. M22x1.5 Plug



UNLESS OTHERWISE SPECIFIED:
DIMENSIONS ARE IN MILLIMETERS
SURFACE FINISH:
TOLERANCES:
LINEAR:
ANGULAR:

FINISH:

DEBURR AND
BREAK SHARP
EDGES

DO NOT SCALE DRAWING

REVISION

	NAME	SIGNATURE	DATE		
DRAWN					
CHK'D					
APP'V'D					
MFG					
Q.A					
				MATERIAL:	
				PLA	
				WEIGHT: 0	

TITLE:
M22x1.5 Plug

DWG NO.
M22x1.5 plug

A4

SCALE: 1:1 SHEET 1 OF 1

E. MATLAB scripts

E.1. Script for plotting Gill 4212 sensor data

```
clc; close all; clear;
load GillData3-1.mat
load timeStamps3-1.mat

GillData = GillData(any(GillData,2),:);

% Extracts the time array from the data
t_end = length(GillData)*0.1;
time = 0:0.1:t_end-0.1;
time = time';

% Converts fine debris voltage signal to debris contamination
fineVoltage = GillData(:, 2);
fine = fineVoltage*(100/10);

% Converts coarse debris voltage signal to debris contamination
coarseVoltage = GillData(:, 4);
coarse = coarseVoltage*(100/10);

% Converts oil voltage signal to oil quality signal
oilVoltage = GillData(:, 3);
oil = oilVoltage*(100/10);

% Plots fine and coarse debris signals
figure('Renderer', 'painters', 'Position', [10 10 960 560])
ax1 = subplot(2, 1, 1, 'Position', [0.1 0.52 0.83 0.37]);
plot(time, [fine coarse], 'LineWidth', 2.5)
title('Particle debris')
legend({'Fine', 'Coarse'}, 'Location', 'northwest', 'NumColumns', 2, 'FontSize', 11)
ylabel('Debris contamination (%)')
xlim([0 time(end)])
ylim([0 100])
ax1.FontSize = 11;
```



```

set(gca, 'linewidth', 1.5)
xline(sedimentTimeStamp(1), '-', {'Step 2', 'Added 50mg'}, 'LabelVerticalAlignment', 'middle', 'LabelHorizontalAlignment',
    ↪ 'center', 'FontSize', 11);
xline(sedimentTimeStamp(2), '-', {'Step 3', 'Added 50mg'}, 'LabelVerticalAlignment', 'middle', 'LabelHorizontalAlignment',
    ↪ 'center', 'FontSize', 11);
xline(sedimentTimeStamp(3), '-', {'Step 4', 'Added 50mg'}, 'LabelVerticalAlignment', 'middle', 'LabelHorizontalAlignment',
    ↪ 'center', 'FontSize', 11);
xline(sedimentTimeStamp(4), '-', {'Step 5', 'Added 50mg'}, 'LabelVerticalAlignment', 'middle', 'LabelHorizontalAlignment',
    ↪ 'center', 'FontSize', 11);
xline(sedimentTimeStamp(5), '-', {'Step 6', 'Added 50mg'}, 'LabelVerticalAlignment', 'middle', 'LabelHorizontalAlignment',
    ↪ 'center', 'FontSize', 11);
xline(sedimentTimeStamp(6), '-', {'Step 7', 'Added 50mg'}, 'LabelVerticalAlignment', 'middle', 'LabelHorizontalAlignment',
    ↪ 'center', 'FontSize', 11);
xline(sedimentTimeStamp(7), '-', {'Step 8', 'Added 50mg'}, 'LabelVerticalAlignment', 'middle', 'LabelHorizontalAlignment',
    ↪ 'center', 'FontSize', 11);
xline(sedimentTimeStamp(8), '-', {'Step 9', 'Added 50mg'}, 'LabelVerticalAlignment', 'middle', 'LabelHorizontalAlignment',
    ↪ 'center', 'FontSize', 11);
xline(sedimentTimeStamp(9), '-', {'Step 10', 'Added 50mg'}, 'LabelVerticalAlignment', 'middle', 'LabelHorizontalAlignment',
    ↪ 'center', 'FontSize', 11);
xline(sedimentTimeStamp(10), '-', {'Step 11', 'Added 50mg'}, 'LabelVerticalAlignment', 'middle',
    ↪ 'LabelHorizontalAlignment', 'center', 'FontSize', 11);

% Plots oil quality signal
ax2 = subplot(2, 1, 2, 'Position', [0.1 0.08 0.83 0.37]);
plot(time, oil, 'Color', [0.9290 0.6940 0.1250], 'LineWidth', 2.5)
title('Oil condition')
legend('Oil condition', 'Location', 'northwest', 'NumColumns', 1, 'FontSize', 11)
ylabel('Oil status alarm (%)')
xlim([0 time(end)])
ylim([0 100])
ax2.FontSize = 11;
set(gca, 'linewidth', 1.5)
linkaxes([ax1, ax2], 'x')
xlabel('Time (s)')

```

```
xline(sedimentTimeStamp(1), '-', {'Step 2', 'Added 50mg'}, 'LabelVerticalAlignment', 'middle', 'LabelHorizontalAlignment',  
↳ 'center', 'FontSize', 11);  
xline(sedimentTimeStamp(2), '-', {'Step 3', 'Added 50mg'}, 'LabelVerticalAlignment', 'middle', 'LabelHorizontalAlignment',  
↳ 'center', 'FontSize', 11);  
xline(sedimentTimeStamp(3), '-', {'Step 4', 'Added 50mg'}, 'LabelVerticalAlignment', 'middle', 'LabelHorizontalAlignment',  
↳ 'center', 'FontSize', 11);  
xline(sedimentTimeStamp(4), '-', {'Step 5', 'Added 50mg'}, 'LabelVerticalAlignment', 'middle', 'LabelHorizontalAlignment',  
↳ 'center', 'FontSize', 11);  
xline(sedimentTimeStamp(5), '-', {'Step 6', 'Added 50mg'}, 'LabelVerticalAlignment', 'middle', 'LabelHorizontalAlignment',  
↳ 'center', 'FontSize', 11);  
xline(sedimentTimeStamp(6), '-', {'Step 7', 'Added 50mg'}, 'LabelVerticalAlignment', 'middle', 'LabelHorizontalAlignment',  
↳ 'center', 'FontSize', 11);  
xline(sedimentTimeStamp(7), '-', {'Step 8', 'Added 50mg'}, 'LabelVerticalAlignment', 'middle', 'LabelHorizontalAlignment',  
↳ 'center', 'FontSize', 11);  
xline(sedimentTimeStamp(8), '-', {'Step 9', 'Added 50mg'}, 'LabelVerticalAlignment', 'middle', 'LabelHorizontalAlignment',  
↳ 'center', 'FontSize', 11);  
xline(sedimentTimeStamp(9), '-', {'Step 10', 'Added 50mg'}, 'LabelVerticalAlignment', 'middle', 'LabelHorizontalAlignment',  
↳ 'center', 'FontSize', 11);  
xline(sedimentTimeStamp(10), '-', {'Step 11', 'Added 50mg'}, 'LabelVerticalAlignment', 'middle',  
↳ 'LabelHorizontalAlignment', 'center', 'FontSize', 11);  
xlim([0 time(end)])  
  
sgtitle('Gill 4212 Experiment 3-1')  
set(0, 'DefaultLegendAutoUpdate', 'off')  
  
export_fig GillExperiment3-1.pdf -a4 -q101 -transparent -nocrop
```

E.2. Script for plotting Poseidon Trident QW3100 sensor data

```

clc; clear; close all;

% Extracts the time array from the data
load Experiment3-1.mat

time = readPoseidon(:, 1);
SSTemp = readPoseidon(1, 4); %Degrees - Steady state temperature

% Filtering based on temperature
for i = 1:length(readPoseidon)
    tempDiff = abs(readPoseidon(i, 5) - readPoseidon(i, 4));
    SSTempDiff = abs(readPoseidon(i, 5) - SSTemp);
    if (tempDiff >= 1 || SSTempDiff >= 10)
        readPoseidon(i, 8) = 0;
    end
end

% Plots relative humidity
figure('Renderer', 'painters', 'Position', [10 10 960 860])
ax1 = subplot(3, 1, 1, 'Position', [0.1 0.66 0.83 0.23]);
plot(time, readPoseidon(:, 2)/100, 'color', [0 0.4470 0.7410], 'LineWidth', 2.5)
ylim([0 100])
ylabel('Relative humidity (%)')
title('Water-in-oil')
legend('% Relative humidity', 'Location', 'northwest', 'NumColumns', 1, 'FontSize', 11);
ax1.FontSize = 11;
set(gca, 'linewidth', 1.5)
xline(sedimentTimeStamp(1), '-', {'Step 2', 'Added 50mg'}, 'LabelVerticalAlignment', 'middle', 'LabelHorizontalAlignment',
    ↪ 'center', 'FontSize', 11);
xline(sedimentTimeStamp(2), '-', {'Step 3', 'Added 50mg'}, 'LabelVerticalAlignment', 'middle', 'LabelHorizontalAlignment',
    ↪ 'center', 'FontSize', 11);
xline(sedimentTimeStamp(3), '-', {'Step 4', 'Added 50mg'}, 'LabelVerticalAlignment', 'middle', 'LabelHorizontalAlignment',
    ↪ 'center', 'FontSize', 11);

```

```

xline(sedimentTimeStamp(4), '-', {'Step 5', 'Added 50mg'}, 'LabelVerticalAlignment', 'middle', 'LabelHorizontalAlignment',
↳ 'center', 'FontSize', 11);
xline(sedimentTimeStamp(5), '-', {'Step 6', 'Added 50mg'}, 'LabelVerticalAlignment', 'middle', 'LabelHorizontalAlignment',
↳ 'center', 'FontSize', 11);
xline(sedimentTimeStamp(6), '-', {'Step 7', 'Added 50mg'}, 'LabelVerticalAlignment', 'middle', 'LabelHorizontalAlignment',
↳ 'center', 'FontSize', 11);
xline(sedimentTimeStamp(7), '-', {'Step 8', 'Added 50mg'}, 'LabelVerticalAlignment', 'middle', 'LabelHorizontalAlignment',
↳ 'center', 'FontSize', 11);
xline(sedimentTimeStamp(8), '-', {'Step 9', 'Added 50mg'}, 'LabelVerticalAlignment', 'middle', 'LabelHorizontalAlignment',
↳ 'center', 'FontSize', 11);
xline(sedimentTimeStamp(9), '-', {'Step 10', 'Added 50mg'}, 'LabelVerticalAlignment', 'middle', 'LabelHorizontalAlignment',
↳ 'center', 'FontSize', 11);
xline(sedimentTimeStamp(10), '-', {'Step 11', 'Added 50mg'}, 'LabelVerticalAlignment', 'middle',
↳ 'LabelHorizontalAlignment', 'center', 'FontSize', 11);

% Plots interfacial impedance
ax2 = subplot(3, 1, 2, 'Position', [0.1 0.37 0.83 0.23]);
plot(time, readPoseidon(:, 8), 'color', [0.8500 0.3250 0.0980], 'LineWidth', 2.5)
hold on
plot(time, readPoseidon(:, 9), 'color', [0.9290 0.6940 0.1250], 'LineWidth', 2.5)
ylim([0 2*1e10])
ylabel('Impedance/Resistance (\Omega)')
title('Interfacial impedance and bulk resistance')
legend({'Interfacial impedance', 'Bulk resistance'}, 'Location', 'northwest', 'NumColumns', 2, 'FontSize', 11);
ax2.FontSize = 11;
set(gca, 'linewidth', 1.5)
xline(sedimentTimeStamp(1), '-', {'Step 2', 'Added 50mg'}, 'LabelVerticalAlignment', 'middle', 'LabelHorizontalAlignment',
↳ 'center', 'FontSize', 11);
xline(sedimentTimeStamp(2), '-', {'Step 3', 'Added 50mg'}, 'LabelVerticalAlignment', 'middle', 'LabelHorizontalAlignment',
↳ 'center', 'FontSize', 11);
xline(sedimentTimeStamp(3), '-', {'Step 4', 'Added 50mg'}, 'LabelVerticalAlignment', 'middle', 'LabelHorizontalAlignment',
↳ 'center', 'FontSize', 11);
xline(sedimentTimeStamp(4), '-', {'Step 5', 'Added 50mg'}, 'LabelVerticalAlignment', 'middle', 'LabelHorizontalAlignment',
↳ 'center', 'FontSize', 11);

```

```

xline(sedimentTimeStamp(5), '-', {'Step 6', 'Added 50mg'}, 'LabelVerticalAlignment', 'middle', 'LabelHorizontalAlignment',
↳ 'center', 'FontSize', 11);
xline(sedimentTimeStamp(6), '-', {'Step 7', 'Added 50mg'}, 'LabelVerticalAlignment', 'middle', 'LabelHorizontalAlignment',
↳ 'center', 'FontSize', 11);
xline(sedimentTimeStamp(7), '-', {'Step 8', 'Added 50mg'}, 'LabelVerticalAlignment', 'middle', 'LabelHorizontalAlignment',
↳ 'center', 'FontSize', 11);
xline(sedimentTimeStamp(8), '-', {'Step 9', 'Added 50mg'}, 'LabelVerticalAlignment', 'middle', 'LabelHorizontalAlignment',
↳ 'center', 'FontSize', 11);
xline(sedimentTimeStamp(9), '-', {'Step 10', 'Added 50mg'}, 'LabelVerticalAlignment', 'middle', 'LabelHorizontalAlignment',
↳ 'center', 'FontSize', 11);
xline(sedimentTimeStamp(10), '-', {'Step 11', 'Added 50mg'}, 'LabelVerticalAlignment', 'middle',
↳ 'LabelHorizontalAlignment', 'center', 'FontSize', 11);

% Plots Temperatures
ax3 = subplot(3, 1, 3, 'Position', [0.1 0.08 0.83 0.23]);
plot(time, readPoseidon(:, 4), 'color', [0.4940 0.1840 0.5560], 'LineWidth', 2.5)
hold on
plot(time, readPoseidon(:, 5), 'color', [0.4660 0.6740 0.1880], 'LineWidth', 2.5)
ylabel(['Temperature (' char(176) 'C)'])
title('Temperatures')
legend({'Temperature pre reference', 'Temperature post sample'}, 'Location', 'northwest', 'NumColumns', 2, 'FontSize', 11);
ax3.FontSize = 11;
set(gca, 'linewidth', 1.5)
ylim([SSTemp-3 SSTemp+3])
linkaxes([ax1, ax2, ax3], 'x')
xlabel('Time (s)')
xline(sedimentTimeStamp(1), '-', {'Step 2', 'Added 50mg'}, 'LabelVerticalAlignment', 'middle', 'LabelHorizontalAlignment',
↳ 'center', 'FontSize', 11);
xline(sedimentTimeStamp(2), '-', {'Step 3', 'Added 50mg'}, 'LabelVerticalAlignment', 'middle', 'LabelHorizontalAlignment',
↳ 'center', 'FontSize', 11);
xline(sedimentTimeStamp(3), '-', {'Step 4', 'Added 50mg'}, 'LabelVerticalAlignment', 'middle', 'LabelHorizontalAlignment',
↳ 'center', 'FontSize', 11);
xline(sedimentTimeStamp(4), '-', {'Step 5', 'Added 50mg'}, 'LabelVerticalAlignment', 'middle', 'LabelHorizontalAlignment',
↳ 'center', 'FontSize', 11);

```

```
xline(sedimentTimeStamp(5), '-', {'Step 6', 'Added 50mg'}, 'LabelVerticalAlignment', 'middle', 'LabelHorizontalAlignment',  
↳ 'center', 'FontSize', 11);  
xline(sedimentTimeStamp(6), '-', {'Step 7', 'Added 50mg'}, 'LabelVerticalAlignment', 'middle', 'LabelHorizontalAlignment',  
↳ 'center', 'FontSize', 11);  
xline(sedimentTimeStamp(7), '-', {'Step 8', 'Added 50mg'}, 'LabelVerticalAlignment', 'middle', 'LabelHorizontalAlignment',  
↳ 'center', 'FontSize', 11);  
xline(sedimentTimeStamp(8), '-', {'Step 9', 'Added 50mg'}, 'LabelVerticalAlignment', 'middle', 'LabelHorizontalAlignment',  
↳ 'center', 'FontSize', 11);  
xline(sedimentTimeStamp(9), '-', {'Step 10', 'Added 50mg'}, 'LabelVerticalAlignment', 'middle', 'LabelHorizontalAlignment',  
↳ 'center', 'FontSize', 11);  
xline(sedimentTimeStamp(10), '-', {'Step 11', 'Added 50mg'}, 'LabelVerticalAlignment', 'middle',  
↳ 'LabelHorizontalAlignment', 'center', 'FontSize', 11);  
xlim([0 time(end)])  
  
sgtitle('Poseidon Trident QW3100 Experiment 3-1')  
set(0, 'DefaultLegendAutoUpdate', 'off')  
  
save('timeStamps3-1.mat', 'sedimentTimeStamp')  
export_fig 'PoseidonExperiment3-1.pdf' -a4 -q101 -transparent -nocrop
```

E.3. Script for plotting Parker Kittiwake MWDS sensor data

```

clc; clear; close all;

data = readtable('Experiment3-1.csv');
load timeStamps3-1.mat

% Extracts the time array from the data
time = str2double(data.Var4(7:end));
ferrouspermin = zeros(length(time), 10);
ferrouspermin(:,1) = str2double(data.Var25(7:end));
ferrouspermin(:,2) = data.Var26(7:end);
ferrouspermin(:,3) = data.Var27(7:end);
ferrouspermin(:,4) = data.Var28(7:end);
ferrouspermin(:,5) = data.Var29(7:end);
ferrouspermin(:,6) = data.Var30(7:end);
ferrouspermin(:,7) = data.Var31(7:end);
ferrouspermin(:,8) = data.Var32(7:end);
ferrouspermin(:,9) = data.Var33(7:end);
ferrouspermin(:,10) = data.Var34(7:end);

nonferrouspermin = zeros(length(time), 10);
nonferrouspermin(:,1) = str2double(data.Var35(7:end));
nonferrouspermin(:,2) = data.Var36(7:end);
nonferrouspermin(:,3) = data.Var37(7:end);
nonferrouspermin(:,4) = data.Var38(7:end);
nonferrouspermin(:,5) = data.Var39(7:end);
nonferrouspermin(:,6) = data.Var40(7:end);
nonferrouspermin(:,7) = data.Var41(7:end);
nonferrouspermin(:,8) = data.Var42(7:end);
nonferrouspermin(:,9) = data.Var43(7:end);
nonferrouspermin(:,10) = data.Var44(7:end);

% Plots all ferrous debris signals
figure('Renderer', 'painters', 'Position', [10 10 960 860])

```

```

ax1 = subplot(2, 1, 1, 'Position', [0.1 0.52 0.83 0.37]);
hold on
plot(time, ferrouspermin(:, 1:7), 'LineWidth', 2)
plot(time, ferrouspermin(:, 8), 'LineWidth', 2, 'Color', [1 1 0])
plot(time, ferrouspermin(:, 9), 'LineWidth', 2, 'Color', [1 0 1])
plot(time, ferrouspermin(:, 10), 'LineWidth', 2, 'Color', [0 1 1])
ylabel('Particles per minute')
title('Ferrous particles')
legend({'A', 'B', 'C', 'D', 'E', 'F', 'G', 'H', 'I', 'J'}, 'Location', 'northwest', 'NumColumns', 10, 'FontSize', 11);
ax1.FontSize = 11;
set(gca, 'linewidth', 1.5)
xline(sedimentTimeStamp(1), '-', {'Step 2', 'Added 50mg'}, 'LabelVerticalAlignment', 'middle', 'LabelHorizontalAlignment',
↳ 'center', 'FontSize', 11);
xline(sedimentTimeStamp(2), '-', {'Step 3', 'Added 50mg'}, 'LabelVerticalAlignment', 'middle', 'LabelHorizontalAlignment',
↳ 'center', 'FontSize', 11);
xline(sedimentTimeStamp(3), '-', {'Step 4', 'Added 50mg'}, 'LabelVerticalAlignment', 'middle', 'LabelHorizontalAlignment',
↳ 'center', 'FontSize', 11);
xline(sedimentTimeStamp(4), '-', {'Step 5', 'Added 50mg'}, 'LabelVerticalAlignment', 'middle', 'LabelHorizontalAlignment',
↳ 'center', 'FontSize', 11);
xline(sedimentTimeStamp(5), '-', {'Step 6', 'Added 50mg'}, 'LabelVerticalAlignment', 'middle', 'LabelHorizontalAlignment',
↳ 'center', 'FontSize', 11);
xline(sedimentTimeStamp(6), '-', {'Step 7', 'Added 50mg'}, 'LabelVerticalAlignment', 'middle', 'LabelHorizontalAlignment',
↳ 'center', 'FontSize', 11);
xline(sedimentTimeStamp(7), '-', {'Step 8', 'Added 50mg'}, 'LabelVerticalAlignment', 'middle', 'LabelHorizontalAlignment',
↳ 'center', 'FontSize', 11);
xline(sedimentTimeStamp(8), '-', {'Step 9', 'Added 50mg'}, 'LabelVerticalAlignment', 'middle', 'LabelHorizontalAlignment',
↳ 'center', 'FontSize', 11);
xline(sedimentTimeStamp(9), '-', {'Step 10', 'Added 50mg'}, 'LabelVerticalAlignment', 'middle', 'LabelHorizontalAlignment',
↳ 'center', 'FontSize', 11);
xline(sedimentTimeStamp(10), '-', {'Step 11', 'Added 50mg'}, 'LabelVerticalAlignment', 'middle',
↳ 'LabelHorizontalAlignment', 'center', 'FontSize', 11);

% Plots all ferrous debris signals
ax2 = subplot(2, 1, 2, 'Position', [0.1 0.08 0.83 0.37]);
hold on

```



```

plot(time, nonferrouspermin(:, 1:7), 'LineWidth', 2)
plot(time, nonferrouspermin(:, 8), 'LineWidth', 2, 'Color', [1 1 0])
plot(time, nonferrouspermin(:, 9), 'LineWidth', 2, 'Color', [1 0 1])
plot(time, nonferrouspermin(:, 10), 'LineWidth', 2, 'Color', [0 1 1])
ylabel('Particles per minute')
title('Non-ferrous particles')
legend({'A', 'B', 'C', 'D', 'E', 'F', 'G', 'H', 'I', 'J'}, 'Location', 'northwest', 'NumColumns', 10, 'FontSize', 11);
ax2.FontSize = 11;
set(gca, 'linewidth', 1.5)
linkaxes([ax1, ax2], 'x')
xlabel('Time (s)')
xline(sedimentTimeStamp(1), '-', {'Step 2', 'Added 50mg'}, 'LabelVerticalAlignment', 'middle', 'LabelHorizontalAlignment',
↳ 'center', 'FontSize', 11);
xline(sedimentTimeStamp(2), '-', {'Step 3', 'Added 50mg'}, 'LabelVerticalAlignment', 'middle', 'LabelHorizontalAlignment',
↳ 'center', 'FontSize', 11);
xline(sedimentTimeStamp(3), '-', {'Step 4', 'Added 50mg'}, 'LabelVerticalAlignment', 'middle', 'LabelHorizontalAlignment',
↳ 'center', 'FontSize', 11);
xline(sedimentTimeStamp(4), '-', {'Step 5', 'Added 50mg'}, 'LabelVerticalAlignment', 'middle', 'LabelHorizontalAlignment',
↳ 'center', 'FontSize', 11);
xline(sedimentTimeStamp(5), '-', {'Step 6', 'Added 50mg'}, 'LabelVerticalAlignment', 'middle', 'LabelHorizontalAlignment',
↳ 'center', 'FontSize', 11);
xline(sedimentTimeStamp(6), '-', {'Step 7', 'Added 50mg'}, 'LabelVerticalAlignment', 'middle', 'LabelHorizontalAlignment',
↳ 'center', 'FontSize', 11);
xline(sedimentTimeStamp(7), '-', {'Step 8', 'Added 50mg'}, 'LabelVerticalAlignment', 'middle', 'LabelHorizontalAlignment',
↳ 'center', 'FontSize', 11);
xline(sedimentTimeStamp(8), '-', {'Step 9', 'Added 50mg'}, 'LabelVerticalAlignment', 'middle', 'LabelHorizontalAlignment',
↳ 'center', 'FontSize', 11);
xline(sedimentTimeStamp(9), '-', {'Step 10', 'Added 50mg'}, 'LabelVerticalAlignment', 'middle', 'LabelHorizontalAlignment',
↳ 'center', 'FontSize', 11);
xline(sedimentTimeStamp(10), '-', {'Step 11', 'Added 50mg'}, 'LabelVerticalAlignment', 'middle',
↳ 'LabelHorizontalAlignment', 'center', 'FontSize', 11);
xlim([0 time(end)])

sgtitle('Parker MWDS Experiment 3-1')
set(0, 'DefaultLegendAutoUpdate', 'off')

```

```
export_fig ParkerExperiment3-1.pdf -a4 -q101 -transparent -nocrop
```

E.4. Script for logging Poseidon Trident QW3100 sensor data

```

clc; clear; close all;
mPoseidon = modbus('serialrtu', 'COM3', 'BaudRate', 115200, 'NumRetries', 10, 'Timeout', 1);

global keep_going
keep_going = 1;
global sedimentNumber
sedimentNumber = 0;
global sedimentTimeStamp
sedimentTimeStamp = [];
fig = figure(100);
title('Stop button here')
stopbutton = uicontrol('string', 'Stop', 'fontsize', 15, 'position', [100,100,100,100], 'ButtonDownFcn', {@stopScript});
increaseSedimentButton = uicontrol('string', 'Add sediment', 'fontsize', 15, 'position', [250,250,200,100],
↳ 'ButtonDownFcn', {@addSediment});
timeText = text(0.5, 0.25, '0', 'fontsize', 15);
timeMinuteText = text(0.5, 0.1, '0', 'fontsize', 15);
maxDiffText = text(0.5, 0.4, '0', 'fontsize', 15);

tic;
Nmax = 100000;
readPoseidon = zeros(Nmax, 9);
i = 1;
sampleFreq = 5;
dt = 1.0/sampleFreq;

lastTime = 0.0;
maxDiff = 0.0;
while true
    tempreadPoseidon = read(mPoseidon, 'holdingregs', 201, [3 6], {'uint16', 'single'});
    readPoseidon(i, 2:3) = tempreadPoseidon(1:2);
    readPoseidon(i, 4:9) = tempreadPoseidon(4:9);
    readPoseidon(i, 1) = toc;
%    disp([num2str(readPoseidon(i, 8))]]);

```

```

timeText.String = [num2str(readPoseidon(i, 1)), 'sec'];
timeMinuteText.String = [num2str(readPoseidon(i, 1)/60), 'min'];
if i >= 2
    if readPoseidon(i, 1) - readPoseidon(i-1, 1) > maxDiff
        maxDiff = readPoseidon(i, 1) - readPoseidon(i-1, 1);
    end
end
maxDiffText.String = num2str(maxDiff);
drawnow;
if keep_going == 0
    close(fig)
    break;
end
i = i + 1;
delta = toc - lastTime;
if delta < dt
    java.lang.Thread.sleep((dt - delta)*1000)
end
lastTime = toc;
end

readPoseidon = readPoseidon(1:i, :);
save(strcat('PoseidonQW3100Data', string(convertTo(datetime('now'), 'posixtime'))), '.mat'), 'readPoseidon',
↳ 'sedimentTimeStamp');

function stopScript(varargin)
    global keep_going
    keep_going = 0;
    disp('Logging stopped')
end

function addSediment(varargin)
    global sedimentNumber
    global sedimentTimeStamp
    sedimentNumber = sedimentNumber + 1;

```

```
disp(['Sediment added ',num2str(sedimentNumber)])  
sedimentTimeStamp(sedimentNumber) = toc;  
end
```

F. Results

F.1. Experiment no. 1

F.1.1. Run no. 1

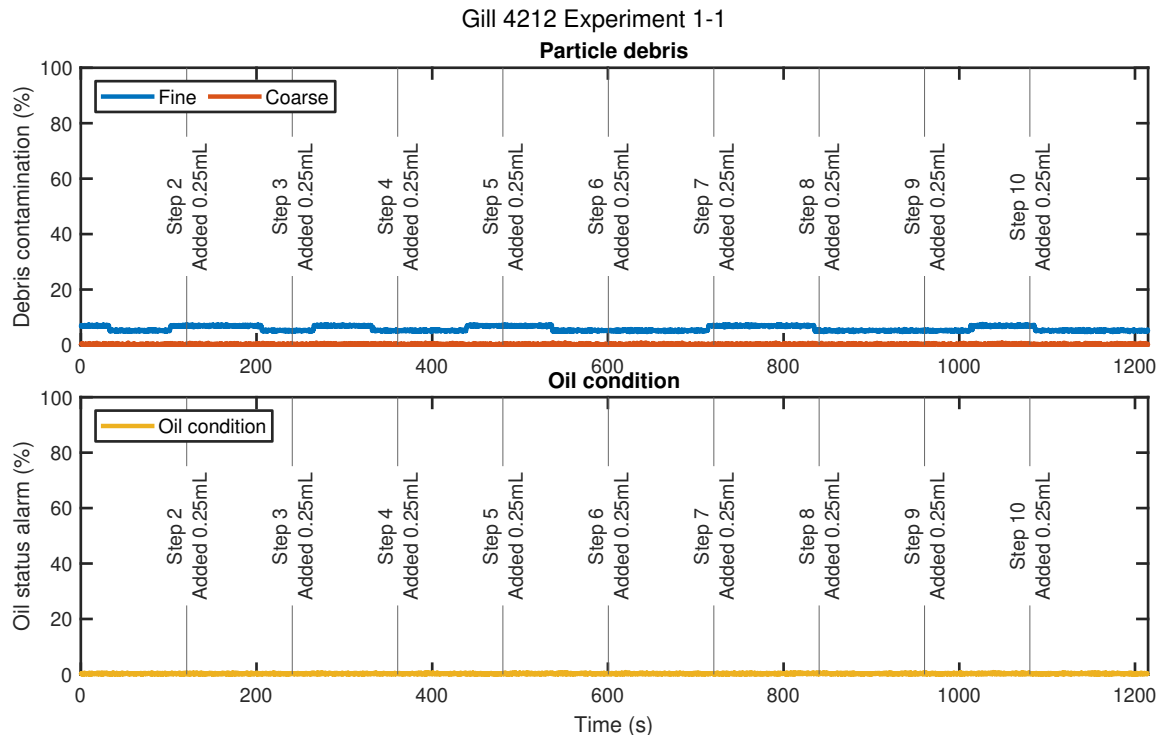


Figure F.1.: Gill 4212 experiment no. 1-1

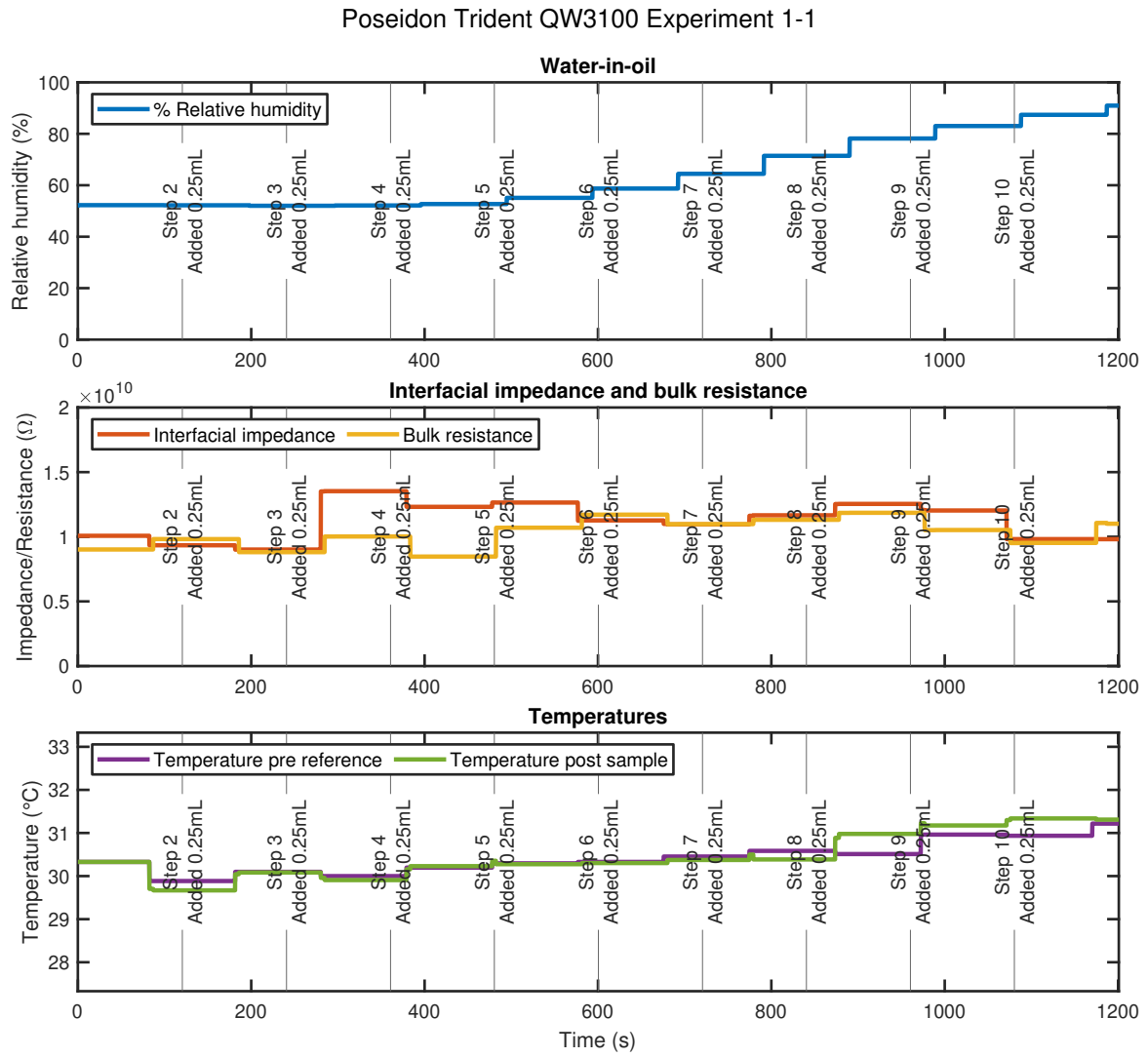


Figure F.2.: Poseidon Trident QW3100 experiment no. 1-1

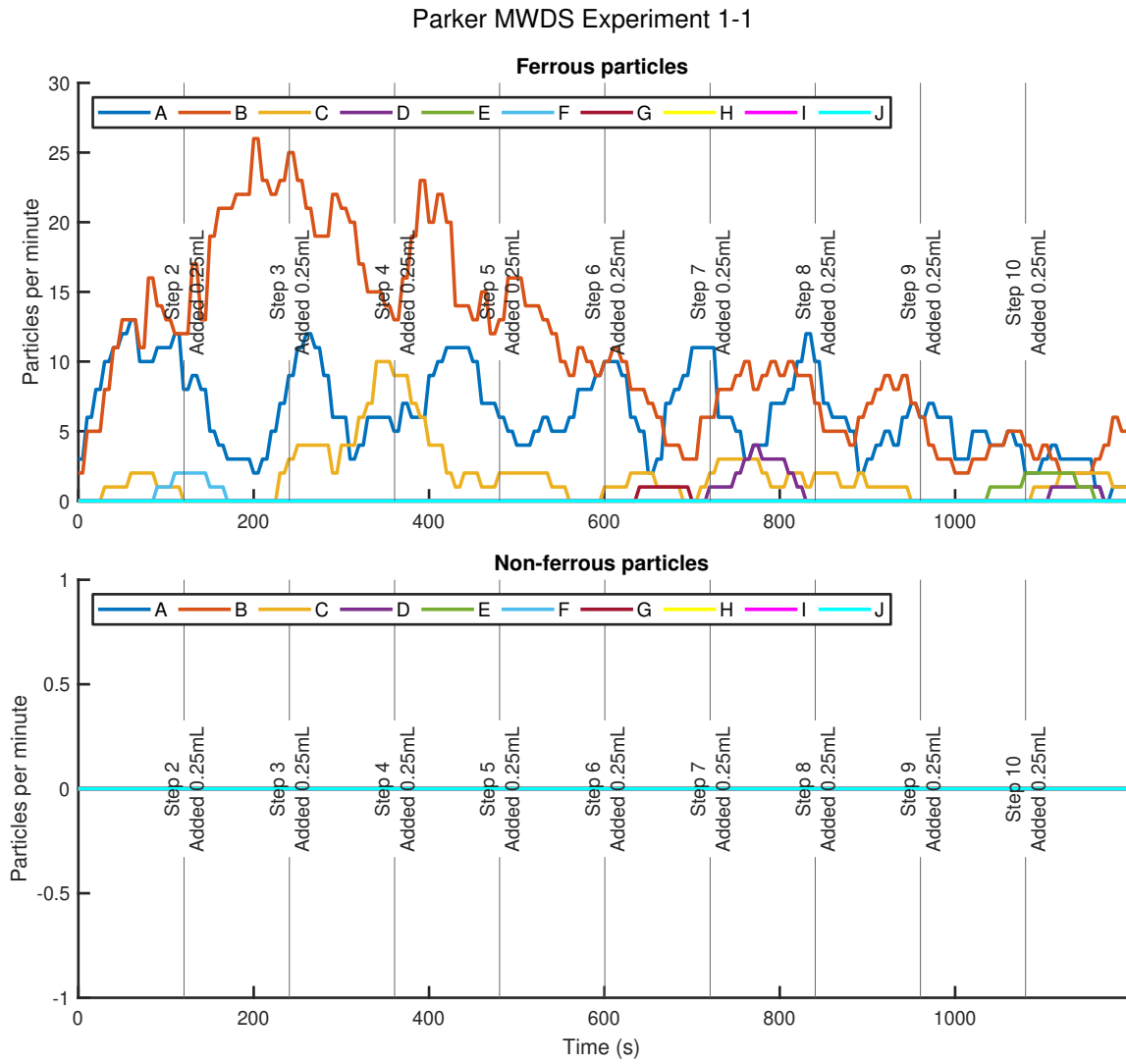


Figure F.3.: Parker MWDS experiment no. 1-1

F.1.2. Run no. 2

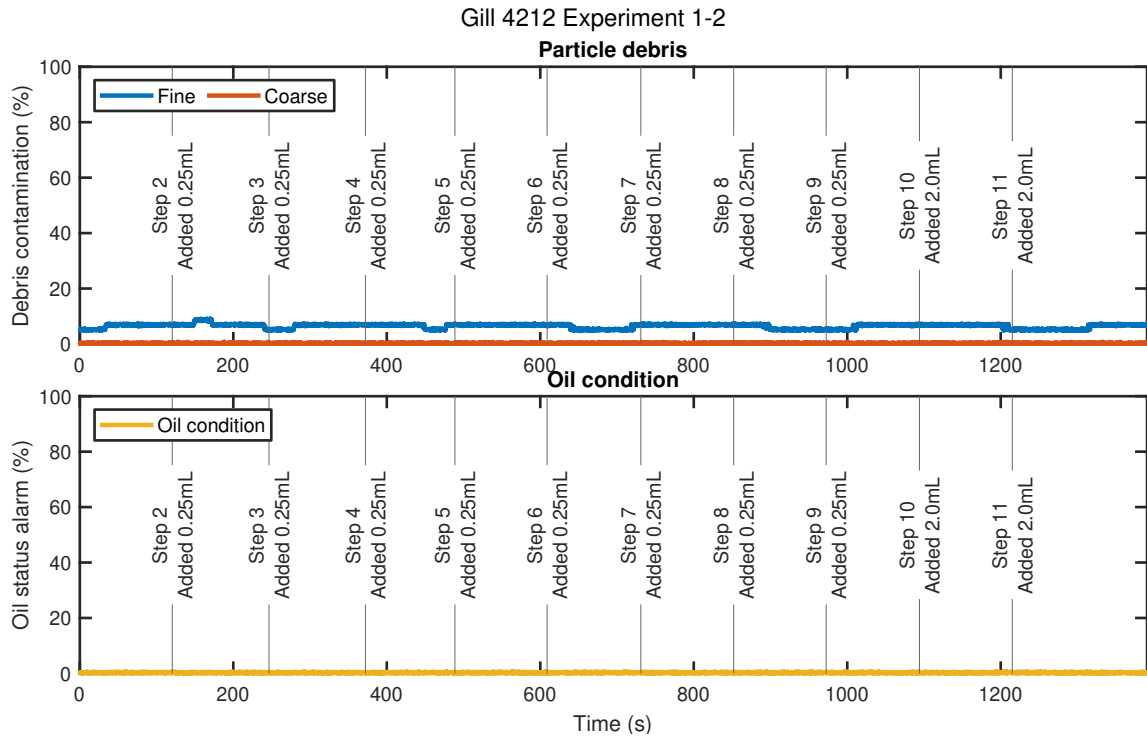


Figure F.4.: Gill 4212 experiment no. 1-2

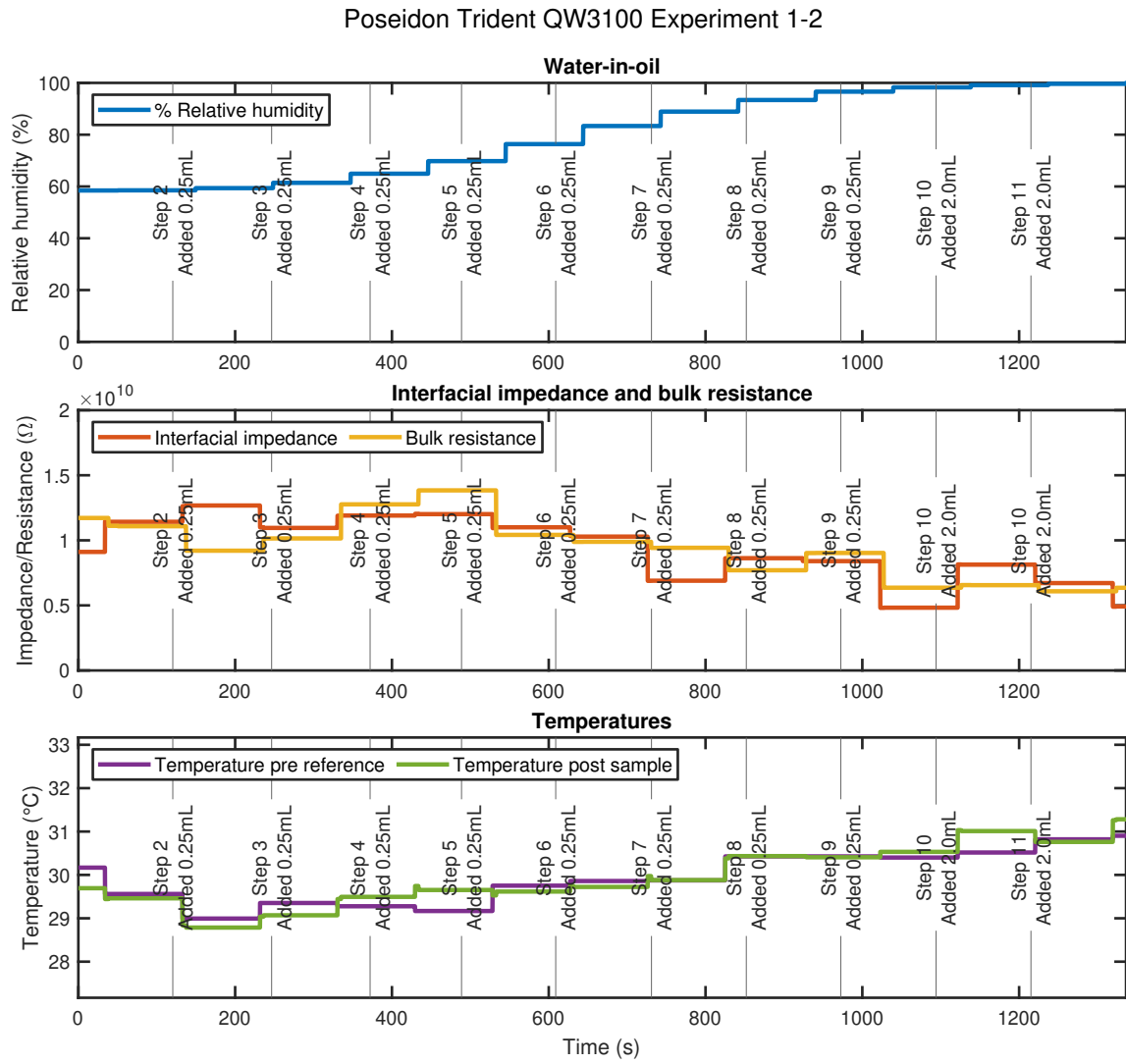


Figure F.5.: Poseidon Trident QW3100 experiment no. 1-2

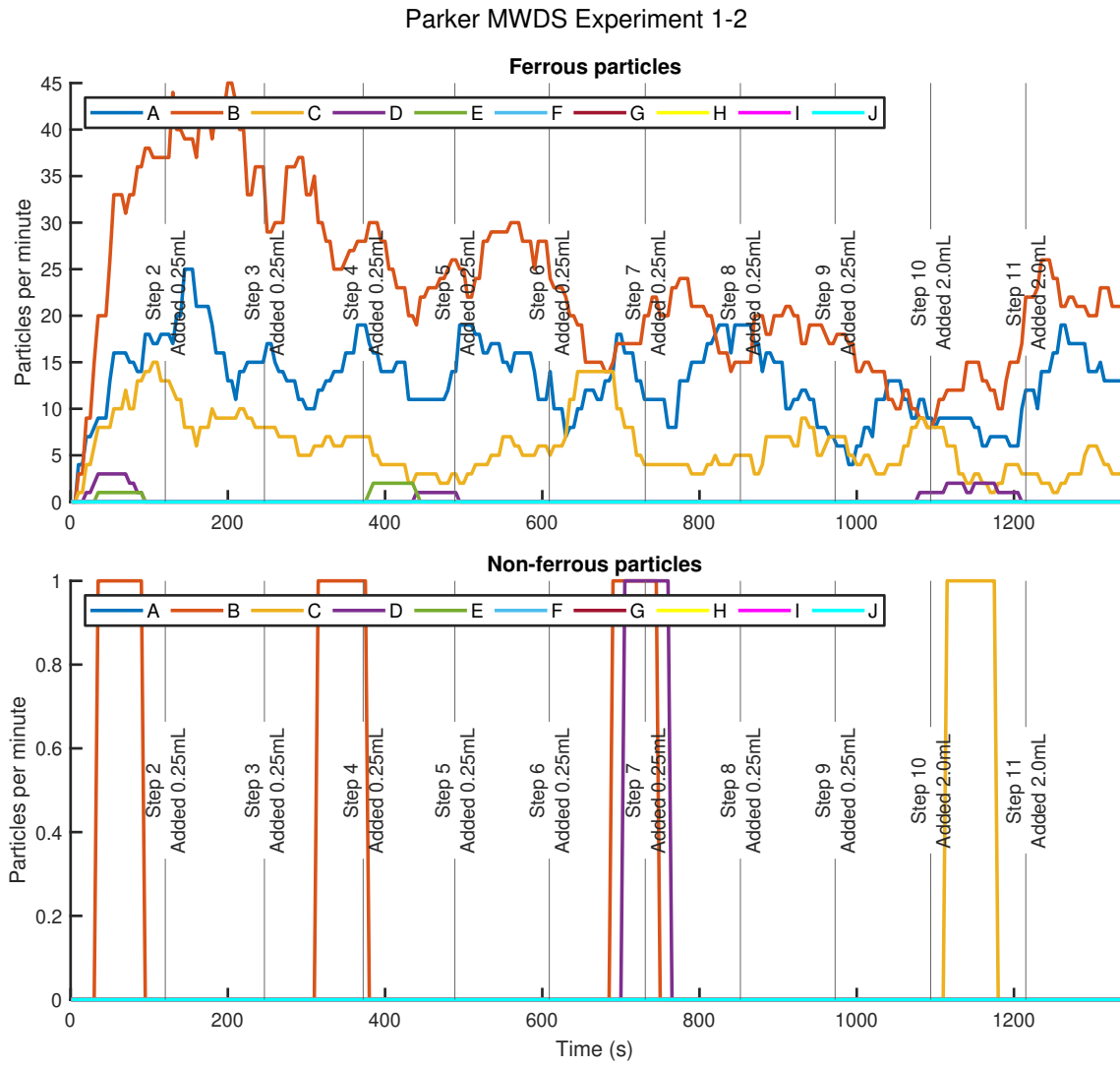


Figure F.6.: Parker MWDS experiment no. 1-2

F.1.3. Run no. 3

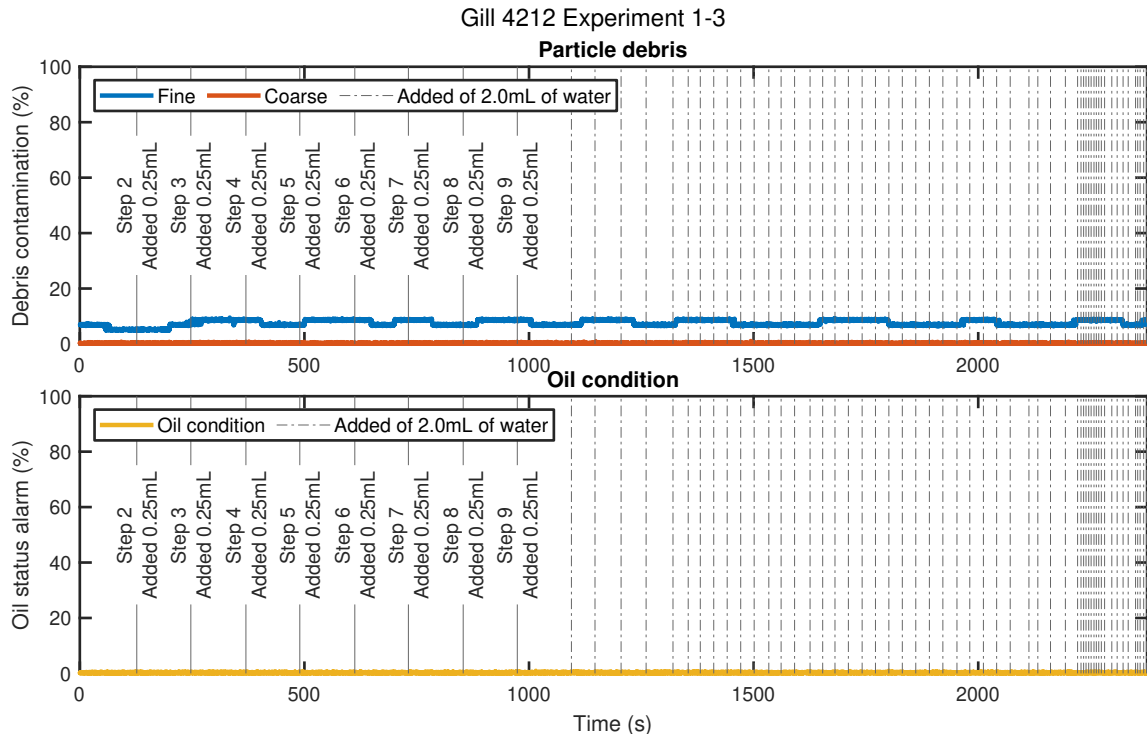


Figure F.7.: Gill 4212 experiment no. 1-3

Poseidon Trident QW3100 Experiment 1-3

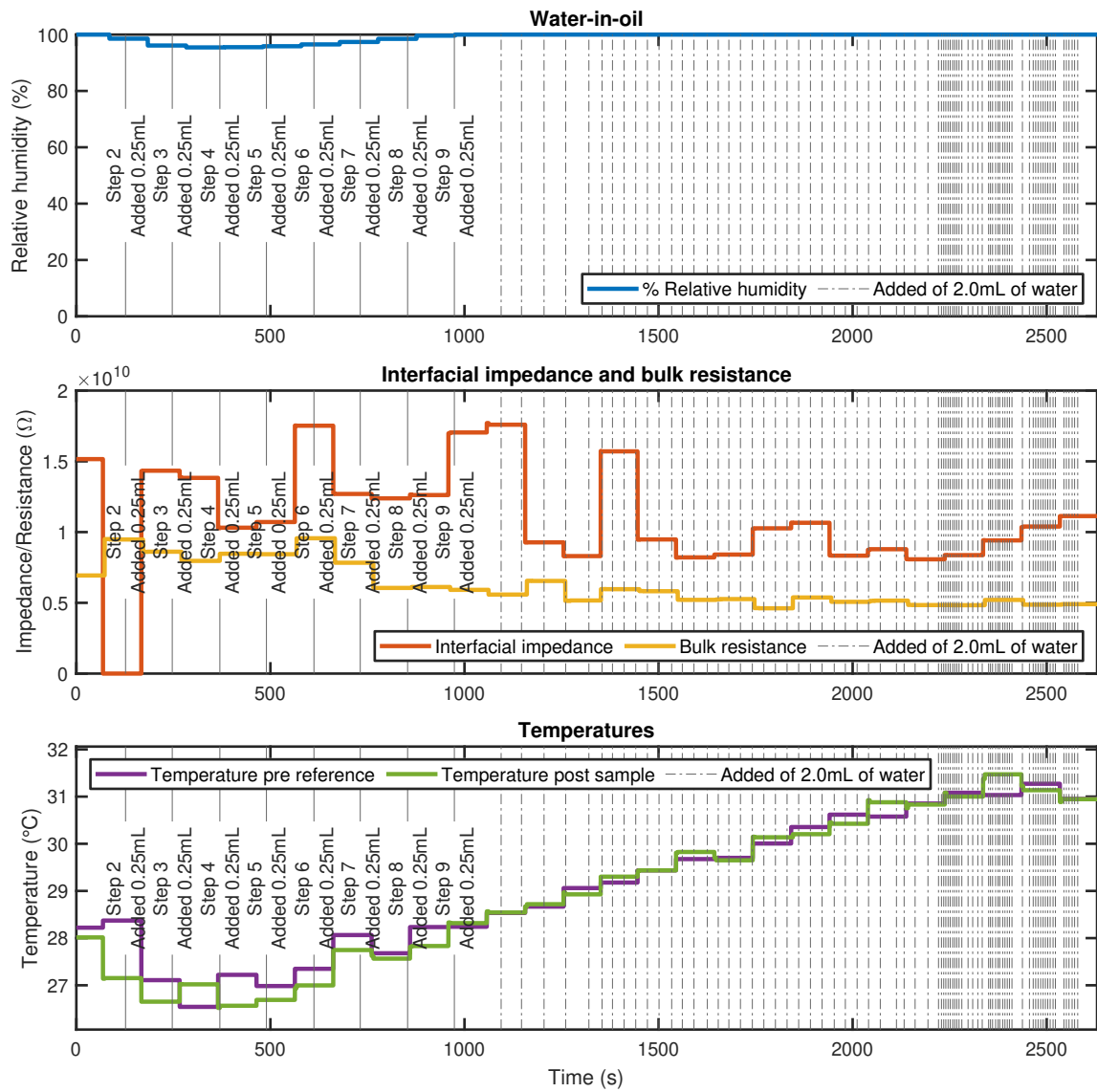


Figure F.8.: Poseidon Trident QW3100 experiment no. 1-3

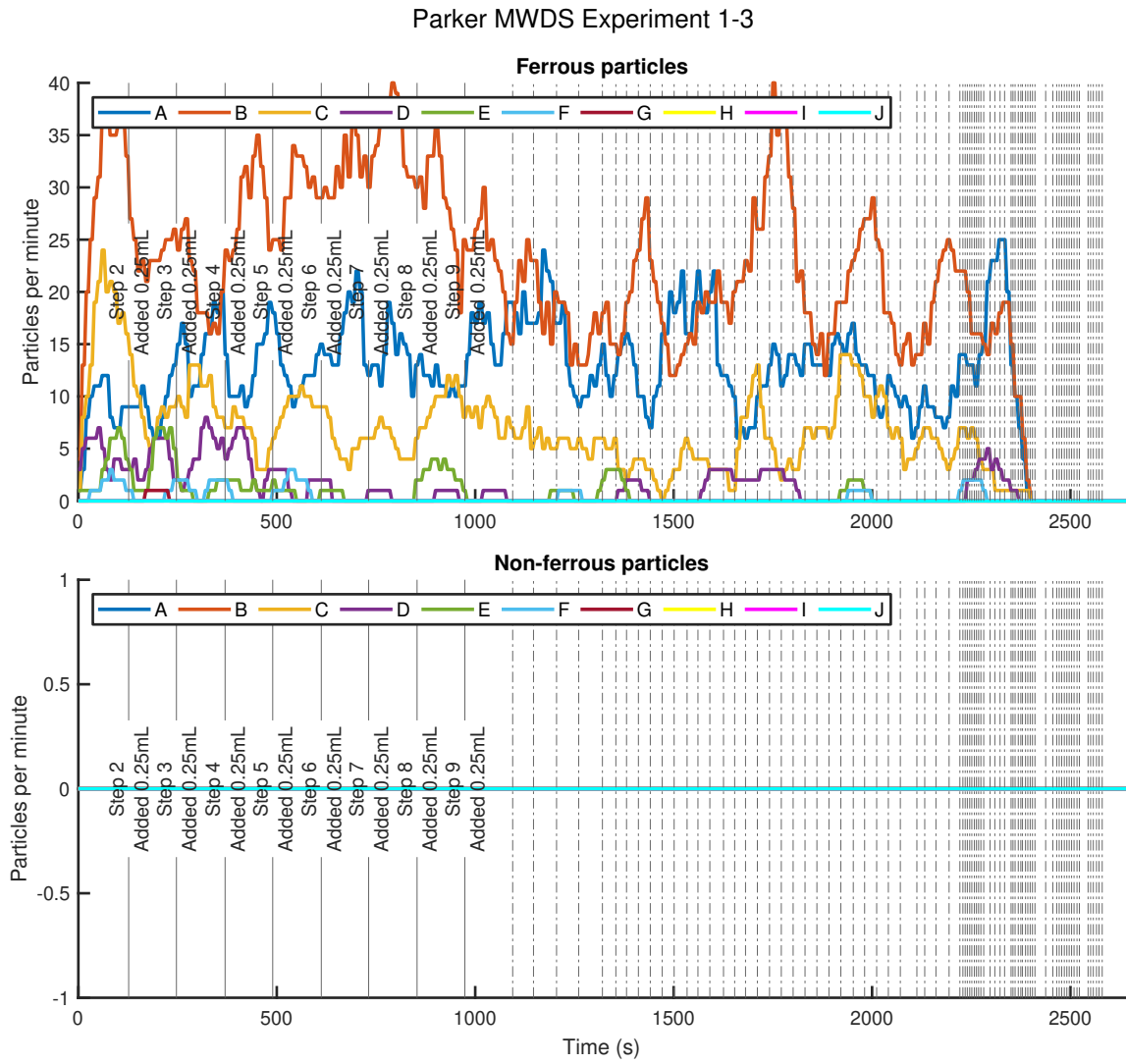


Figure F.9.: Parker MWDS experiment no. 1-3

F.2. Experiment no. 2

F.2.1. Run no. 1

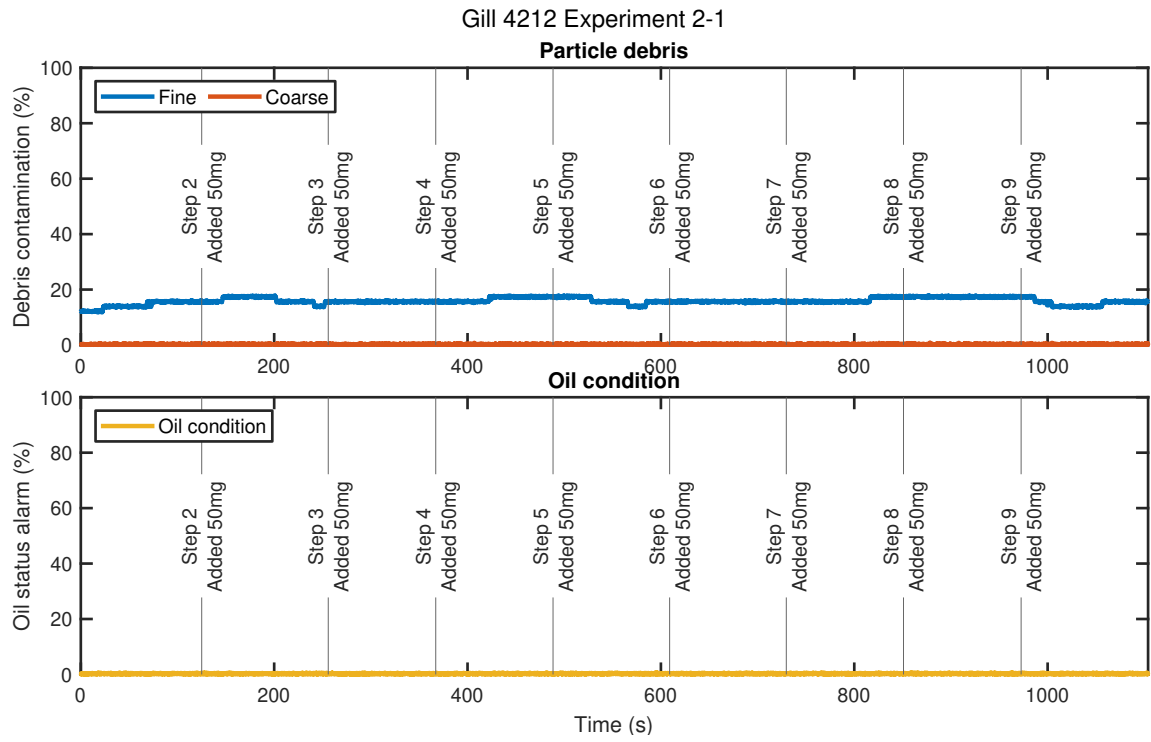


Figure F.10.: Gill 4212 experiment no. 2-1

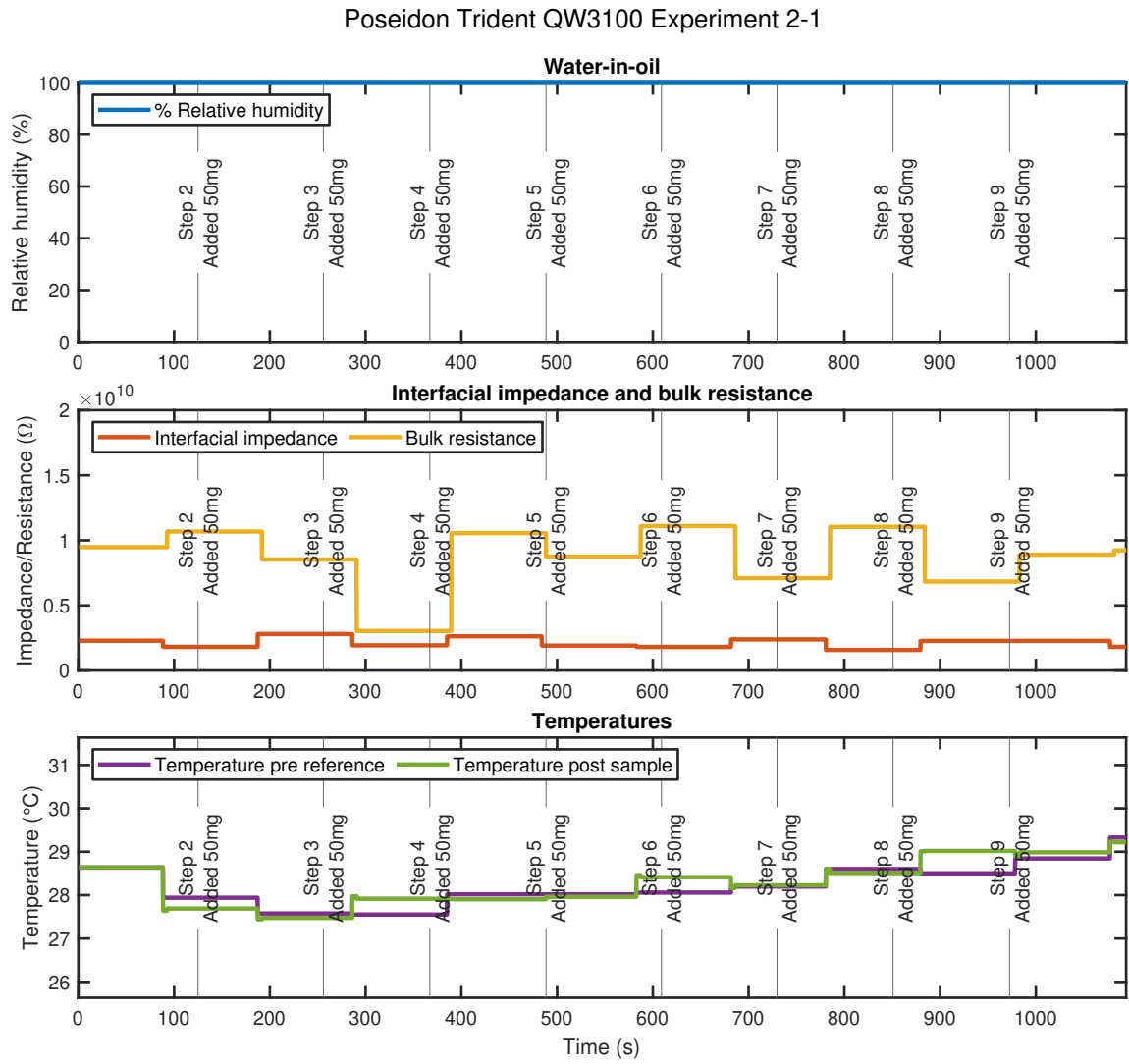


Figure F.11.: Poseidon Trident QW3100 experiment no. 2-1

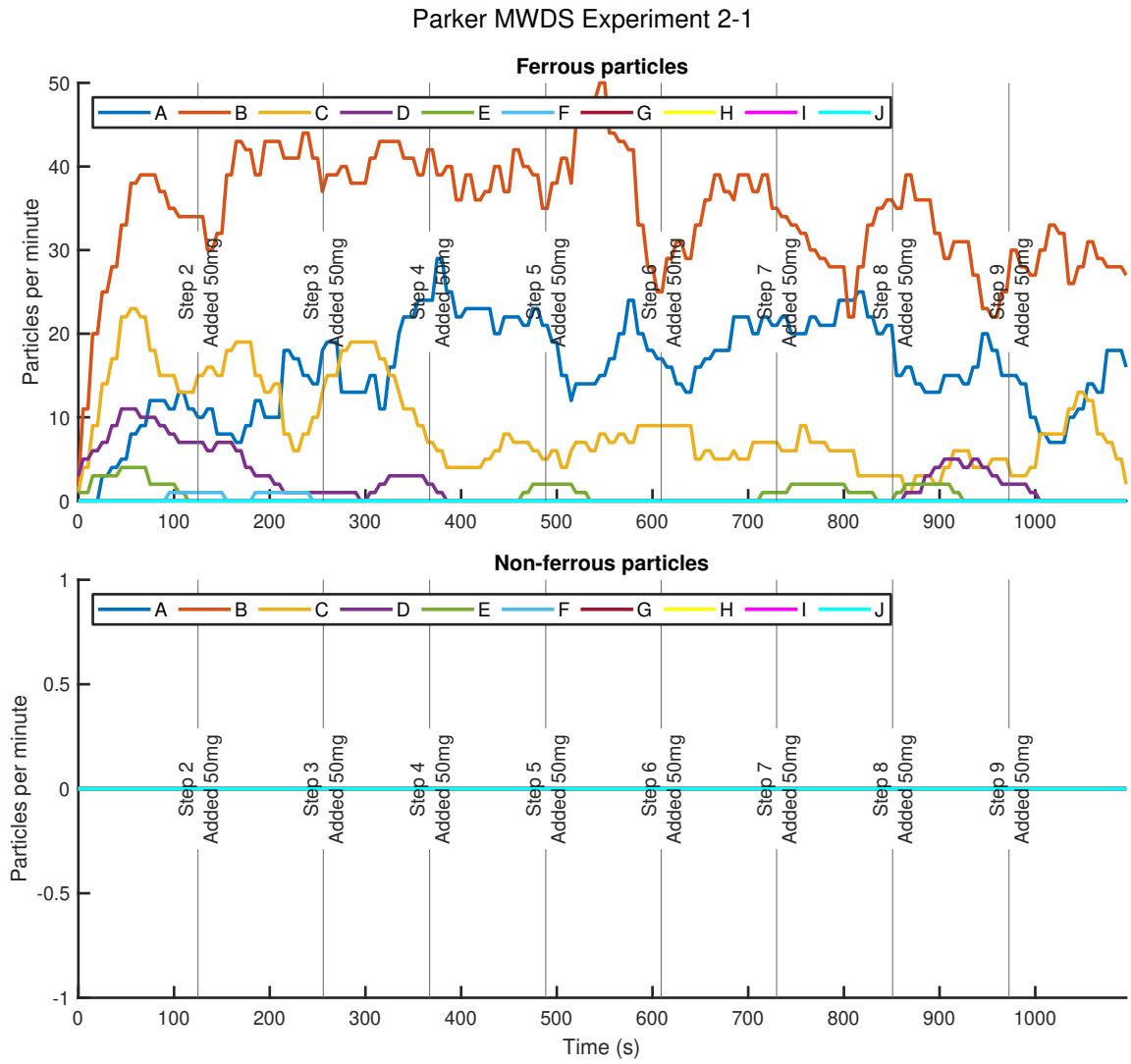


Figure F.12.: Parker MWDS experiment no. 2-1

F.2.2. Run no. 2

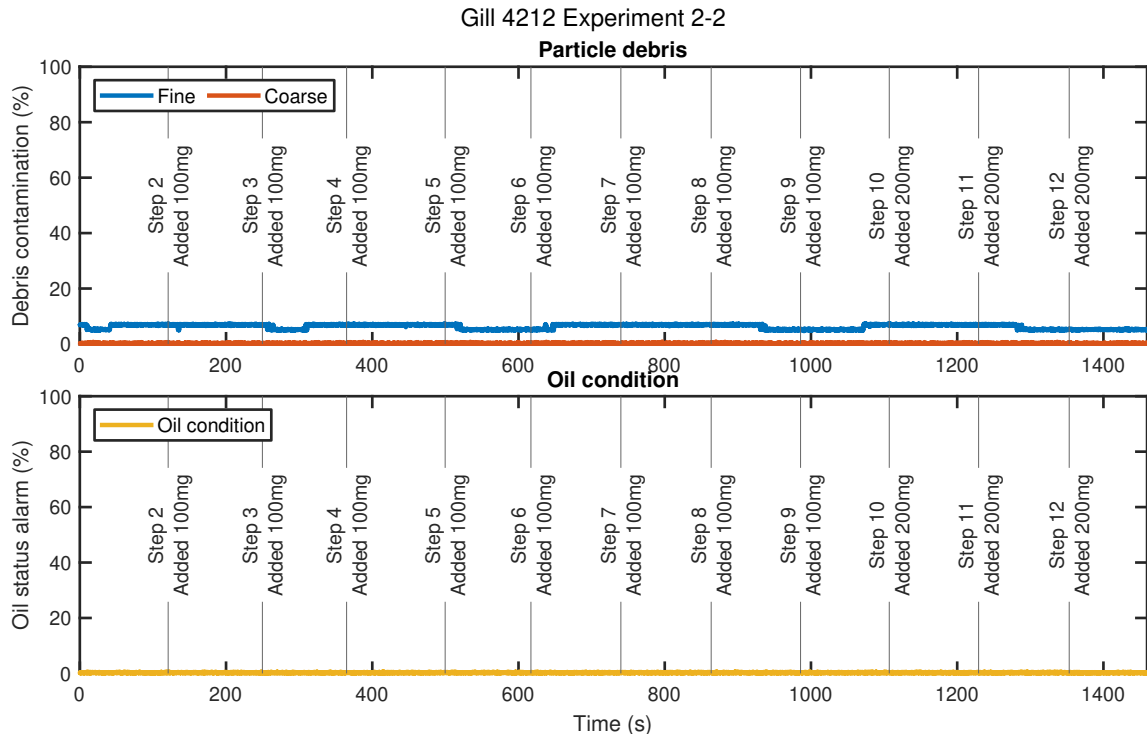


Figure F.13.: Gill 4212 experiment no. 2-2

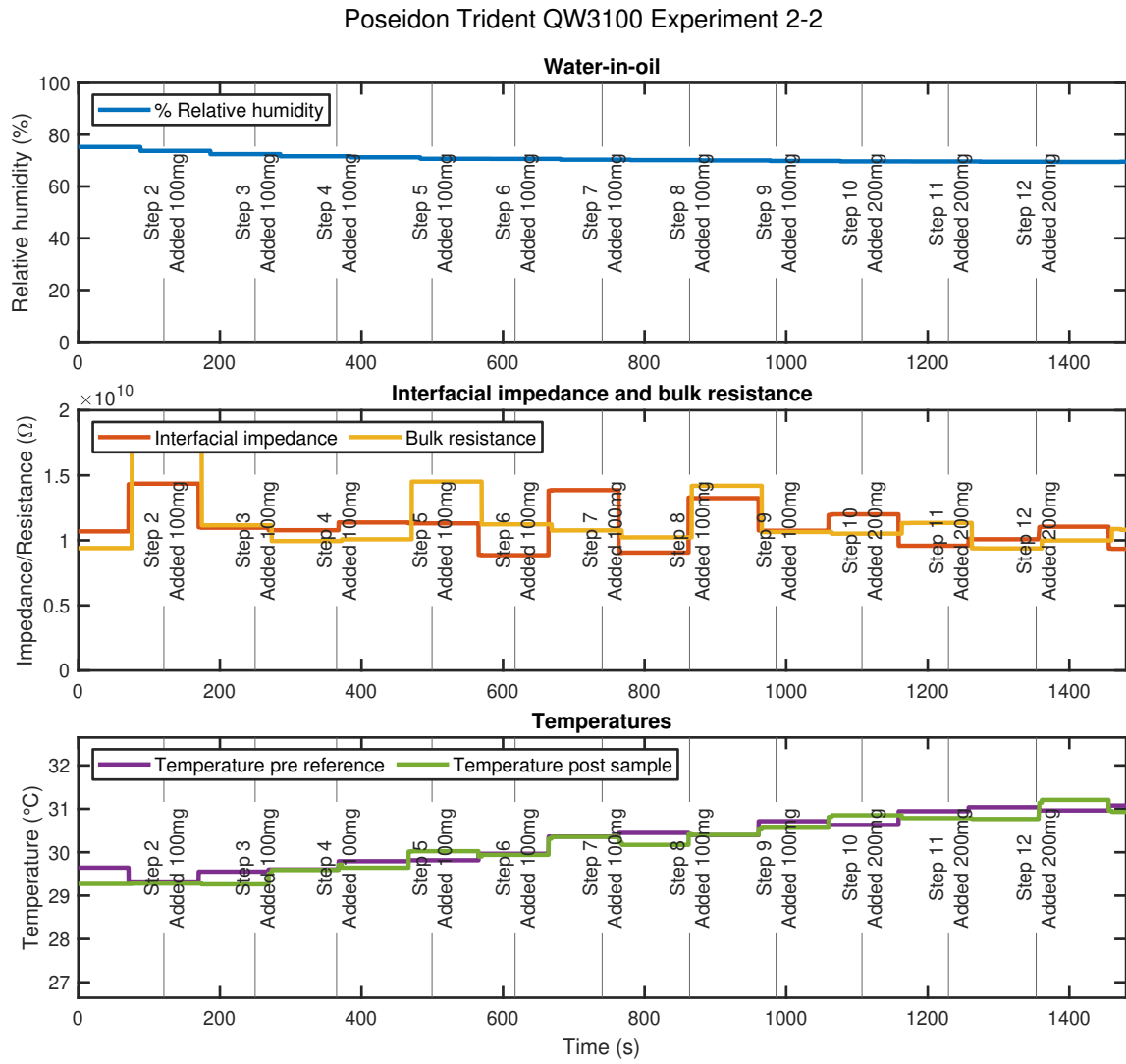


Figure F.14.: Poseidon Trident QW3100 experiment no. 2-2

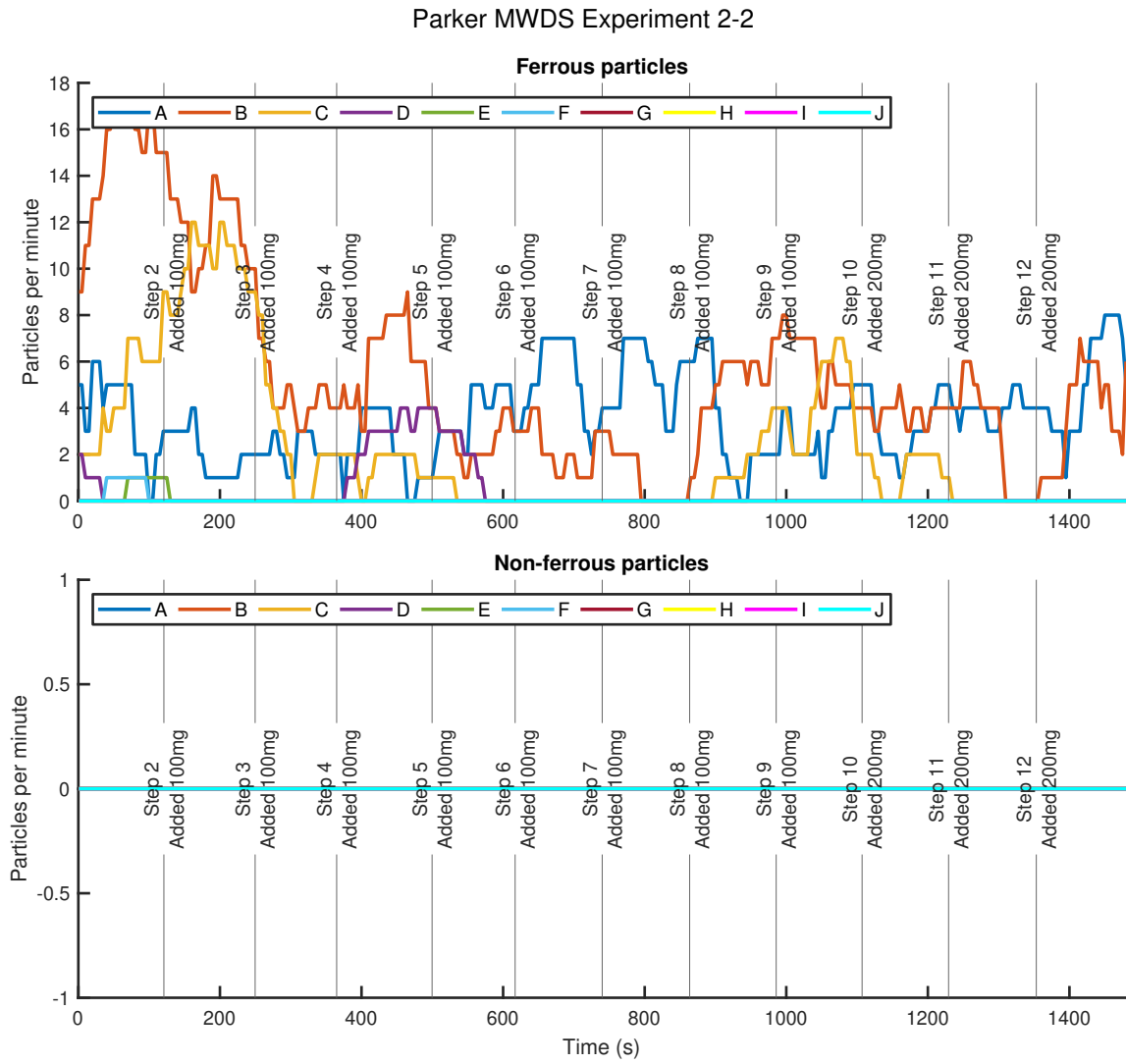


Figure F.15.: Parker MWDS experiment no. 2-2

F.2.3. Run no. 3

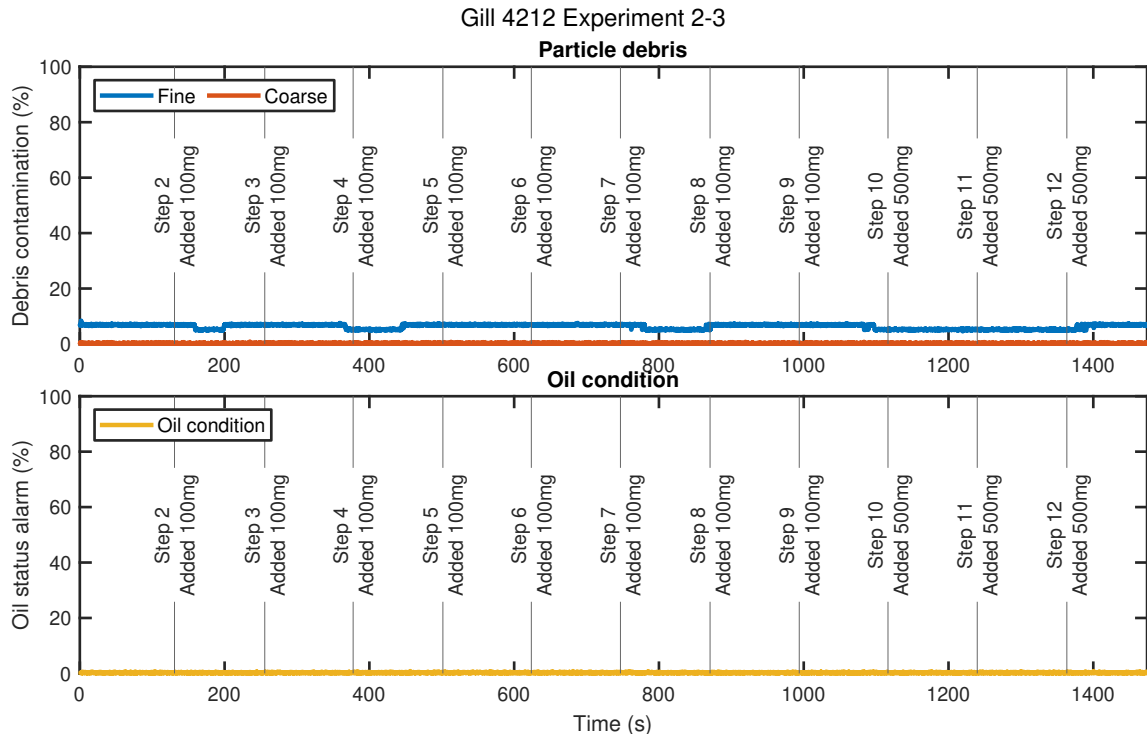


Figure F.16.: Gill 4212 experiment no. 2-3

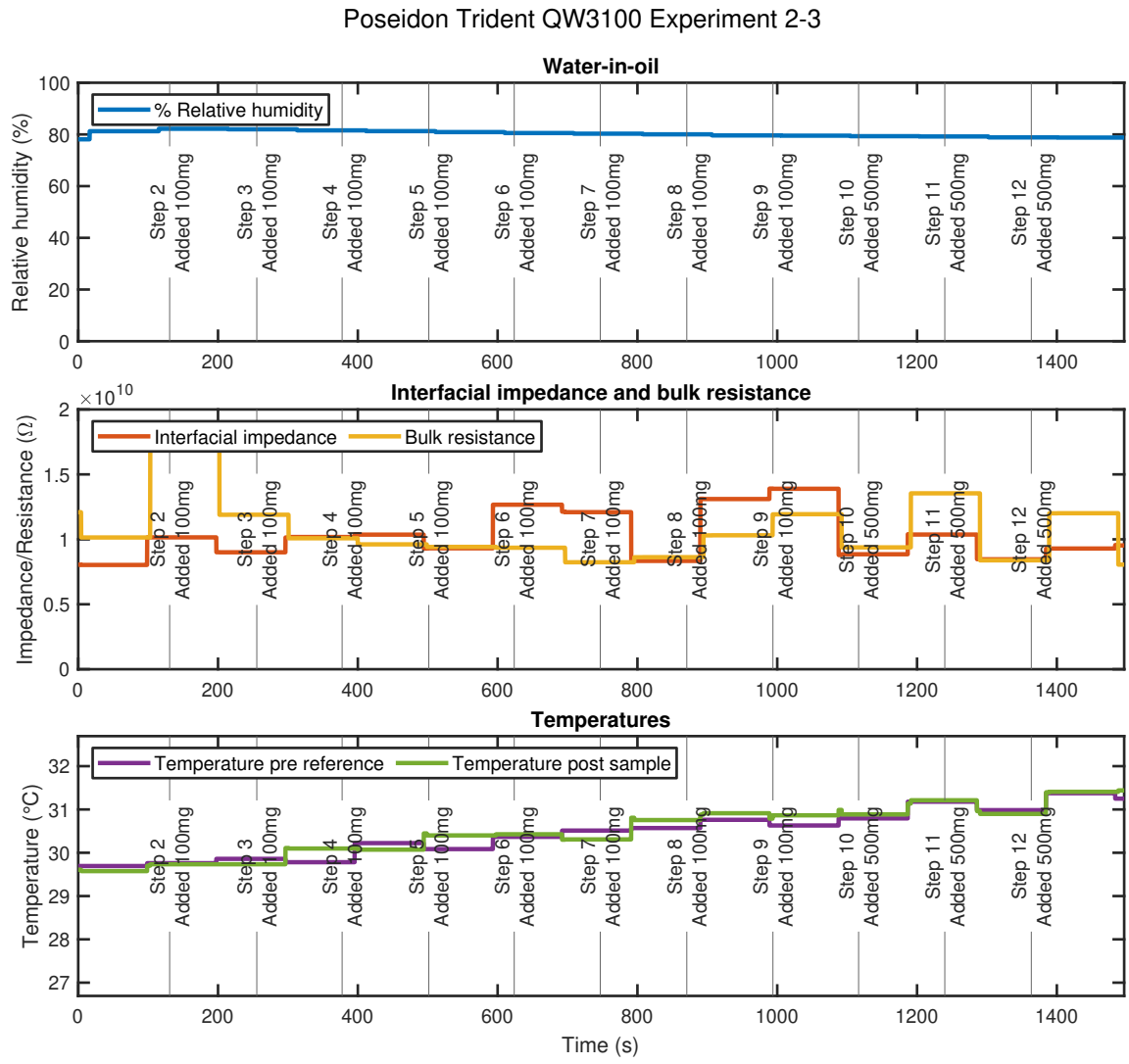


Figure F.17.: Poseidon Trident QW3100 experiment no. 2-3

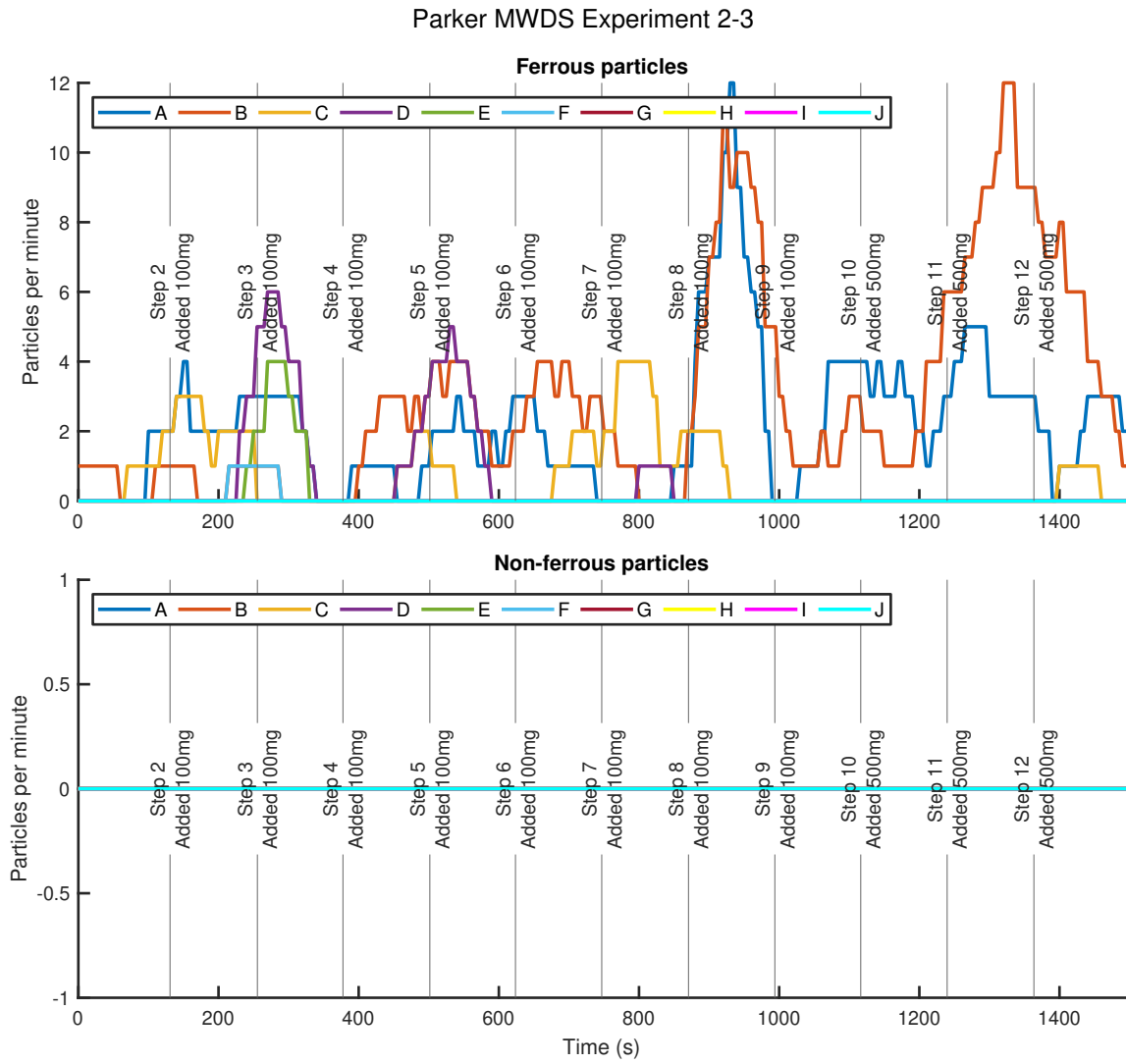


Figure F.18.: Parker MWDS experiment no. 2-3

F.3. Experiment no. 3

F.3.1. Run no. 1

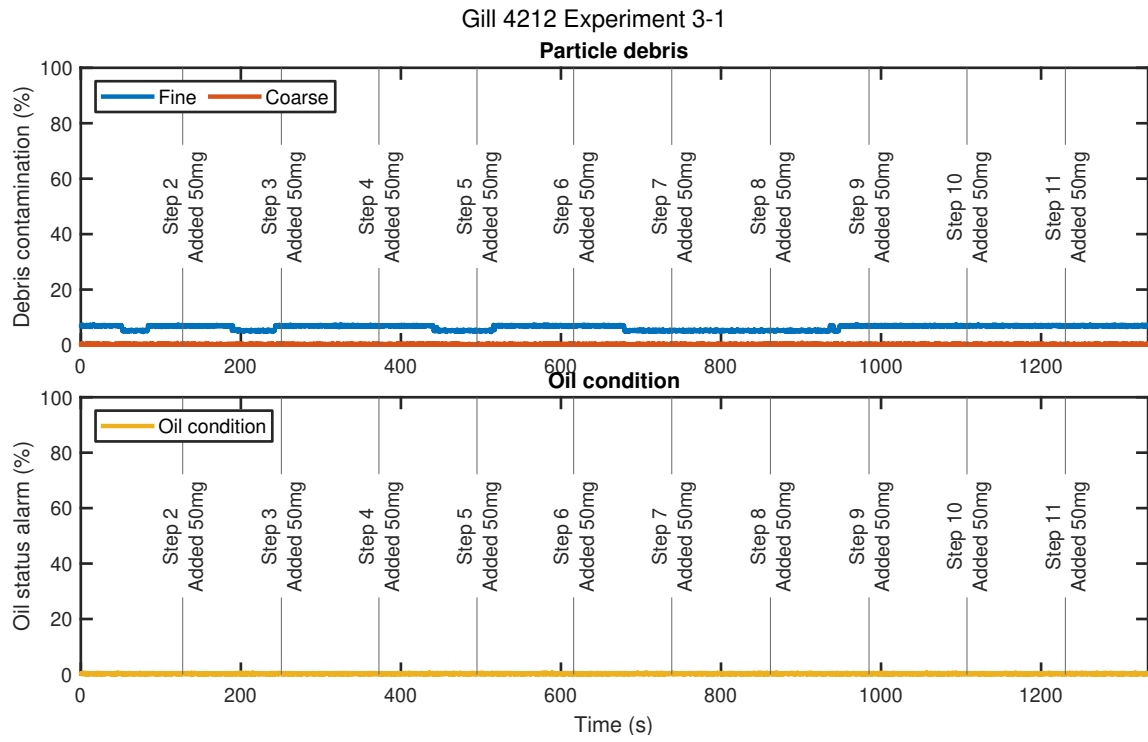


Figure F.19.: Gill 4212 experiment no. 3-1

Poseidon Trident QW3100 Experiment 3-1

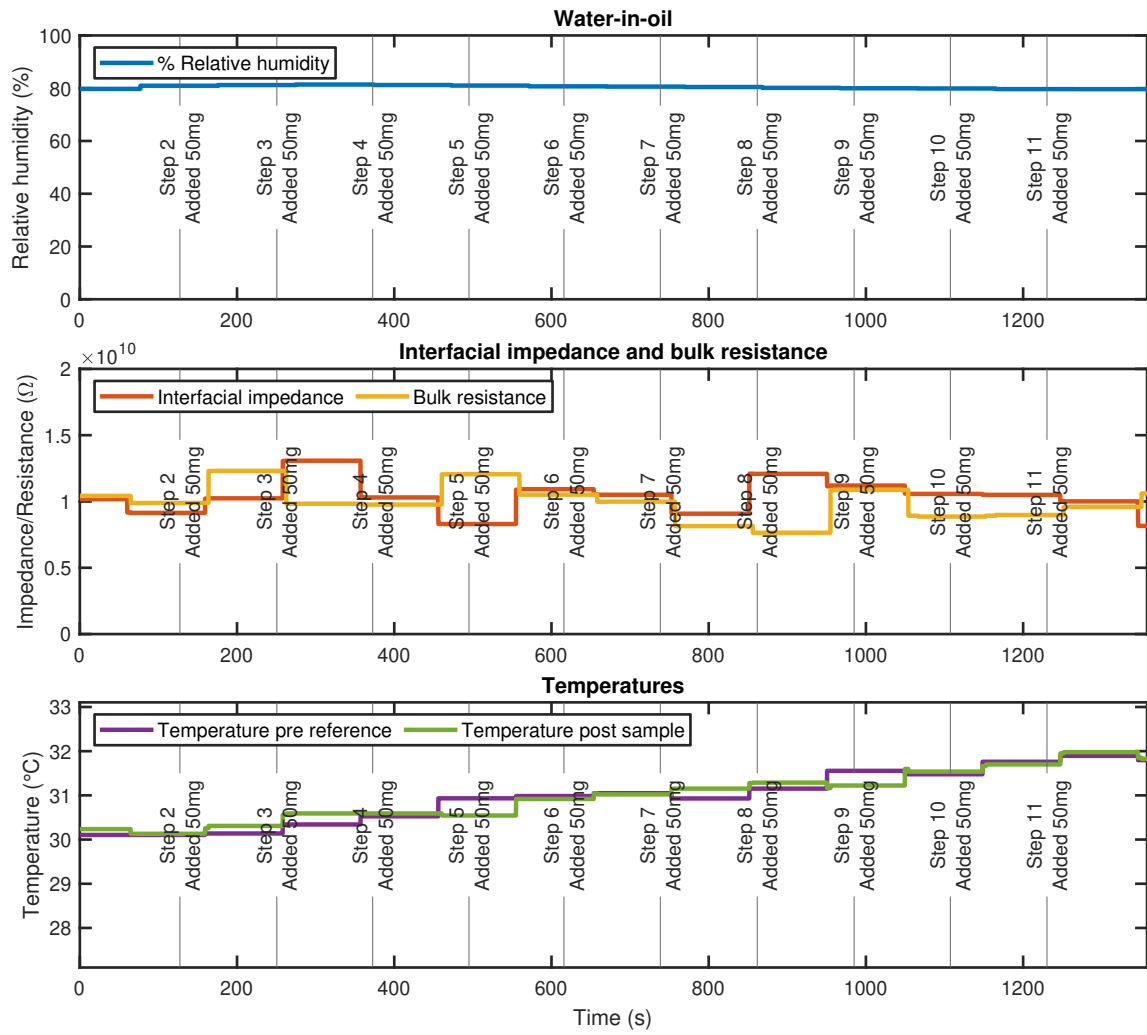


Figure F.20.: Poseidon Trident QW3100 experiment no. 3-1

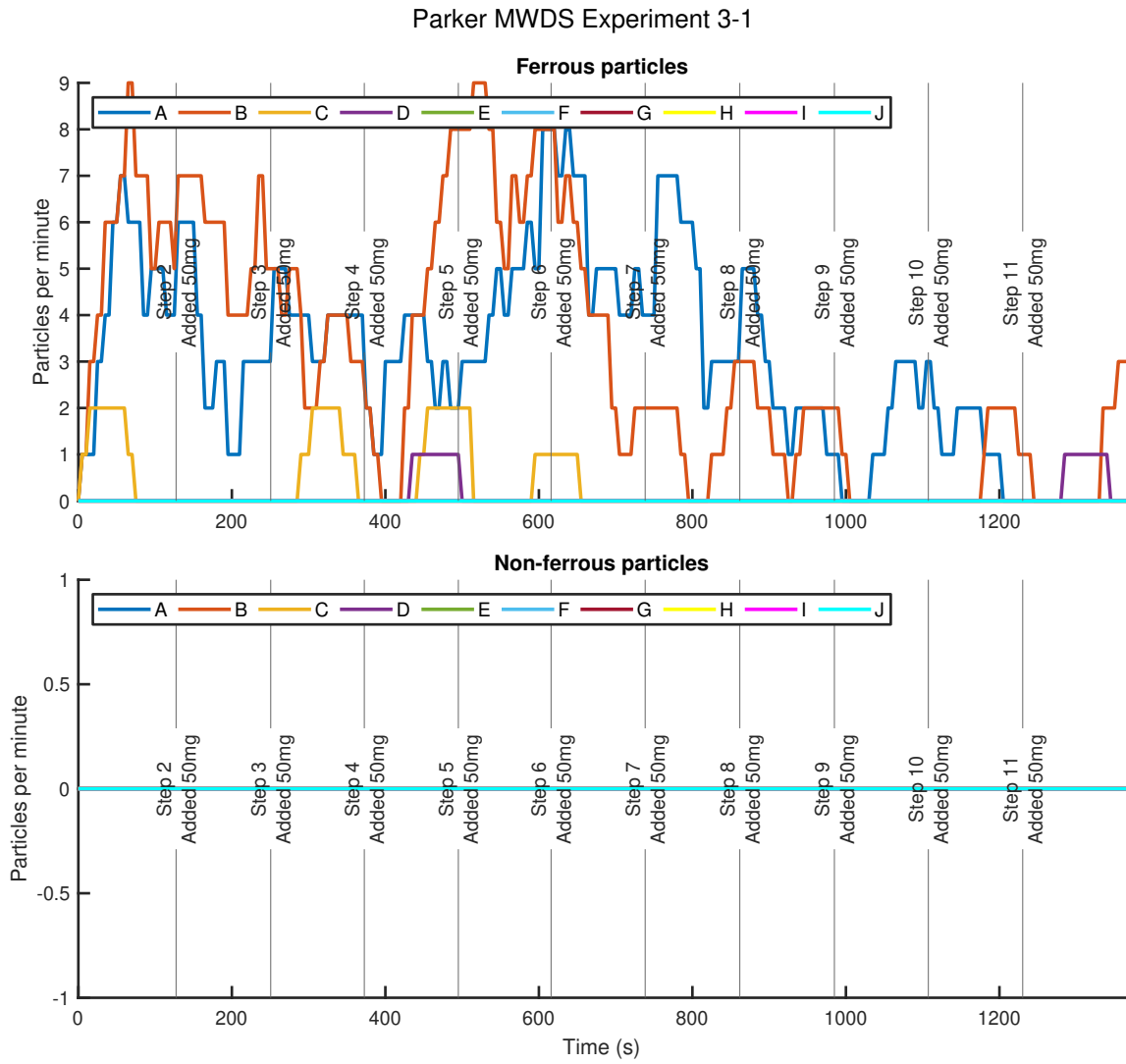


Figure F.21.: Parker MWDS experiment no. 3-1

F.3.2. Run no. 2

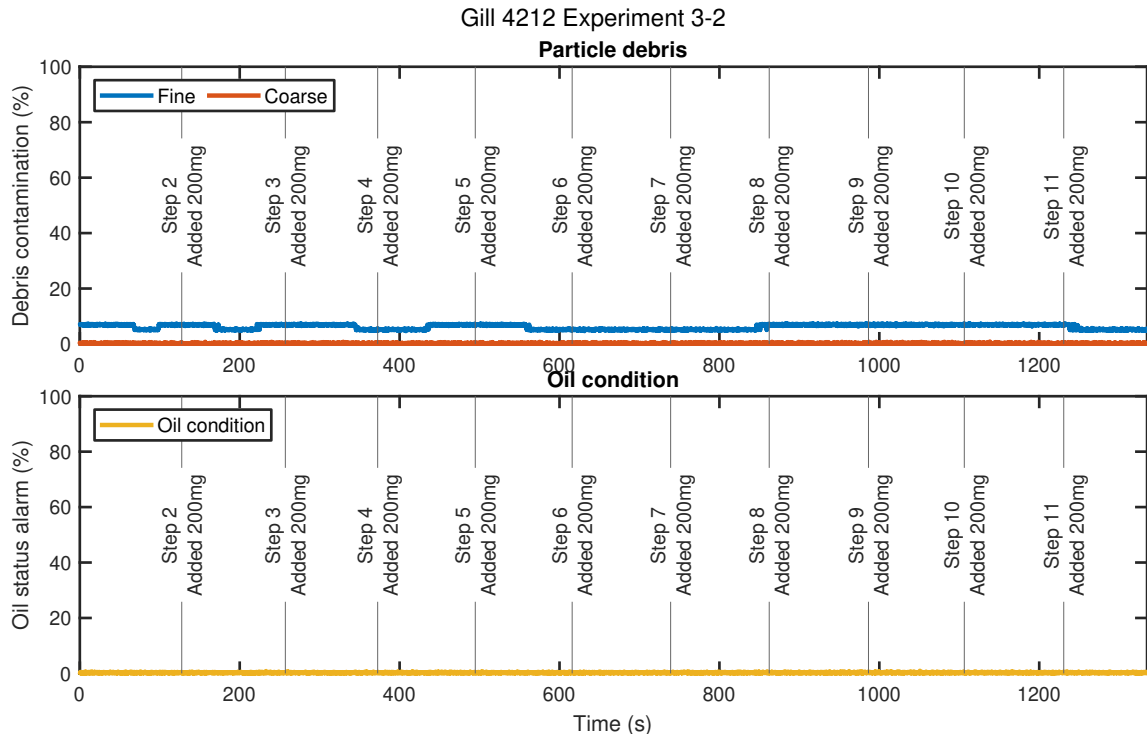


Figure F.22.: Gill 4212 experiment no. 3-2

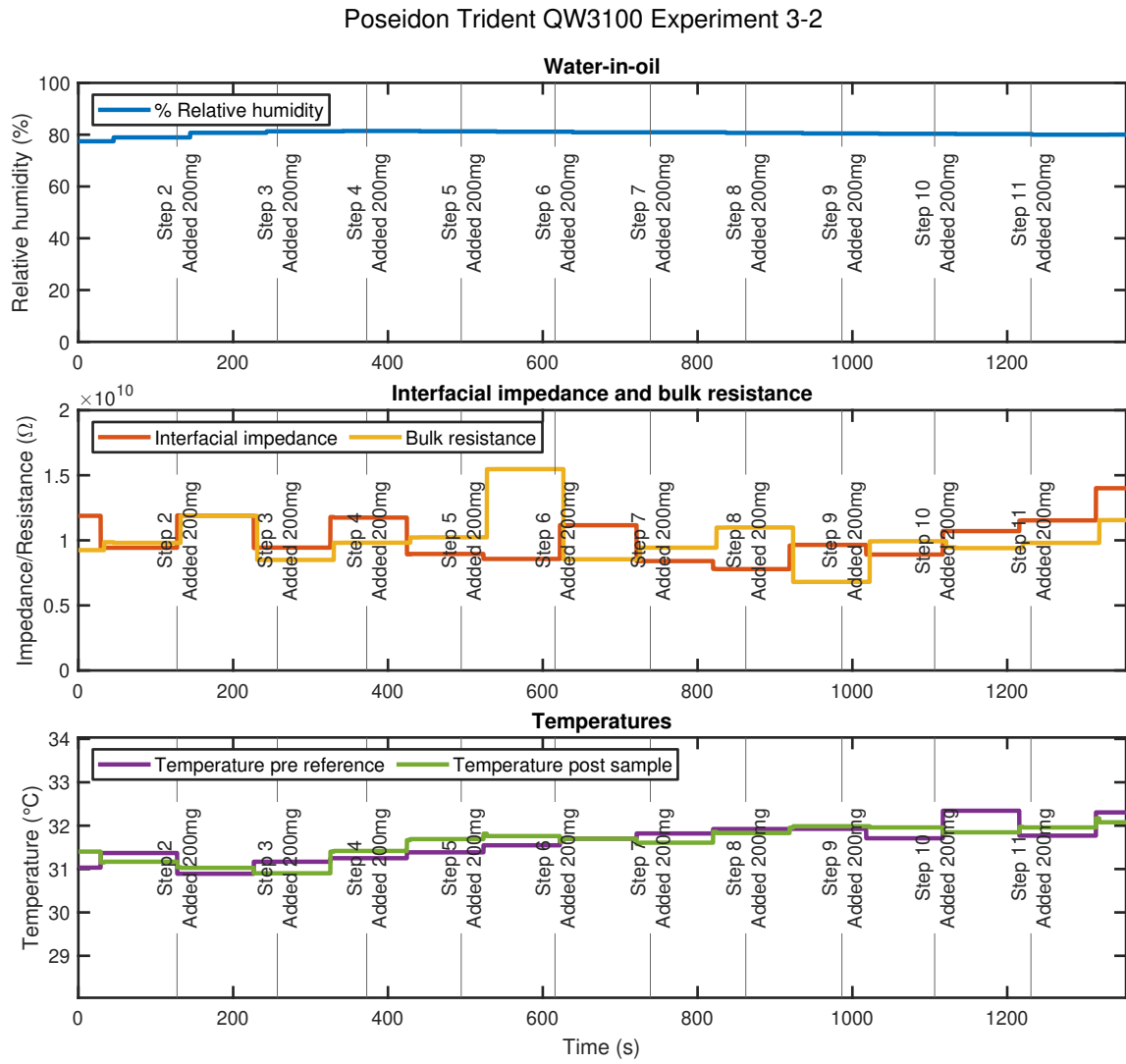


Figure F.23.: Poseidon Trident QW3100 experiment no. 3-2

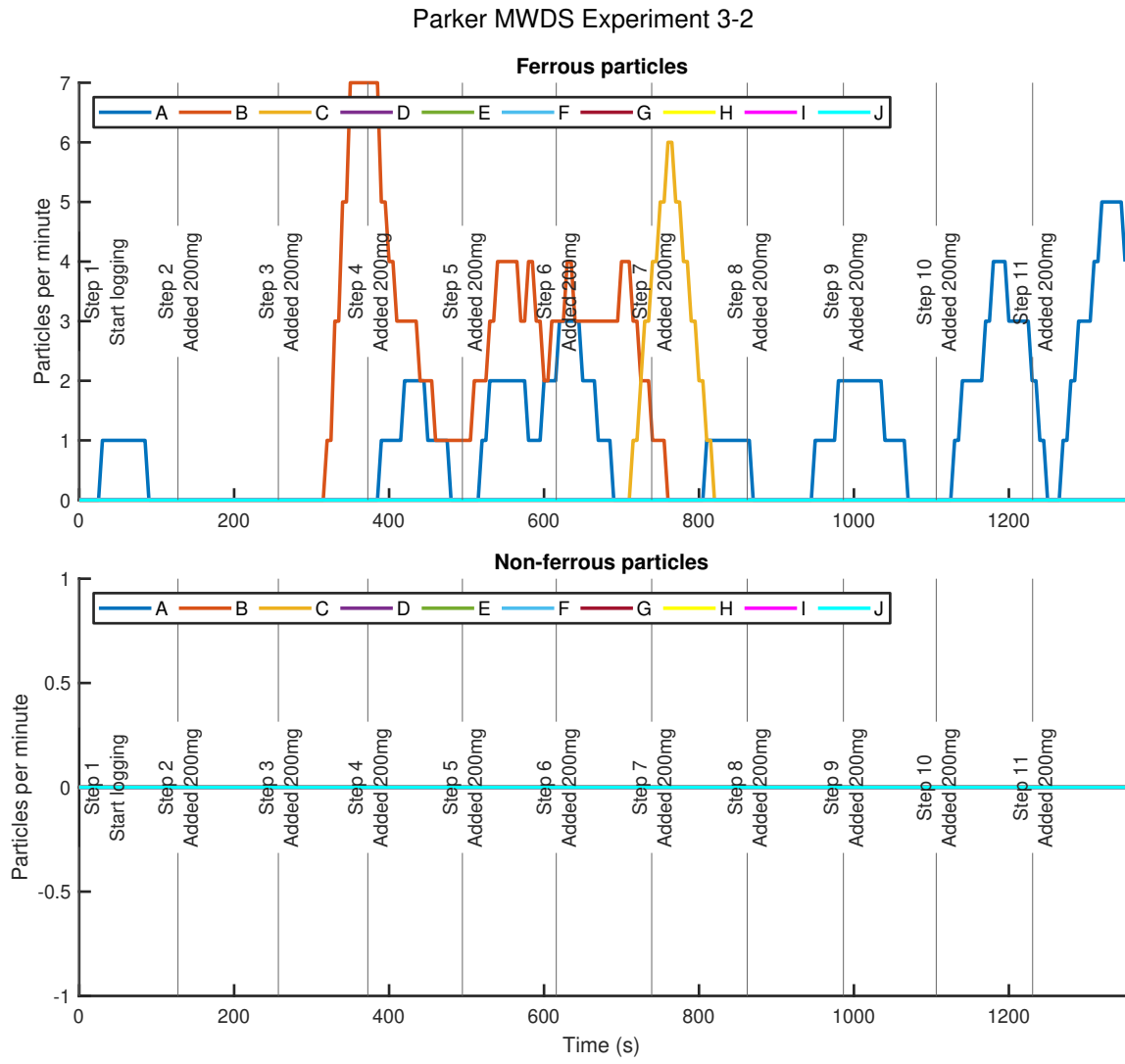


Figure F.24.: Parker MWDS experiment no. 3-2

F.3.3. Run no. 3

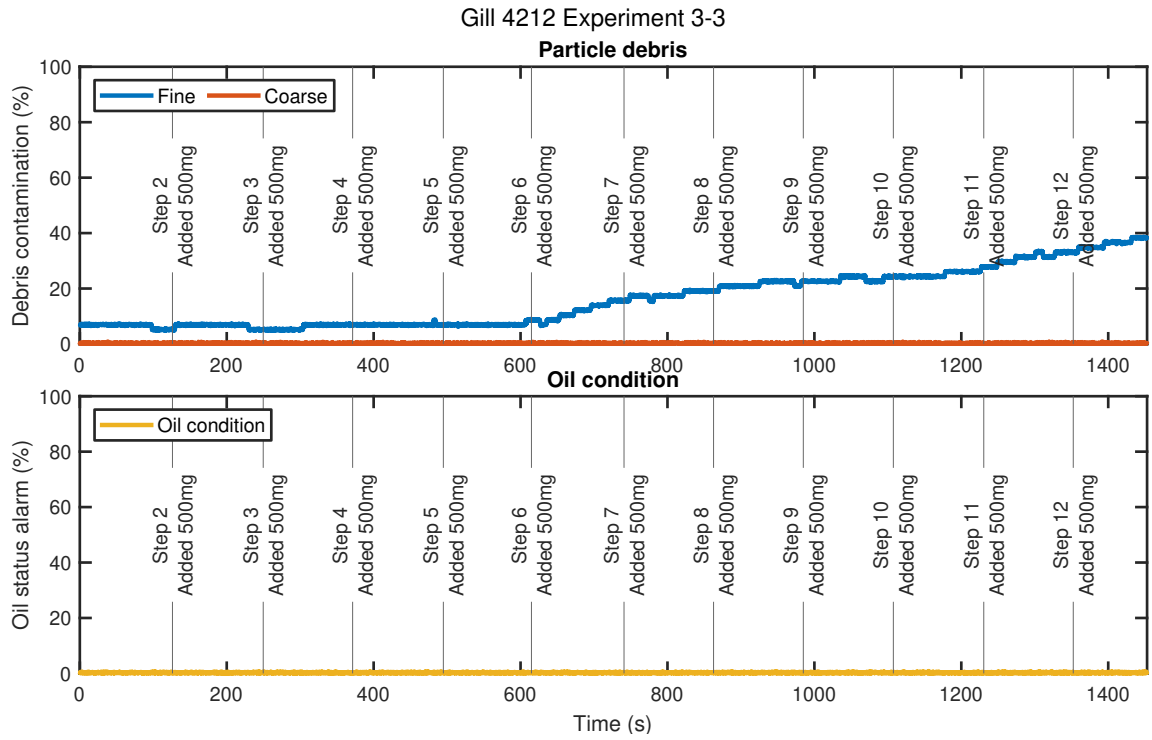


Figure F.25.: Gill 4212 experiment no. 3-3

Poseidon Trident QW3100 Experiment 3-3

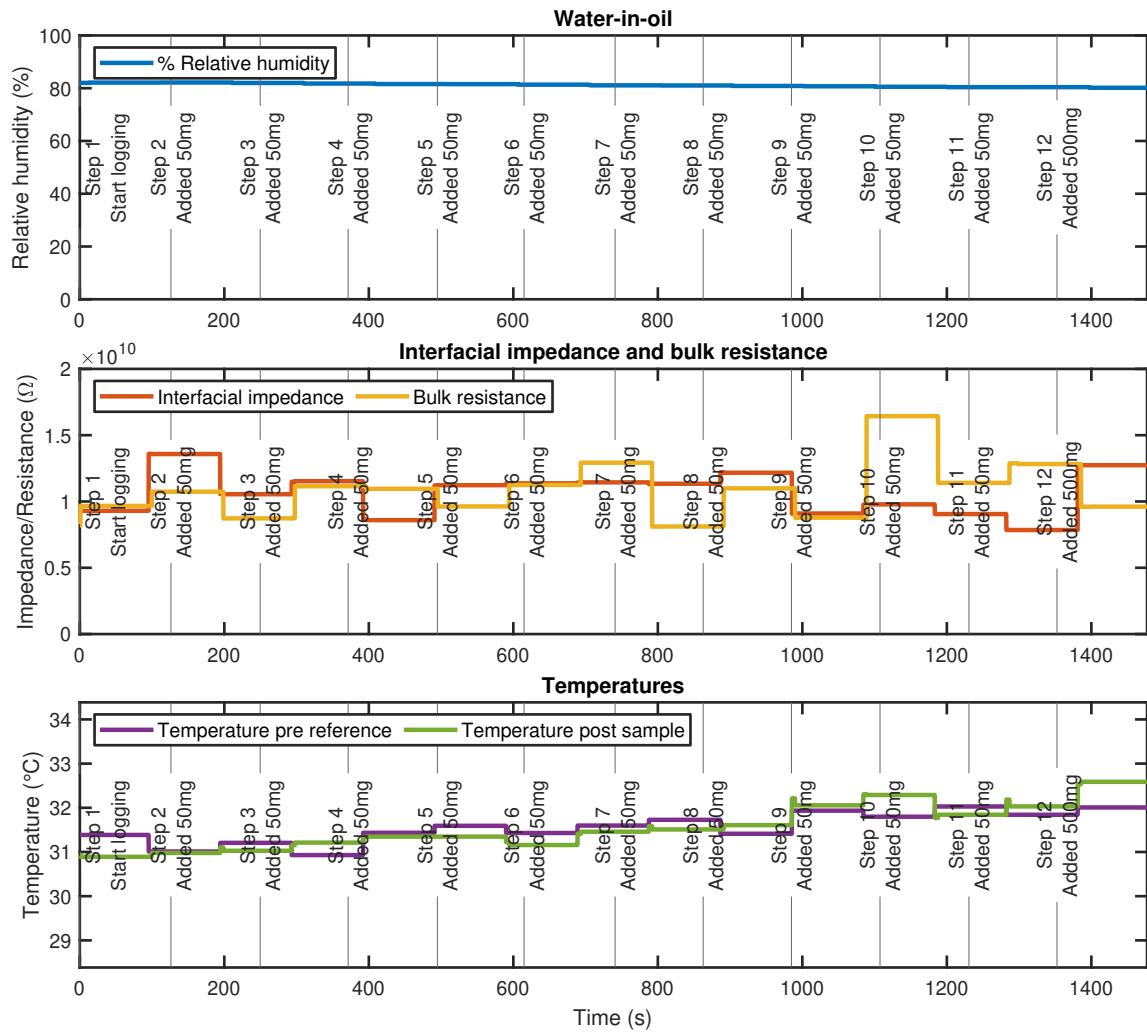


Figure F.26.: Poseidon Trident QW3100 experiment no. 3-3

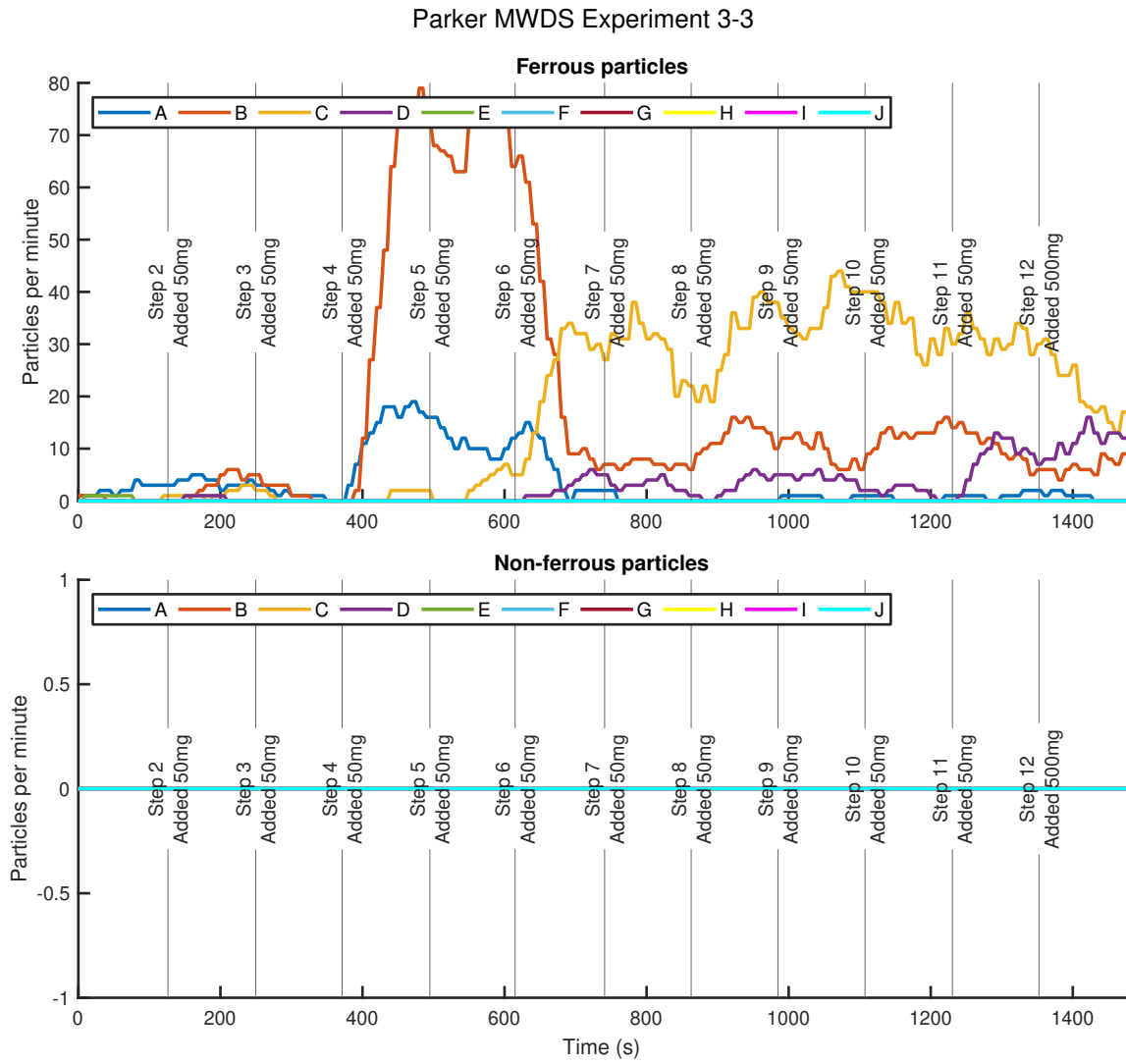


Figure F.27.: Parker MWDS experiment no. 3-3

F.4. Experiment no. 4

F.4.1. Run no. 1

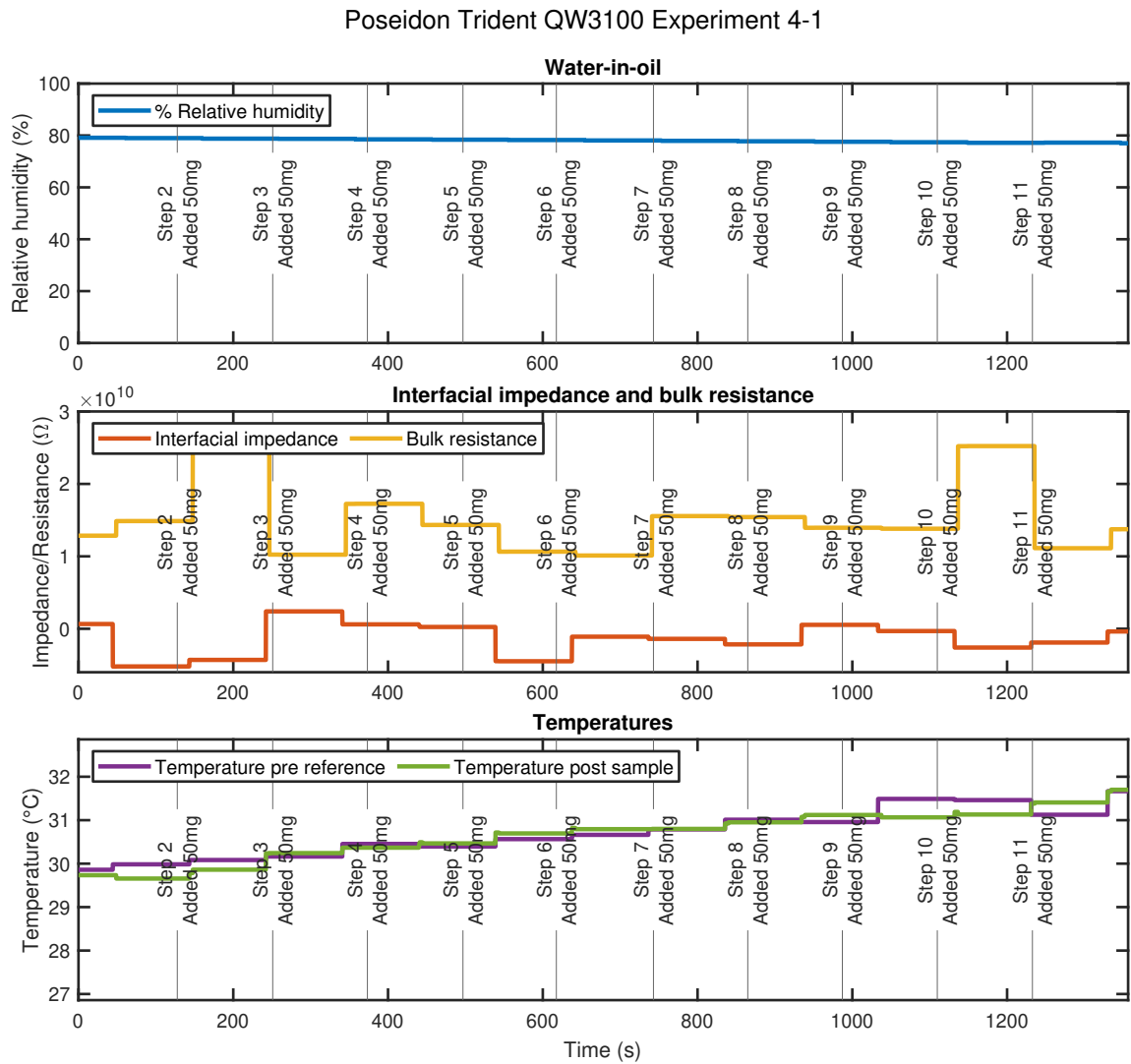


Figure F.28.: Poseidon Trident QW3100 experiment no. 4-1

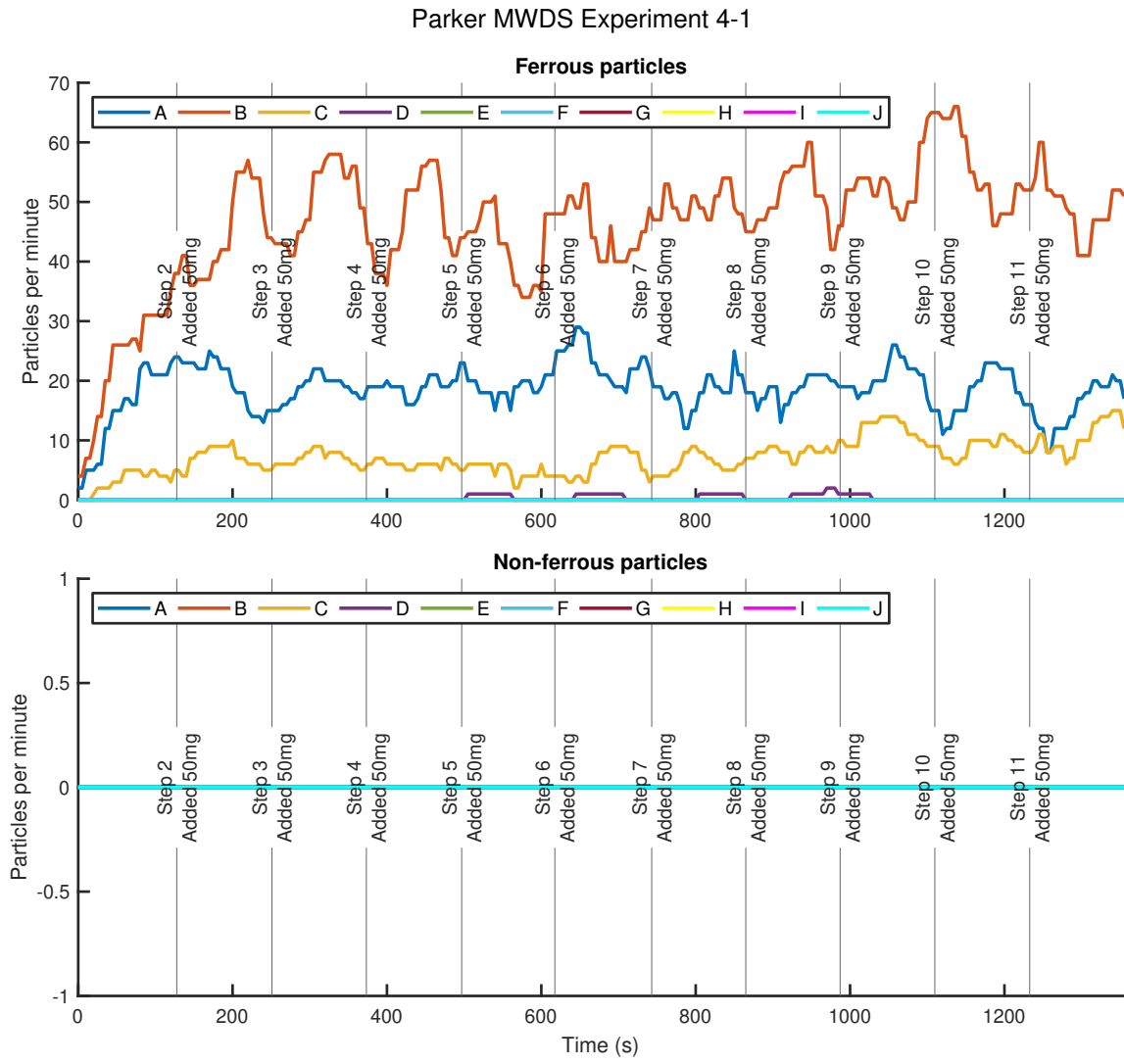


Figure F.29.: Parker MWDS experiment no. 4-1

F.4.2. Run no. 2

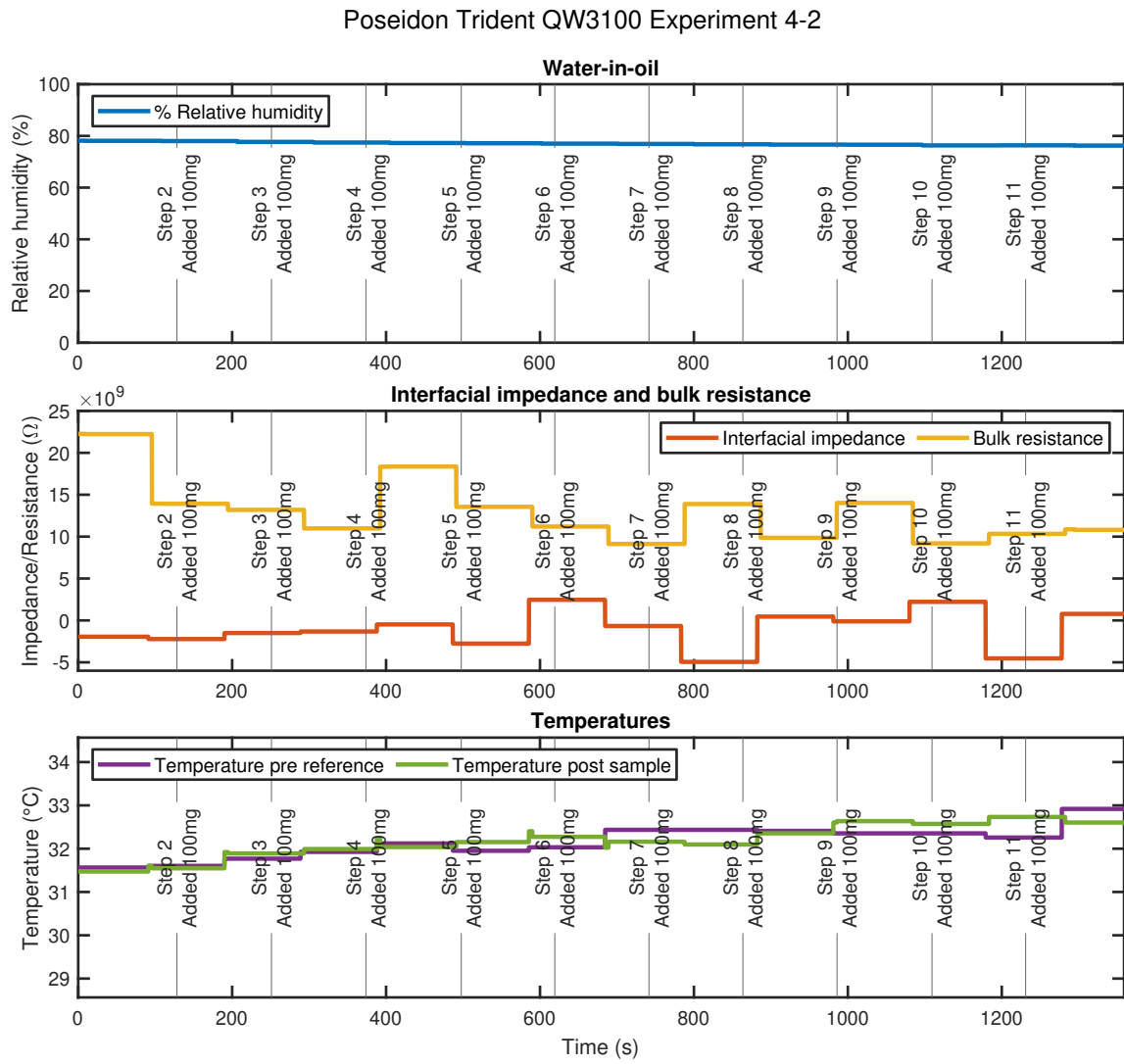


Figure F.30.: Poseidon Trident QW3100 experiment no. 4-2

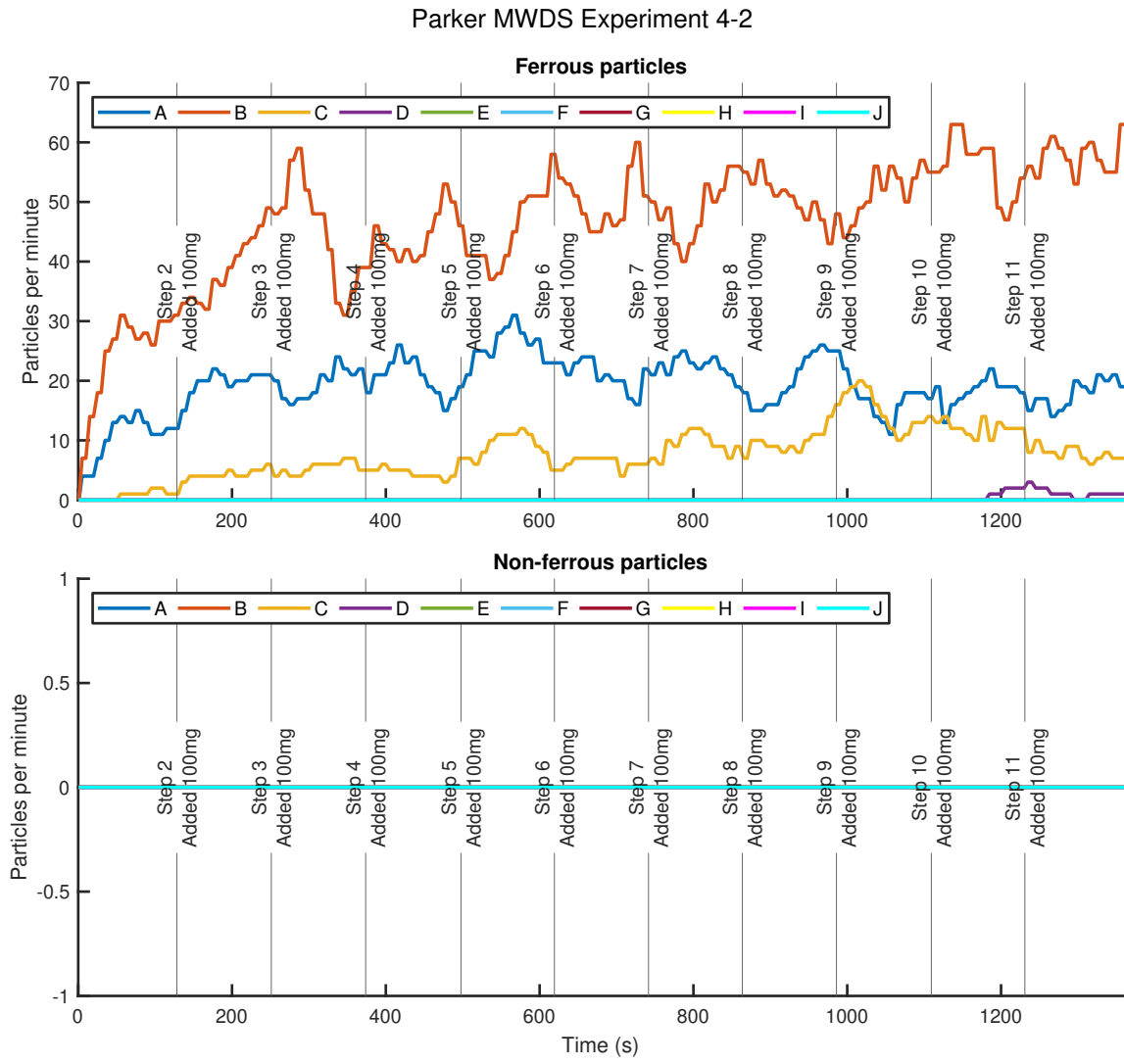


Figure F.31.: Parker MWDS experiment no. 4-2

F.4.3. Run no. 3

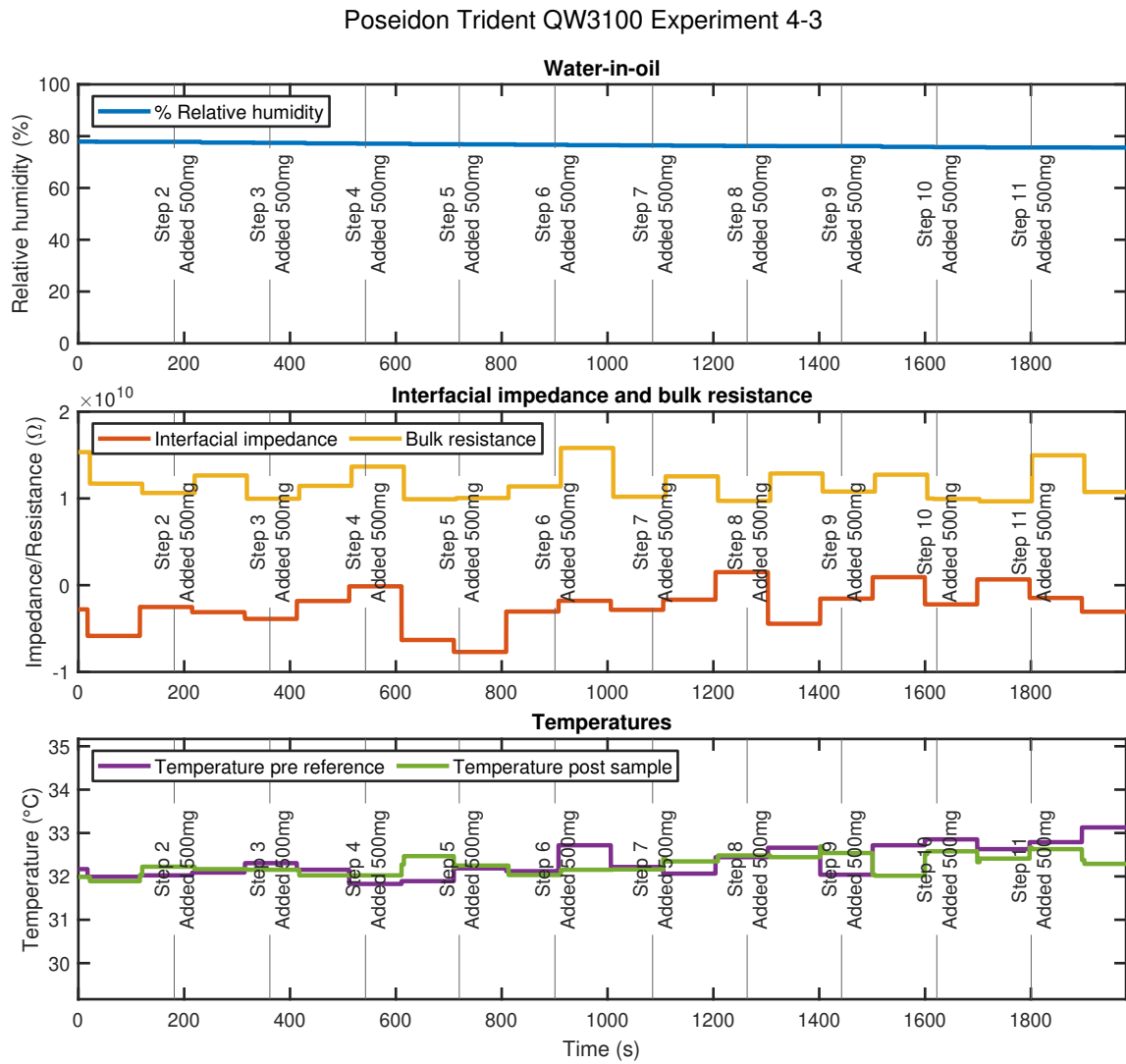


Figure F.32.: Poseidon Trident QW3100 experiment no. 4-3

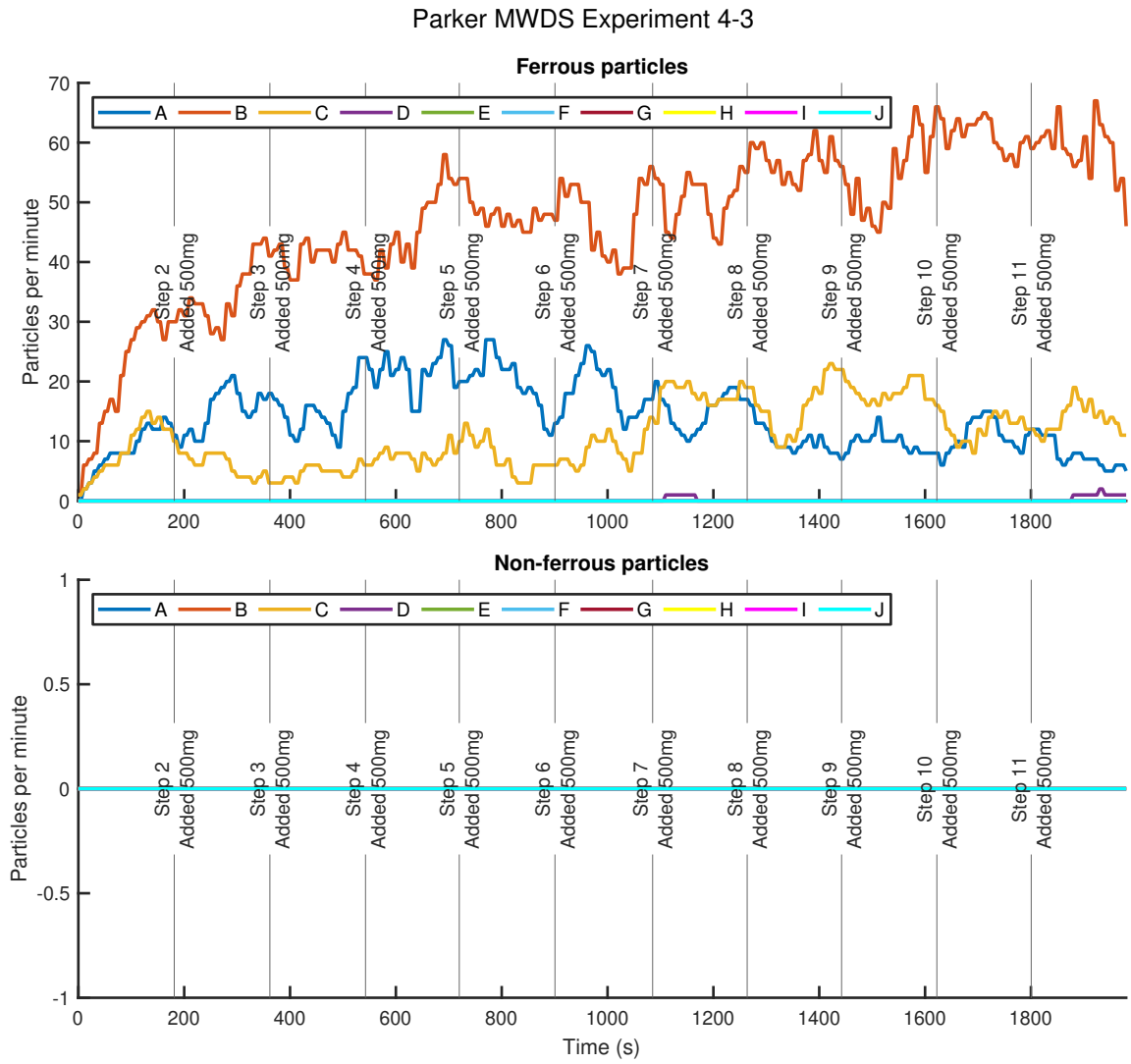


Figure F.33.: Parker MWDS experiment no. 4-3

F.4.4. Run no. 4

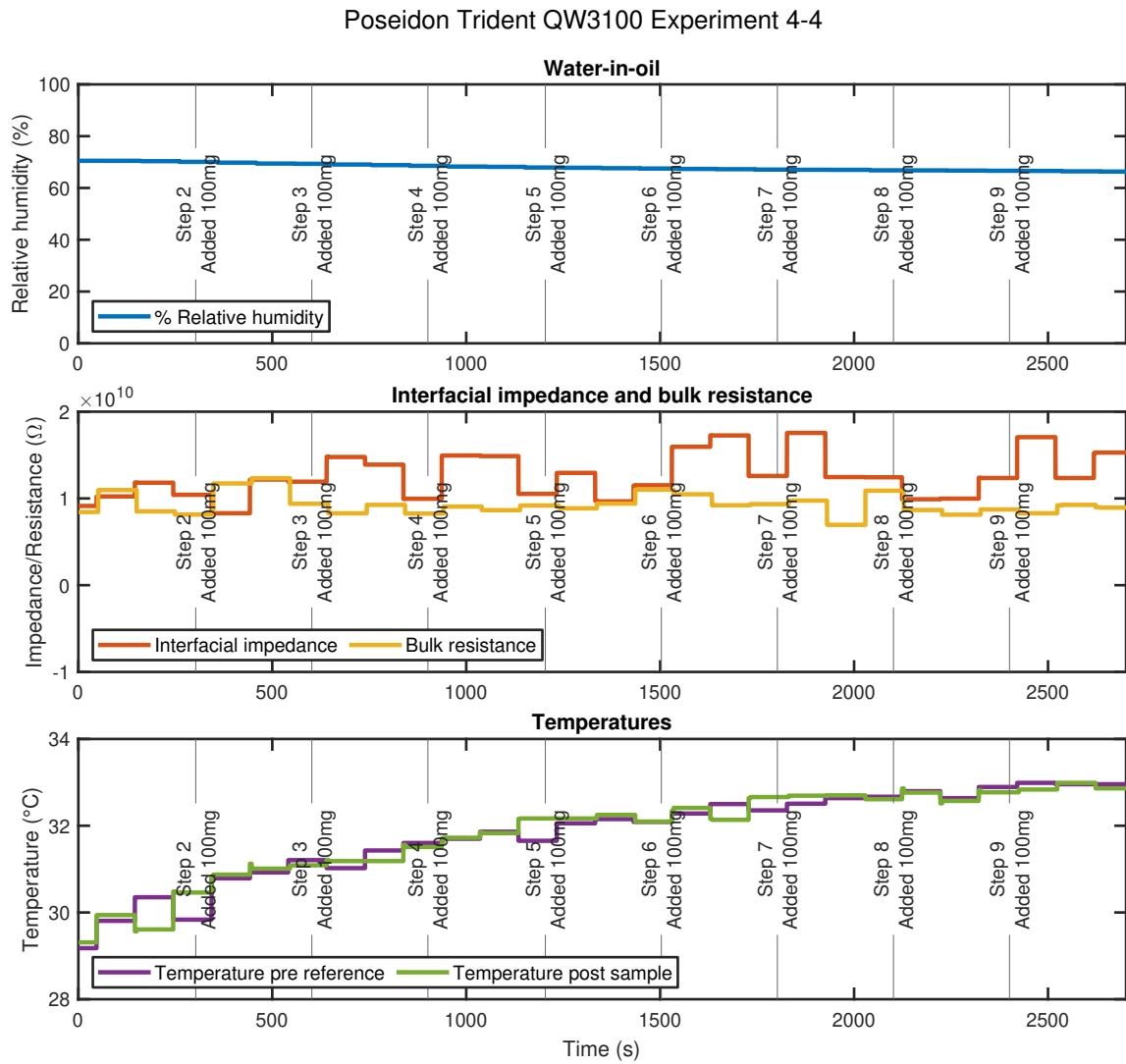


Figure F.34.: Poseidon Trident QW3100 experiment no. 4-4

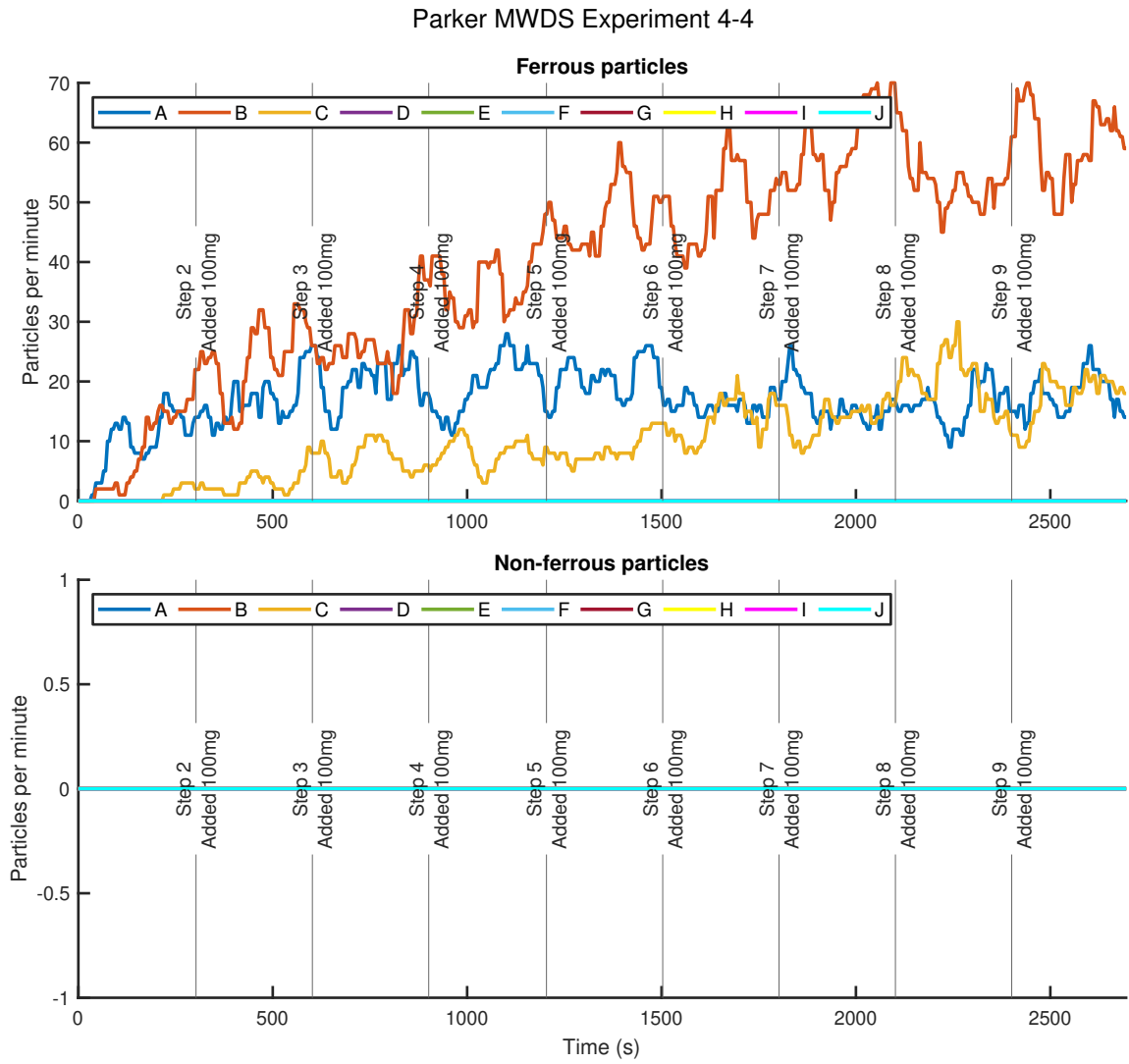


Figure F.35.: Parker MWDS experiment no. 4-4

F.5. Experiment no. 5

F.5.1. Run no. 1

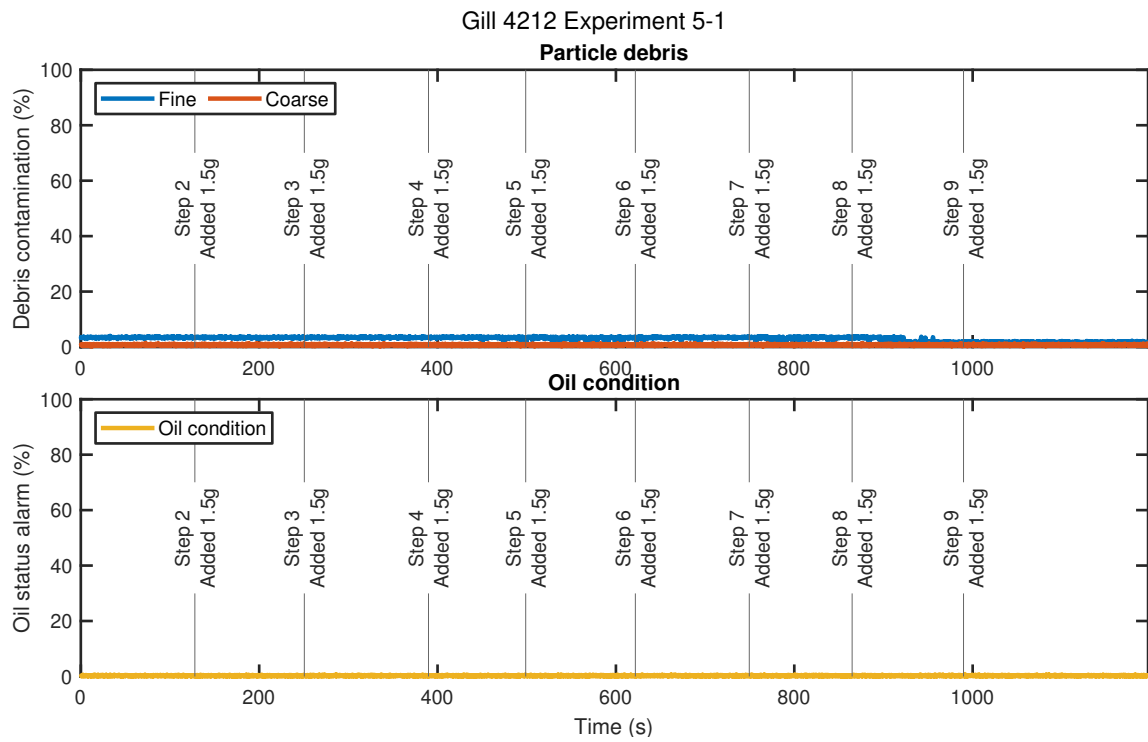


Figure F.36.: Gill 4212 experiment no. 5-1

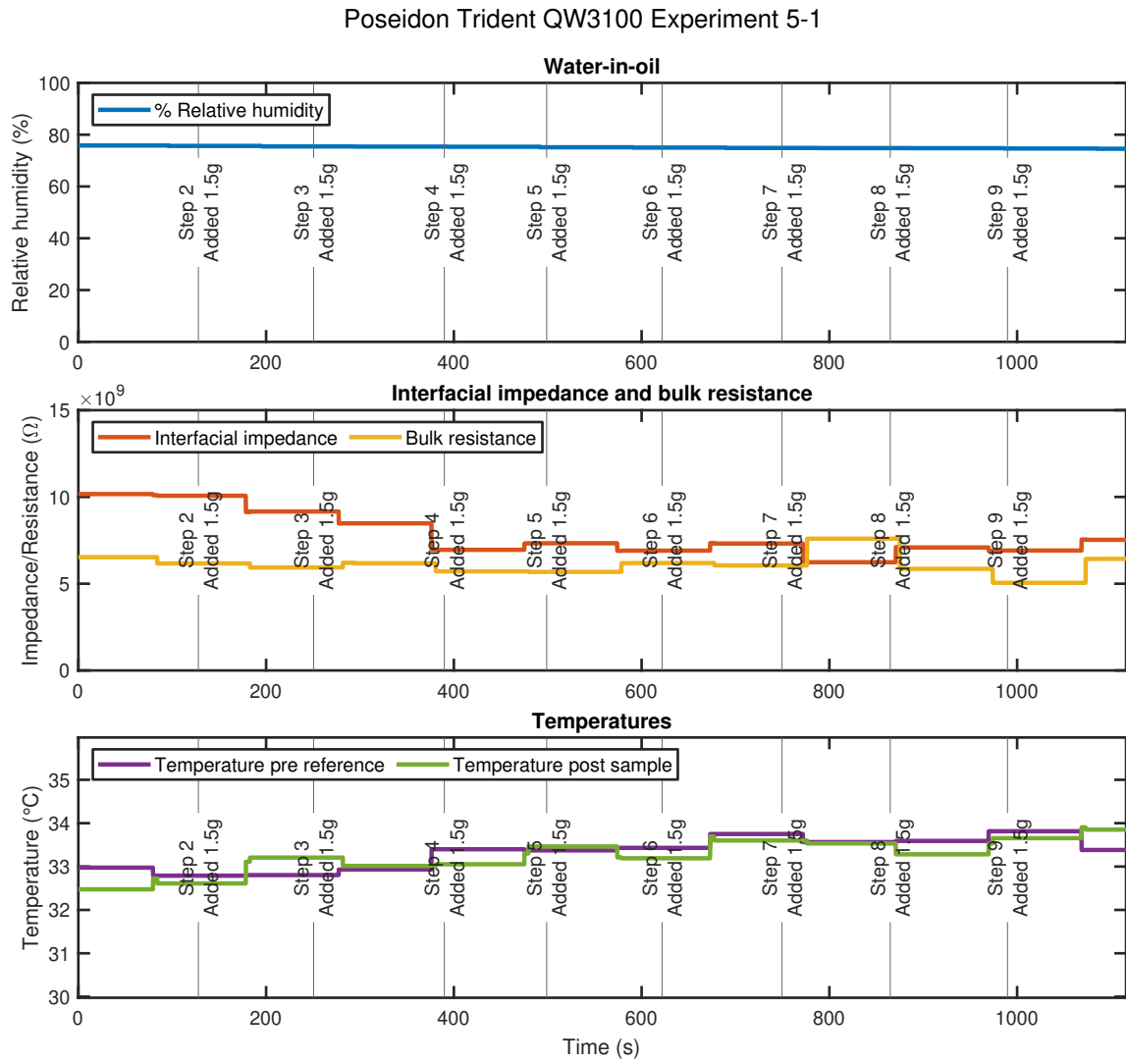


Figure F.37.: Poseidon Trident QW3100 experiment no. 5-1

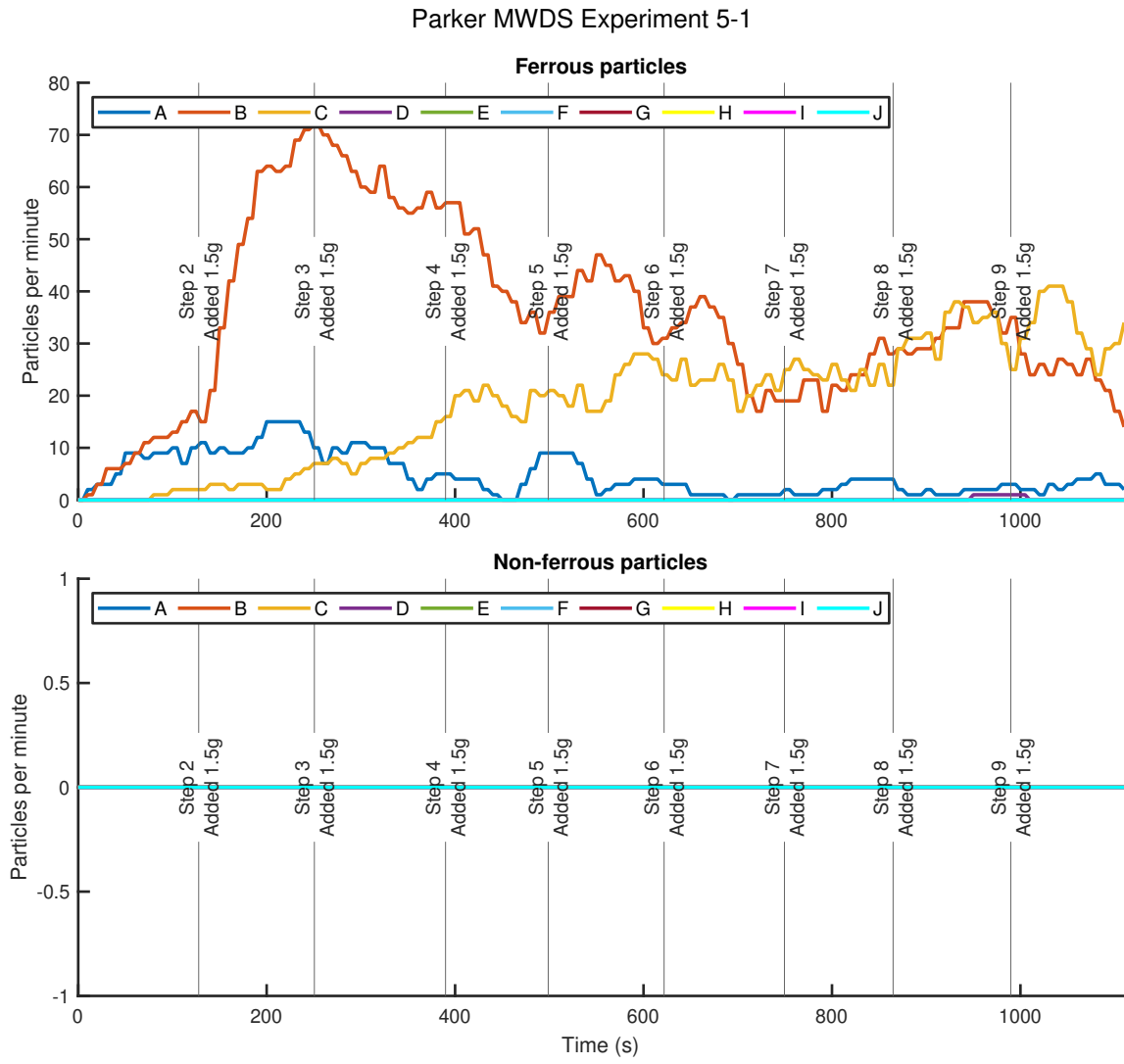


Figure F.38.: Parker MWDS experiment no. 5-1

F.5.2. Run no. 2

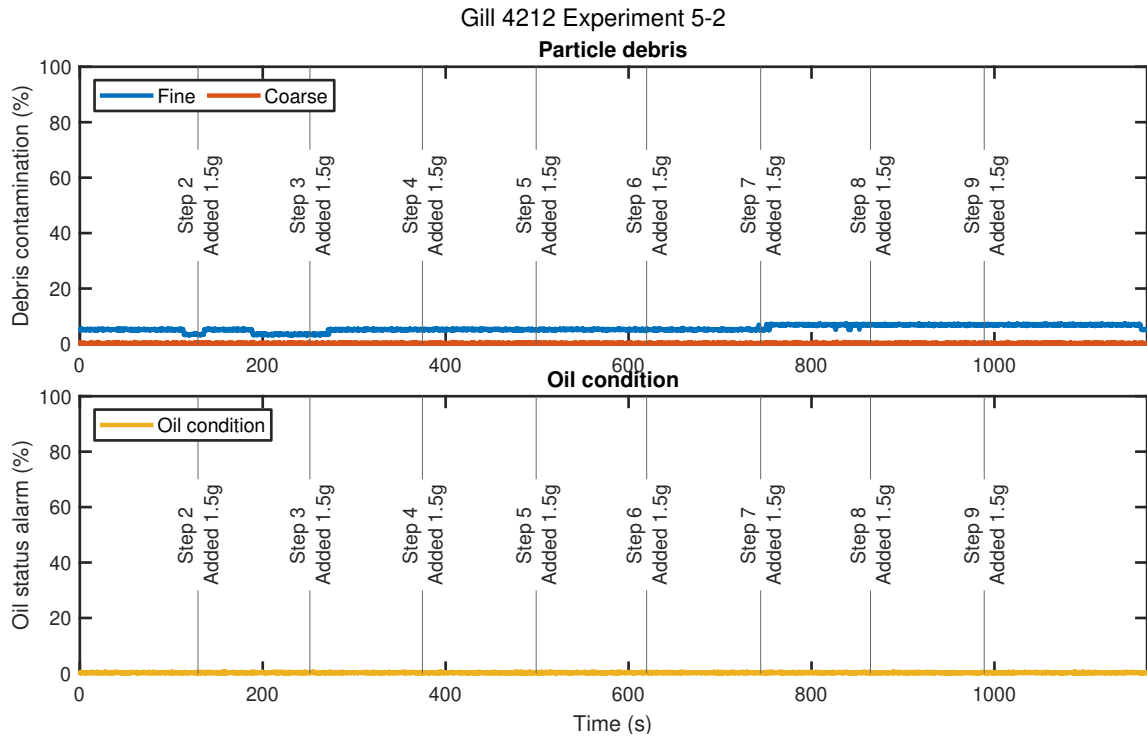


Figure F.39.: Gill 4212 experiment no. 5-2

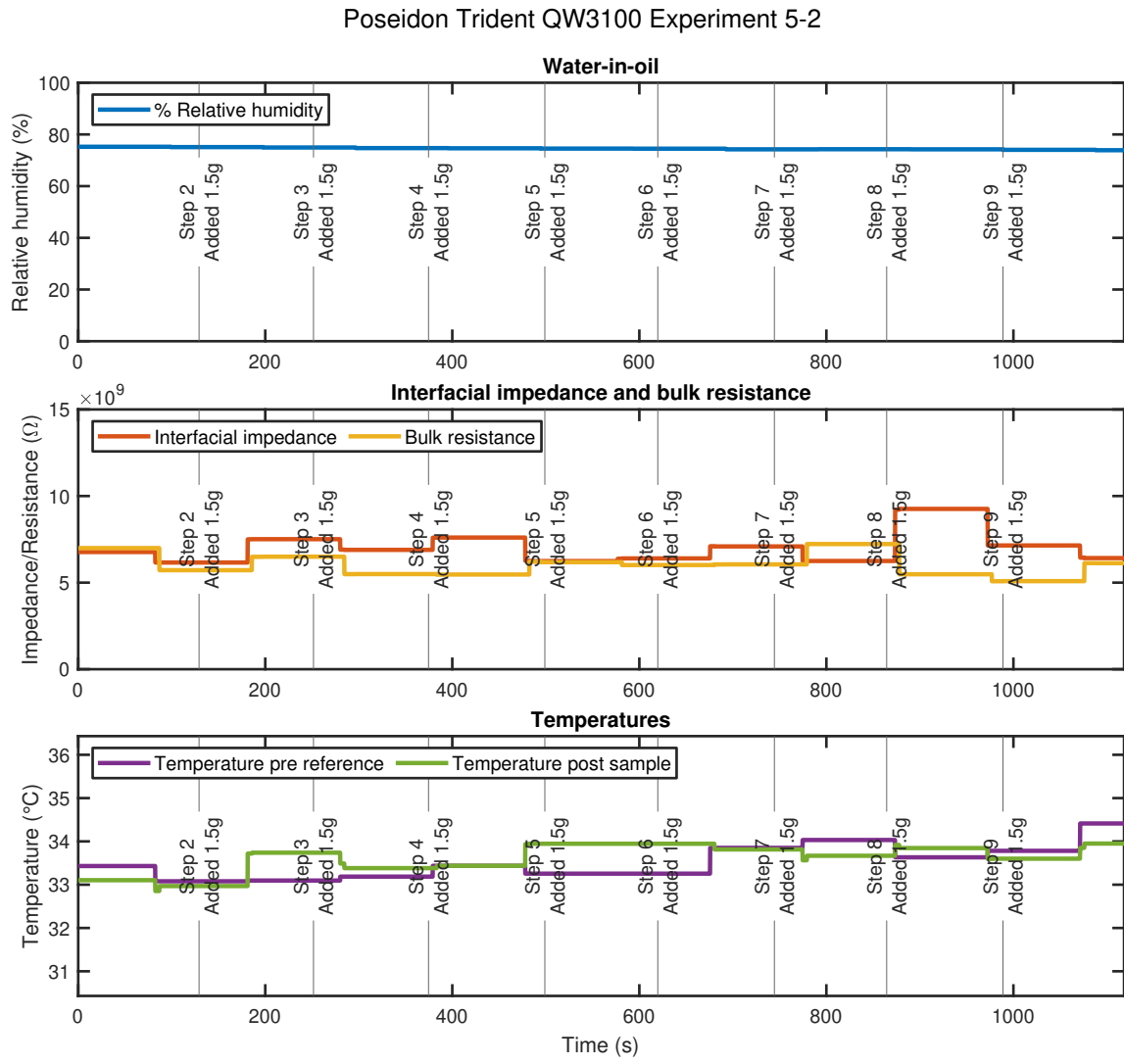


Figure F.40.: Poseidon Trident QW3100 experiment no. 5-2

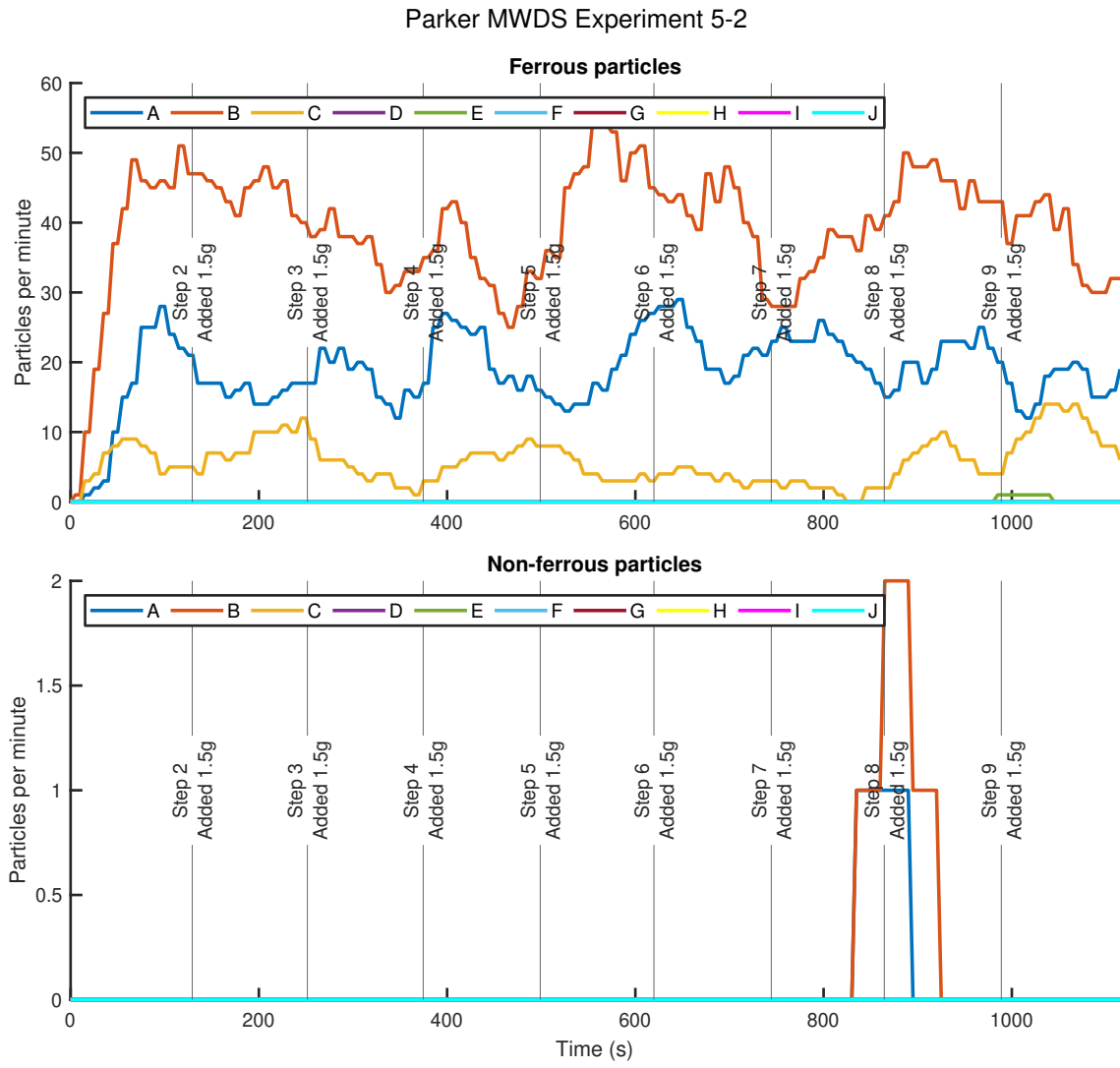


Figure F.41.: Parker MWDS experiment no. 5-2

F.5.3. Run no. 3

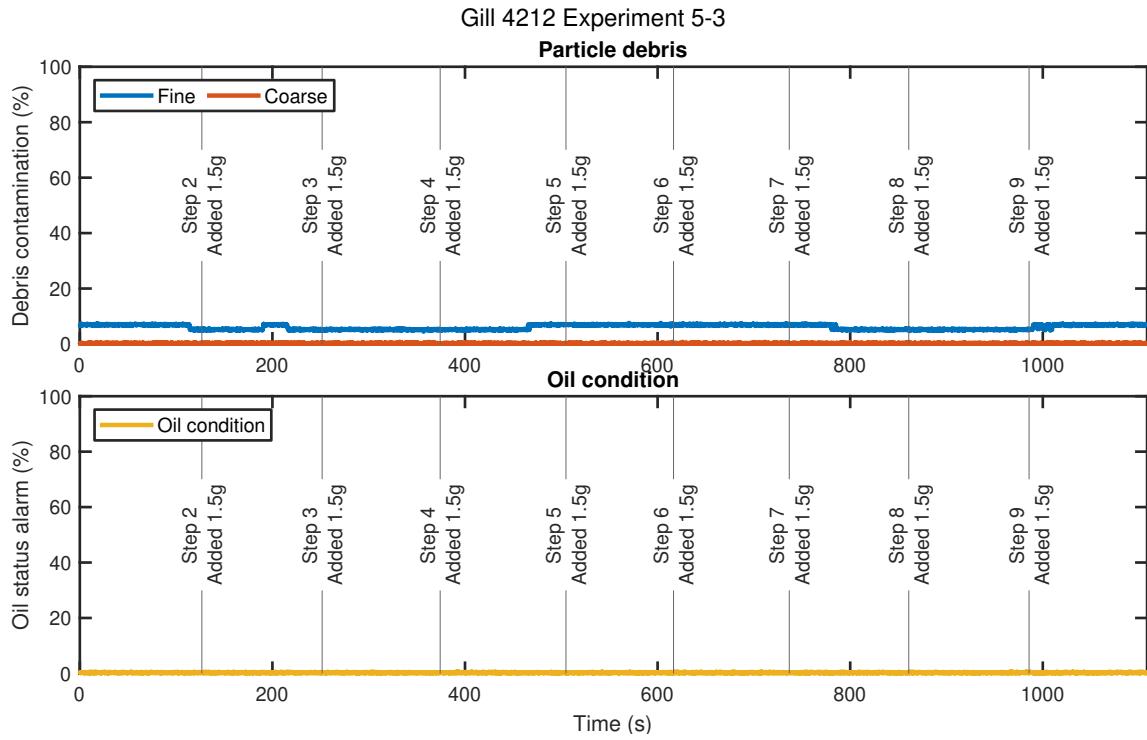


Figure F.42.: Gill 4212 experiment no. 5-3

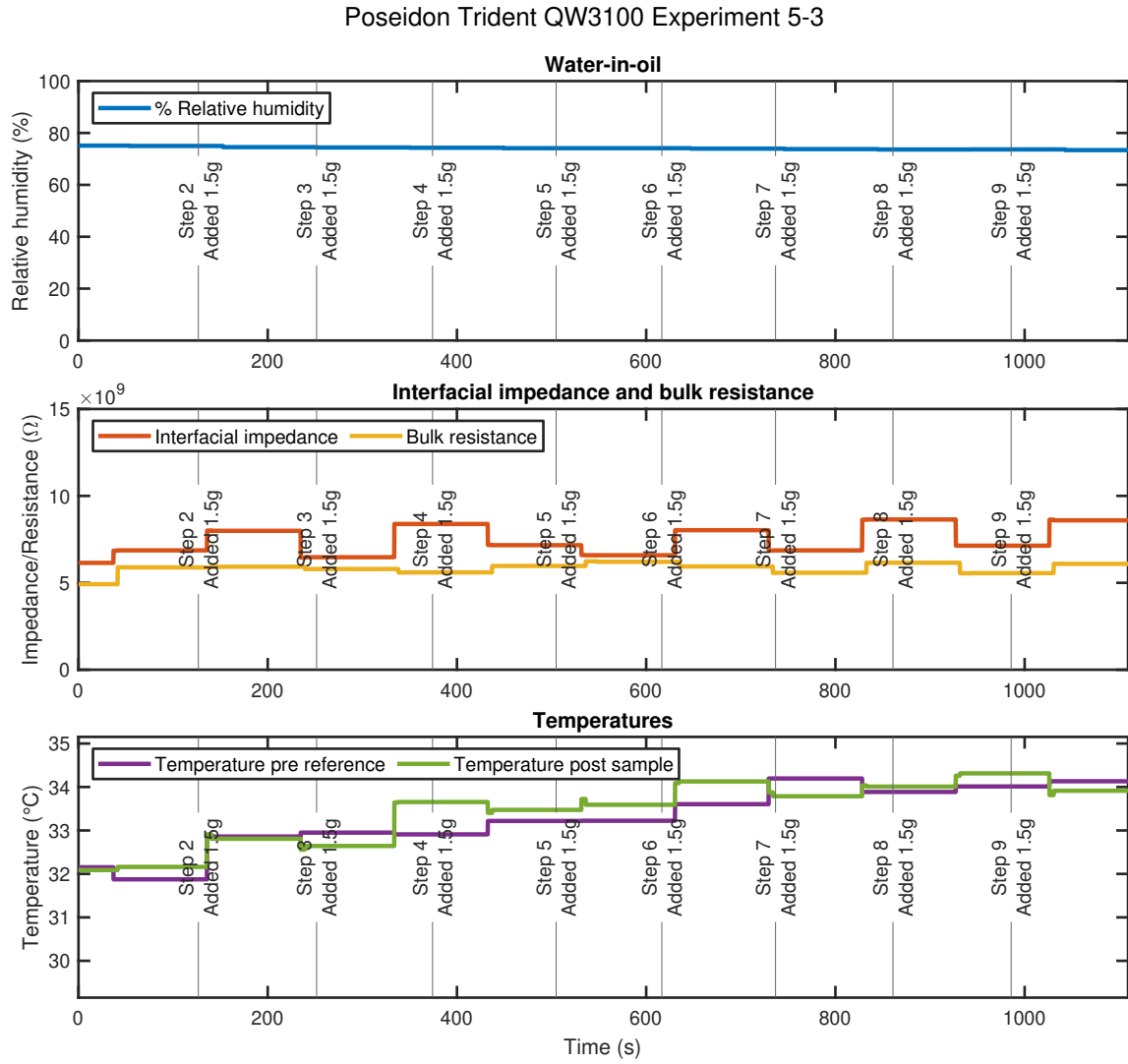


Figure F.43.: Poseidon Trident QW3100 experiment no. 5-3

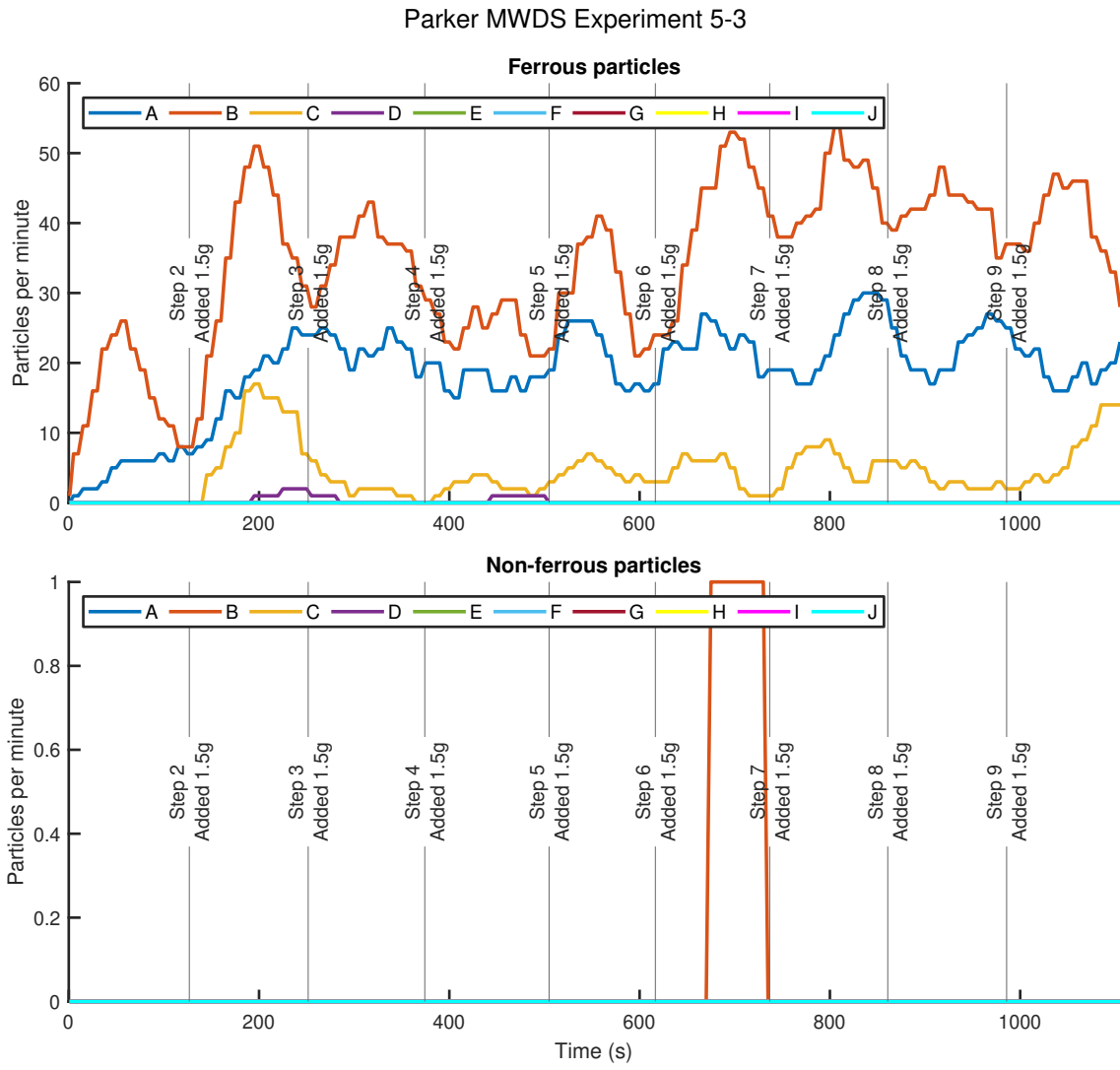


Figure F.44.: Parker MWDS experiment no. 5-3